# Intensity Modulated Brachytherapy for the Treatment of Cervical Cancer


**Marc Morcos**

Medical Physics Unit
Department of Bioengineering and Biomedical Engineering
McGill University

A thesis submitted to McGill University in partial fulfillment
of the requirements of the degree of
*Doctor of Philosophy*

 December 2021

# ABSTRACT

The critical limitation with brachytherapy is the rotationally symmetric dose distribution provided by brachytherapy sources, delivering high dose to the tumor but often with poor tumor conformity due to the non-symmetrical shape of the tumors resulting in dose spillage to surrounding healthy tissues. Intensity modulated brachytherapy (IMBT) utilizes radiation-attenuating shields to produce highly anisotropic dose distributions. Dynamic shield IMBT makes use of shield(s) which rotate around a conventional high dose rate brachytherapy source. By varying the position of the source and amount of time it dwells at each position combined with the rotation angle of the shield, a patient-specific dose distribution can be produced which better conforms to the tumor topology while reducing dose to radiosensitive organs-at-risk (OARs).

Conventional intracavitary cervix brachytherapy provides a cylindrically symmetric pear-shaped dose distribution, adequate for treating small tumors contained within the uterine body. Large tumors extending into the parametrial and/or paravaginal tissues cannot be safely treated without overdosing nearby OARs. In advanced cases, the intracavitary implant is supplemented with interstitial brachytherapy needles, enabling conformal dose delivery to the tumor while reducing dose to the OARs. Magnetic resonance imaging (MRI) guided hybrid intracavitary-interstitial high dose rate brachytherapy has increased the local control without increasing morbidity for large tumors, compared to the intracavitary brachytherapy alone. Interstitial brachytherapy, which allows the clinicians to treat large or irregular tumors that are hard to reach, is the most invasive, complex and resource demanding brachytherapy technique. Despite the excellent clinical results, this treatment is not available to all patients due to its invasive nature, lack of resources and trained radiation oncologists.

Intracavitary dynamic shield cervix IMBT holds the promise of safely increasing the tumoricidal dose coverage to the irregular tumor periphery. Intracavitary dynamic shield IMBT will increase the therapeutic ratio and the probability of a curative outcome with minimal quality of life detriment without use of interstitial needles, which will make it available to a larger population of patients. The aim of this thesis was to investigate a novel method of delivering dynamic shield IMBT for the treatment of cervical cancer.

This work was carried out in several steps. First, an open-source Monte Carlo based treatment planning system, RapidBrachyMCTPS was further developed with the ability to transport radiation through matter during dynamic shield motion. Next, three candidate shields were designed that would fit within the intrauterine brachytherapy applicator component known as the tandem. To further leverage the theoretical advantage of intensity modulation, two lower average photon

energy emitting brachytherapy radionuclides ($^{75}$Se & $^{169}$Yb) were investigated in addition to the clinically ubiquitous $^{192}$Ir. The combination of candidate shields, and radionuclides were studied in terms of their resulting dosimetric properties.

A retrospective treatment planning study was then carried out to demonstrate the dosimetric benefit of dynamic shield IMBT using our most promising shield design (flute). Using images from 36 cervical cancer patients, conventional brachytherapy was compared to our IMBT applicator using $^{192}$Ir, $^{75}$Se and $^{169}$Yb. For women with smaller (<30 cm$^3$) tumor volumes, IMBT achieved a significantly higher tumor dose up to 6.7% while simultaneously reducing dose to OARs by up to 7.7%. IMBT benefits increase with decreasing radionuclide average photon energy ($^{192}$Ir$\rightarrow$$^{75}$Se$\rightarrow$$^{169}$Yb). For patients with larger (>30 cm$^3$) tumor volumes which regularly require the addition of interstitial brachytherapy needles, needle-free IMBT was comparable with $^{169}$Yb-based IMBT further improving tumor dose and reducing sigmoid dose by 1.5% and 1.9%, respectively, all without having to implant needles.

Finally, this work involved evaluation of the impact of dose reporting schemes and tissue/applicator material heterogeneities for $^{192}$Ir-, $^{75}$Se- and $^{169}$Yb-based conventional brachytherapy and IMBT on dose metrics. The historical assumption that patients' tissues can be approximated as water equivalent for the purposes of dose calculation are not valid in the presence of high-density applicators and pelvic bones. Additionally, with the advent of MRI guided brachytherapy, we also investigated that dosimetric impact resulting from moving away from computed tomography imaging and having to estimate the mass-density on an entire organ-to-organ basis. We reported our findings and have made recommendations regarding the clinical adoption of IMBT and lower energy radionuclides. Dynamic shield cervix IMBT system holds great promise for increasing the therapeutic ratio and making brachytherapy accessible to more patients.

# RÉSUMÉ

La principale limite de la curiethérapie est la distribution de dose symétrique fournie par les sources de curiethérapie, qui délivrent une dose élevée à la tumeur, mais dont la conformité à la tumeur est souvent médiocre en raison de la forme non symétrique des tumeurs, ce qui entraîne un déversement de la dose dans les tissus sains environnants. La curiethérapie à modulation d'intensité (IMBT) utilise des boucliers atténuant le rayonnement pour produire des distributions de dose hautement anisotropes. L'IMBT à bouclier dynamique utilise un ou plusieurs boucliers qui tournent autour d'une source conventionnelle de curiethérapie à haut débit de dose. En faisant varier la position de la source et le temps qu'elle passe dans chaque position, ainsi que l'angle de rotation de l'écran, il est possible de produire une distribution de dose spécifique au patient qui se conforme mieux à la topologie de la tumeur tout en réduisant la dose reçue par les organes à risque (OAR) radiosensibles.

La curiethérapie intracavitaire conventionnelle du col de l'utérus fournit une distribution de dose en forme de poire à symétrie cylindrique, adéquate pour traiter les petites tumeurs contenues dans le corps utérin. Les tumeurs de grande taille s'étendant dans les tissus paramétriaux et/ou paravaginaux ne peuvent pas être traitées en toute sécurité sans surdoser les OAR voisins. Dans les cas avancés, l'implant intracavitaire est complété par des aiguilles de curiethérapie interstitielles, ce qui permet de délivrer une dose conforme à la tumeur tout en réduisant la dose aux OAR. La curiethérapie hybride intracavitaire-interstitielle à haut débit de dose guidée par l'imagerie par résonance magnétique (IRM) a permis d'améliorer le contrôle local sans augmenter la morbidité pour les tumeurs de grande taille, par rapport à la curiethérapie intracavitaire seule. La curiethérapie interstitielle, qui permet aux cliniciens de traiter des tumeurs volumineuses ou irrégulières difficiles à atteindre, est la technique de curiethérapie la plus invasive, la plus complexe et la plus gourmande en ressources. Malgré d'excellents résultats cliniques, ce traitement n'est pas accessible à tous les patients en raison de sa nature invasive, du manque de ressources et de radio-oncologues formés.

L'IMBT du col de l'utérus avec bouclier dynamique intracavitaire promet d'augmenter en toute sécurité la couverture de la dose tumoricide à la périphérie irrégulière de la tumeur. L'IMBT à bouclier dynamique intracavitaire augmentera le ratio thérapeutique et la probabilité d'un résultat curatif avec un préjudice minimal à la qualité de vie sans utiliser d'aiguilles interstitielles, ce qui la rendra accessible à une plus grande population de patients. L'objectif de cette thèse était d'étudier une nouvelle méthode d'administration de la IMBT à bouclier dynamique pour le traitement du cancer du col de l'utérus.

Ce travail a été réalisé en plusieurs étapes. Tout d'abord, un système de planification de traitement basé sur la méthode Monte Carlo, RapidBrachyMCTPS, a été développé avec la capacité de transporter le rayonnement à travers la matière pendant le mouvement dynamique du bouclier. Ensuite, trois boucliers candidats ont été conçus pour s'adapter à l'applicateur de curiethérapie intra-utérine connu sous le nom de tandem. Pour mieux exploiter l'avantage théorique de la modulation d'intensité, deux radionucléides de curiethérapie émettant une énergie photonique moyenne plus faible (sélénium-75 et ytterbium-169) ont été étudiés en plus de l'iridium-192, omniprésent en clinique. La combinaison des boucliers candidats et des radionucléides a été étudiée en termes de propriétés dosimétriques résultantes.

Une étude rétrospective de planification du traitement a ensuite été réalisée pour démontrer l'avantage dosimétrique de la IMBT à bouclier dynamique en utilisant notre modèle de bouclier le plus prometteur (flûte). En utilisant les images de 36 patientes atteintes d'un cancer du col de l'utérus, la curiethérapie conventionnelle a été comparée à notre applicateur IMBT utilisant l'iridium-192, le sélénium-75 et l'ytterbium-169. Pour les femmes présentant des volumes tumoraux plus petits (<30 $cm^3$), l'IMBT a permis d'obtenir une dose tumorale significativement plus élevée, jusqu'à 6,7%, tout en réduisant simultanément la dose aux OAR jusqu'à 7,7%. Les avantages de l'IMBT augmentent avec la diminution de l'énergie photonique moyenne du radionucléide. Pour les patients présentant des volumes tumoraux plus importants (>30 $cm^3$) qui nécessitent régulièrement l'ajout d'aiguilles de curiethérapie interstitielle, l'IMBT sans aiguille était comparable à l'IMBT à base d'ytterbium-169 améliorant davantage la dose tumorale et réduisant la dose sigmoïde de 1,5% et 1,9%, respectivement, le tout sans avoir à implanter d'aiguilles.

Enfin, ce travail a permis d'évaluer l'impact sur les mesures de dose des systèmes de rapport de dose et des hétérogénéités des tissus/applicateurs pour la curiethérapie conventionnelle et l'IMBT à base d'iridium-192, de sélénium-75 et d'ytterbium-169. L'hypothèse historique selon laquelle les tissus des patients peuvent être assimilés à un équivalent d'eau aux fins du calcul de la dose n'est pas valable en présence d'applicateurs à haute densité et d'os pelviens. De plus, avec l'avènement de la curiethérapie guidée par IRM, nous avons également étudié l'impact dosimétrique résultant de l'abandon de l'imagerie par tomographie assistée par ordinateur et de la nécessité d'estimer la masse volumique sur une base d'organe à organe. Nous avons présenté nos résultats et formulé des recommandations concernant l'adoption clinique de l'IMBT et des radionucléides de plus faible énergie. Le système IMBT à bouclier dynamique pour le col de l'utérus est très prometteur pour augmenter le ratio thérapeutique et rendre la curiethérapie accessible à un plus grand nombre de patients.

# ACKNOWLEDGEMENT

I am indebted to my supervisor, Dr. Shirin Abbasinejad Enger, for her support and guidance - which I'm certain will continue throughout my career. I would like to acknowledge my supervisory committee, Dr. Asa Carlsson Tedgren and Dr. Ahmad Haidar for their valuable input towards this project. I would like to thank the students in the Enger Lab for their camaraderie and constructive criticisms on this project. A special thanks to Majd Antaki, for his friendship and indulging me with our never ending thought experiments. I would like to thank Drs. John Wong and Akila N. Viswanathan for their mentorship and support which motivated me to pursue my studies. I would like to acknowledge financial support from the Natural Sciences and Engineering Research Council of Canada (NSERC) grant(#241018), Collaborative Health Research Projects grant (#248490). I would like to thank everyone in the McGill Medical Physics Unit, specifically Dr. Slobodan Devic, Dr. Jan Seuntjens, Margery Knewstubb and Tatjana Nisic, who have influenced me greatly over the years and for providing such a wonderful environment to learn and perform research. Finally, I would like to express my gratitude to my wife Fanny, my parents Mohsen, Heidy and Marie-Helene, and my siblings Sandra, Ramy, Dina and Daniel for their love, support and patience.

# Table of contents

# List of figures

# List of tables

# Chapter 1

# Introduction

## 1.1 Motivation

Brachytherapy (BT) is a form of radiation therapy (or radiotherapy) used in the treatment of cancer. BT consists of temporarily placing small gamma-emitting, sealed radioactive sources directly within or in proximity of the tumour. The radioactive source, often referred to as a seed, travels to the tumour site within implanted hollow catheters in the patient. The catheters are connected to an afterloader, which is a machine containing a single radioactive source at the end of a wire. The source is pushed into each of the catheters, one by one under computer control and guided to the tumor site. The computer controls where along the catheter the source should pause to deliver its radiation (dwell positions) and how long it dwells at each position (dwell time). After the desired dose is delivered, the source is pulled back to the afterloader and the catheters are removed. Generally, BT is delivered using either intracavitary BT, interstitial BT or a combination of the two (intracavitary/interstitial BT). In intracavitary BT, the hollow catheters are embedded within a BT applicator, which is a device placed into a natural body cavity (e.g.: tandem & ring placed into the intrauterine canal, cylinder placed into the vagina or mold applicator placed into the rectum; Figure 1.1). Intracavitary BT applicators are often specific to the anatomical treatment site. For example, in cervical cancer, the tandem & ring applicator is placed into the intrauterine canal via the vagina. Interstitial BT applicators are simply hollow needles which are used to access the tumor when there is no naturally occurring body cavity to grant access. Common interstitial BT treatment sites include (i) advanced cervical cancer where the tumor has spread from the cervix to the nearby parametrium and paravaginal tissues, (ii) prostate cancer where BT needles are placed trans-perineally or (iii)

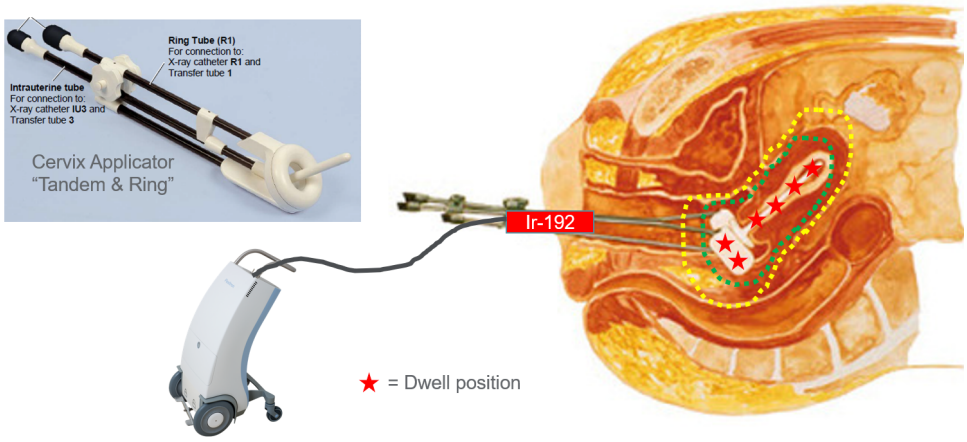


Figure 1.1: Cable-driven radionuclide is controlled by the brachytherapy afterloader into applicators via catheters.

localized breast cancer where IS needles are used to access the center of the lumpectomy site, post-resection. Of these examples, cervical cancer is unique as it can be treated with either intracavitary or a combination of intra- and interstitial BT depending on the size and extent of the tumor (Figure 1.2).

Despite improvements in screening and prevention, cervical cancer remains a significant societal burden in terms of morbidity and mortality. Worldwide, cervical cancer is the third most common cancer in women after breast and colorectal cancers and is one of the leading causes of death among women in the world. In Canada, an estimated 1,350 women were diagnosed in 2020 with 410 dying from the disease. [1] In the United States, over 13,000 new cases are expected annually, resulting in more than 4250 deaths [2]. Cervical cancer mortality rates are highest in low income and developing countries due to a lack of resources to properly manage these patients. Statistics globally are far worse with over 600,000 new cases and 260,000 deaths [3].

The standard course of treatment for women with locally advanced cervical cancer includes external beam radiotherapy (EBRT) with concurrent chemotherapy followed by a BT boost [4]. EBRT which treats the entire pelvis and adjacent nodal regions provides approximately 50% of the total dose. BT provides the remaining course of radiation to treat the tumor cells which survive EBRT. Recent advances in magnetic resonance image (MRI) guided BT have significantly improved local control: 95-100% in limited stages (FIGO IB-IIB) and 85-90% in more

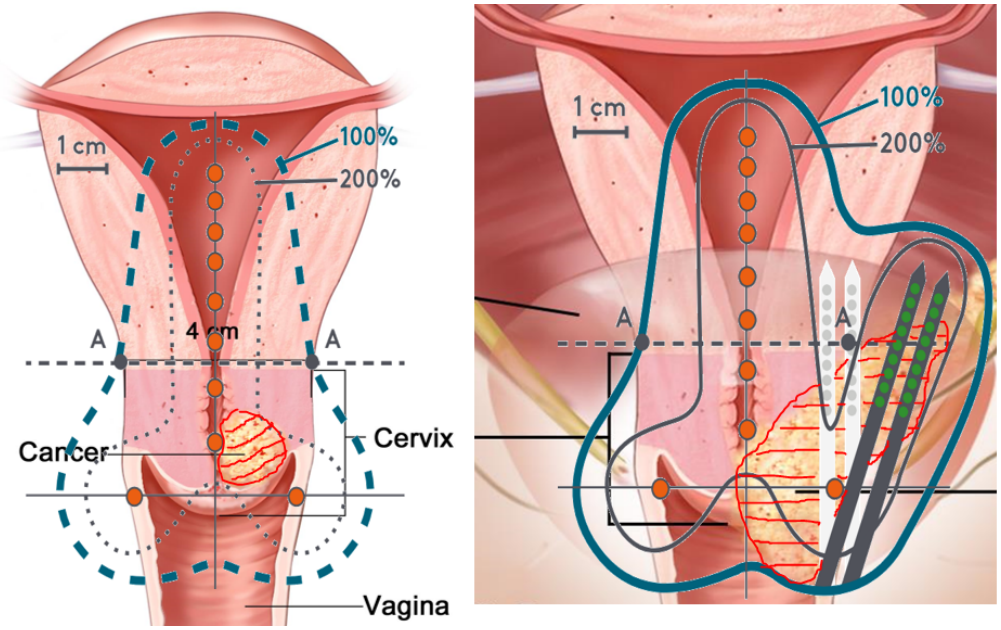


Figure 1.2: The dose distribution achieved with intracavitary BT is adequate for treating small cervical cancers contained within the uterus (left). In the case of larger tumors which extend into the parametrium and/or paravaginal tissues, the addition of interstitial needles is conventionally required to adequately extend the dose to the tumor periphery (right).

advanced stages [5]. Intracavitary cervix BT provides a cylindrically symmetric pear-shaped dose distribution, adequate for treating small tumors contained within the uterine body. Large tumors which extend into the parametrial and/or paravaginal tissues cannot, in most cases, be safely treated without overdosing nearby organs at risk (OARs). In advanced cases, supplementing the intracavitary implant with interstitial BT needles enables conformal dose delivery to the tumor while reducing OAR doses [4]. Despite the excellent outcomes achieved with BT, there are an increasing number of reports testifying on a systemic decline in BT utilization in the US [6–8]. The reasons for the decline are multifaceted. However, the main factors are lack of resources and expertise as is evidenced by a request from the American Board of Radiology to implement the Focused Practice Recognition in BT as an element of its Maintenance of Certification [7]. Of the various BT techniques, the most complex and resource intensive is interstitial BT. Regardless of the reason, the grim reality is that women around the globe, specifically women in rural areas, in developing countries and/or in a lower socioeconomic status, do not have access to this standard-of-care and life-saving treatment modality.

The main motivation of this thesis is to propose a technologically innovative solution which will improve access to care as well as improve the therapeutic ratio, i.e., increase the radiation dose to the tumour while maintaining or reducing the absorbed dose to the OARs.

Conventional BT sources emit radiation isotropically. When tumors are large and/or irregular it becomes impossible to deliver a dose distribution which conforms to the tumor periphery without overdosing the OARs. In recent years, the intensity modulated BT (IMBT) technique has become a topic of renewed interest in the radiation oncology community. The IMBT concept was first introduced by Ebert in 2002 [9]. By incorporating highly (radiation) attenuating metal shields to partially shield the BT source, radiation can be directed towards the tumor and shielded from the OARs. Coupling the shielding to a motorized system can enable dynamic intensity modulation of the radiation dose distribution. In addition to optimizing dwell positions and dwell times, IMBT offers another degree of freedom, shield rotation angle which enables directed radiation beam orientation. This is likely to achieve superior treatment plans to those achieved with conventional BT. Finally, by incorporating the dynamic shield(s) into existing intracavitary BT applicators, we hypothesize that an overall therapeutic benefit should be observed relative to conventional intracavitary BT. The dosimetric benefit achieved with intracavitary IMBT is also proposed to potentially be equivalent to complex intracavitary/interstitial BT, but without implanting a single interstitial needle - thereby significantly reducing implant-related toxicities such as bleeding and organ perforations and giving clinicians and institutions around the globe the ability to treat women with advanced cervical cancer who may not have the resources or expertise to perform the hybrid intracavitary/interstitial BT.

## 1.2 Overview of thesis

This thesis is organized as follows. **Chapter 2** presents clinical and physical aspects of BT followed by the historical progression from classical one-size-fits all cervical cancer BT treatment to present day, patient-specific, image-guided BT. **Chapter 2** then summarizes the limitations of current conventional techniques and introduces the concept of IMBT, and presents a literature review of the various applications of IMBT. The review discusses the differences between static vs. dynamic shielding techniques, and shielded-source vs. shielded-applicator techniques. **Chapter 3** presents a study that uses the Monte Carlo dose calculation method to investigate the resulting dose distributions from three proposed dynamic, MRI-compatible, IMBT shield designs in combination with three candidate BT radionuclides. **Chapter 4** presents a retrospective dosimetric study which evalutes IMBT on a cohort of 36 cervical cancer

patients. Conventional intracavitary and intracavitary/interstitial BT techniques are compared to IMBT using three candidate radionuclides $^{192}$Ir, $^{75}$Se and $^{169}$Yb. **Chapter 5** evaluates the impact of dose reporting, patient tissue heterogeneities and implanted applicator/shield material heterogeneities on absorbed dose to the target volume as well as the OARs. Conventional and IMBT techniques using three candidate BT radionuclides were used for this analysis on a cohort of patients previously treated for cervical cancer. Finally, **Chapter 6** discusses future directions for this project and outlook for the field of IMBT in general.

## 1.3 Author contributions

The core work of this thesis consists of three published peer-reviewed articles. These articles consist of original work and distinct contributions to knowledge. A breakdown of each author's contribution to the published articles is listed below.

The first article (Chapter 3), "Monte Carlo Dosimetry Study of Novel Rotating MRI-Compatible Shielded Tandems for Intensity Modulated Cervix Brachytherapy", Marc Morcos, Shirin A. Enger. Marc Morcos designed and carried out the experiments and the simulations, performed the data analysis and wrote the manuscript. Shirin A. Enger provided expert knowledge, consultation and supervision throughout the course of the study. Both authors corrected and commented the manuscript.

The second article (Chapter 4), "A novel minimally invasive dynamic shield intensity modulated brachytherapy system for cervical cancer", Marc Morcos, Majd Antaki, Akila N. Viswanathan, Shirin A. Enger, presents work conducted by Marc Morcos. Majd Antaki was involved in software development. Marc Morcos designed and carried out the experiments and the simulations, performed the data analysis and wrote the manuscript. Akila N. Viswanathan provided clinical insight. Shirin A. Enger provided expert knowledge, consultation and supervision throughout the course of the study. All authors corrected and commented the manuscript.

The third article (Chapter 5), "On the impact of absorbed dose specification, tissue heterogeneities and applicator heterogeneities on Monte Carlo-based dosimetry of Ir-192, Se-75 and Yb-169 in conventional and intensity modulated brachytherapy for the treatment of cervical cancer", Marc Morcos, Akila N. Viswanathan, Shirin A. Enger, presents work conducted by Marc Morcos. Marc Morcos designed and carried out the experiments and the simulations,

performed the data analysis and wrote the manuscript. Akila N. Viswanathan provided clinical insight. Shirin A. Enger provided expert knowledge, consultation and supervision throughout the course of the study. All authors corrected and commented the manuscript.

## 1.4 Publications

### 1.4.1 Thesis Publications

The following articles are considered the core work of this thesis:

1. **M.Morcos** and S.A.Enger (2020). “Monte Carlo dosimetry study of novel rotating MRI-compatible shielded tandems for intensity modulated cervix brachytherapy”. Physica Medica.

2. **M.Morcos**, M.Antaki, A.N.Viswanathan, and S.A.Enger (2020). “A novel minimally invasive dynamic shield intensity modulated brachytherapy system for cervical cancer”. Medical Physics.

3. **M.Morcos**, A.N.Viswanathan, and S.A.Enger (2021). “On the impact of absorbed dose specification, tissue heterogeneities and applicator heterogeneities on Monte Carlo-based dosimetry of Ir-192, Se-75 and Yb-169 in conventional and intensity modulated brachytherapy for the treatment of cervical cancer”. Medical Physics.

### 1.4.2 Peripheral Publications

The following articles were published in parallel to my studies. Thanks to the intersection between my doctoral thesis subject and my ten years of clinical expertise in cervical cancer brachytherapy, I was fortunate to be able to contribute to the following works in parallel:

1. AL Gunderman, EJ Schmidt, Q Xiao, JTokuda, RT Seethamraju, L Neri, HR Halperin, C Kut, AN Viswanathan, **M Morcos**, Y Chen. "MRI-Conditional Eccentric-Tube Injection Needle: Design, Fabrication, and Animal Trial". *In preparation*

2. F Zabihollahy, AN Viswanathan, EJ Schmidt, **M Morcos**, J Lee. "Fully Automated Multi-Organ Segmentation of Female Pelvic Magnetic Resonance Images with Coarse-to-Fine Convolutional Neural Network". *Accepted pending proofs*

3. **M.Morcos**, J Vogel, S Bartolac, JR Garcia, V Gomez-Lobo, AN Viswanathan (2021). "Treatment of pediatric vaginal rhabdomyosarcoma with the use of a real-time tracked 3D printed applicator". Brachytherapy *(Accepted pending proofs)*.

4. A.Alipour, A.N.Viswanathan, R.D.Watkins, H.Elahi, W.Loew, E.Meyer, **M.Morcos**, HR.Halperin, EJ.Schmidt (2021) "An Endovaginal Array with a Forward-Looking Coil for MRI-Guided Cervical Cancer Brachytherapy Procedures: Design and Initial Results". Medical Physics.

5. Gunderman, A.L., E.J.Schmidt, **M.Morcos**, J.Tokuda, R.T.Seethamraju, H.R.Halperin, A.N.Viswanathan, and Y.Chen (2021). "MR-Tracked Deflectable Stylet for Gynecologic Brachytherapy". IEEE/ASME Transactions on Mechatronics.

6. J.Chino, C.M.Annunziata, S.Beriwal, L.Bradfield, B.A.Erickson, E.C.Fields, K.Fitch, M.M.Harkenrider, C.H.Holschneider, M.Kamrava, E.Leung, L.L.Lin, J.S.Mayadev, **M.Morcos**, C.Nwachukwu, D.Petereit, and A.N.Viswanathan (2020)."Radiation Therapy for Cervical Cancer: Executive Summary of an ASTRO Clinical Practice Guideline". Practical Radiation Oncology.

7. E.C.Fields, S.Hazell, **M.Morcos**, E.J.Schmidt, C.Chargari, and A.N.Viswanathan (2020). "Image-Guided Gynecologic Brachytherapy for Cervical Cancer". Seminars in radiation oncology.

8. J.Chino, C.M. Annunziata, S.Beriwal, L.Bradfield, B.A.Erickson, E.C.Fields, K.Fitch, M.M.Harkenrider, C.H.Holschneider, M.Kamrava, E.Leung, L.L.Lin, J.S.Mayadev, **M.Morcos**, C.Nwachukwu, D.Petereit, and A.N.Viswanathan (2020). "The ASTRO clinical practice guidelines in cervical cancer: Optimizing radiation therapy for improved outcomes". Gynecologic oncology.

9. N.E.Chernavsky, **M.Morcos**, P.Wu, A.N.Viswanathan, and J.H.Siewerdsen (2019). "Technical assessment of a mobile CT scanner for image-guided brachytherapy". Journal of applied clinical medical physics.

10. W.T.Hrinivich, **M.Morcos**, A.Viswanathan, and J.Lee (2019). "Automatic tandem and ring reconstruction using MRI for cervical cancer brachytherapy". Medical Physics.

11. S.Devic, L.Liang, N.Tomic, H.Bekerat, **M.Morcos**, M.Popovic, P.Watson, S.Aldelaijan, and J.Seuntjens (2019). "Dose measurements nearby low energy electronic brachytherapy sources using radiochromic film". Physica Medica.

### 1.4.3 Patents

The synergistic effect of combining my doctoral studies with my clinical experience has also contributed to the filing of three patents, two of which are provisional:

1. MRI-guided active injection needle for brachytherapy (2021) C16600-P15500-01
2. Patient-specific real-time tracked brachytherapy applicators (2021) 63/139,961
3. IMBT radiation shields for brachytherapy (2020) PCT/CA2020/050821

# References

[1] Cancer facts & Figures 2020;. Available from: https://www.cancer.ca/en/cancer-information/cancer-type/cervical/statistics/?region=on.

[2] Cancer facts & Figures 2020;. Available from: https://www.cancer.org/research/cancer-facts-statistics/all-cancer-facts-figures/cancer-facts-figures-2020.html.

[3] Ferlay J. GLOBOCAN 2008 v1. 2, Cancer incidence and mortality world-wide: IARC Cancer Base No. 10. http://globocan iarc. 2010.

[4] Viswanathan AN, Beriwal S, De Los Santos JF. American Brachytherapy Society consensus guidelines for locally advanced carcinoma of the cervix. Brachytherapy;11:47–52. Available from: https://doi.org/10.1016/J.BRACHY.2011.07.002.

[5] Sturdza A, Pötter R, Fokdal LU. Image guided brachytherapy in locally advanced cervical cancer: Improved pelvic control and survival in RetroEMBRACE, a multicenter cohort study. Radiother Oncol;120:428–433. Available from: https://doi.org/10.1016/j.radonc.2016.03.011.

[6] Han K, Milosevic M, Fyles A, Pintilie M, Viswanathan AN. Trends in the utilization of brachytherapy in cervical cancer in the United States. Int J Radiat Oncol Biol Phys;87:111–119. Available from: https://doi.org/10.1016/j.ijrobp.2013.05.033.

[7] Petereit DG, Frank SJ, Viswanathan AN. Brachytherapy: Where Has It Gone? J Clin Oncol;33:980–982. Available from: https://doi.org/10.1200/JCO.2014.59.8128.

[8] Orio PF, Nguyen PL, Buzurovic I, Cail DW, Chen YW. The decreased use of brachytherapy boost for intermediate and high-risk prostate cancer despite evidence supporting its effectiveness. Brachytherapy;15:701–706. Available from: https://doi.org/10.1016/j.brachy.2016.05.001.

[9] Ebert MA. Possibilities for intensity-modulated brachytherapy: Technical limitations on the use of non-isotropic sources. Phys Med Biol;47:2495–2509. Available from: https://doi.org/10.1088/0031-9155/47/14/309.

# Chapter 2

# Background and literature review

## 2.1 Brachytherapy Sources

Photon-emitting BT sources, commonly referred to as radioactive seeds or sources are composed of a radioactive core encapsulated inside a metal case usually stainless steel to attenuate undesired decay products and prevent contamination. Hence, these sources are called sealed sources. Radioactive materials used in BT sources are produced by either neutron activation or are a product of nuclear fission or may be naturally occurring (i.e. Radium-226). In neutron activation, a stable isotope of an element (i.e. Iridium-191) is placed in a neutron field in a nuclear reactor. As the nuclei of the element captures a neutron, a radioactive isotope (i.e. Iridium-192) is obtained, which emits gamma radiation as a decay product. The yield of the radioactive isotope will depend on the reactor's neutron flux and energy, interaction cross-section with the material under irradiation, the half-life of the radioactive isotope and the amount of time the sample is in the reactor. For radioactive materials obtained as a by-product of nuclear fission, the desired product often has to be separated from other fission products. The most common example is Cesium-137 which is a fission by-product of uranium fuel rods in a reactor. Physical properties of photon-emitting BT sources are listed in table 2.1.

Radium-226 was the first radioactive material used for BT applications. Radium-226 decays by alpha emission to Radon-222. Radon-222 which is also radioactive, decays by beta and gamma emission and emits a complex photon spectrum with a maximum energy of 2450 keV with the alpha and beta particles absorbed by the encapsulation ( 0.5 mm of Platinum was historically used [1]). In the following section, we describe early dosimetry systems using Radium-226. Radium-226 has several disadvantages including: (i) the high energy photon

Table 2.1: Physical properties of photon-emitting radionuclides.

| Radionuclide | Decay mode | Half-life | Mean photon energy (keV) | HVL (mm Pb) |
|---|---|---|---|---|
| $^{226}$Ra | $\alpha$ | 1620 y | 2450 (Max) | 17.0 |
| $^{60}$Co | $\beta$ | 5.3 y | 1250 | 11.0 |
| $^{137}$Cs | $\beta$ | 30.2 y | 662 | 5.5 |
| $^{192}$Ir | $\beta$ (95%), EC (5%) | 73.8 d | 380 | 2.5 |
| $^{75}$Se | EC | 118.5 d | 210 | 1.0 |
| $^{57}$Co | EC | 272 d | 114 | 0.6 |
| $^{169}$Yb | EC | 32.0 d | 93 | 0.48 |
| $^{153}$Gd | EC | 240.4 d | 60 | 0.12 |
| $^{131}$Cs | EC | 9.7 d | 30 | 0.030 |
| $^{125}$I | EC | 59.5 d | 28 | 0.025 |
| $^{103}$Pd | EC | 17.0 d | 21 | 0.008 |

emission from Radium-226 BT source requires thick shielding to protect hospital personnel, (ii) the risk of ingestion of Radium salt should the encapsulation be compromised and (iii) it has a low specific activity, limiting how small the source can be constructed while maintaining a practically high radioactivity. Due to these listed disadvantages and the availability of more convenient radionuclides, Radium-226 has been discontinued in most of the world.

In the treatment of cervical cancer, Radium-226 has been almost entirely replaced by Iridium-192. With an average photon energy of 380 keV, Iridium-192 is more easily shielded, requiring about 7 times less lead compared to Radium-226. Iridium-192's half-life is 73.8 days, requiring frequent ( 4 times per year) source replacements but its very high specific activity which is 3 orders of magnitude greater than Radium-226 enables placement of a high radioactivity in the core. Introduction of Iridium-192 as a source made it possible to produce sources small enough (diameter < 1 mm) to fit inside BT needles and deliver tumorcidal dose in minutes.

## 2.2 History of Cervix Brachytherapy

The treatment of cervical cancer is one of the earliest applications of radionuclides in medicine. Shortly after Marie Curie's discovery of Radium-226 in 1898 [2], the use of Radium in the treatment of cervical cancer became widespread. The first documented treatment of cervical cancer with Radium was performed by American surgeon Robert Abbe in 1910 [3]. Over the last century, the basic premise of cervical cancer BT has remained the same. A hollow

intracavitary applicator with two main components is implanted to allow the radionuclide to treat the tumor from within the applicator (Figure 2.1). Specifically, a tandem is placed within the cervix, through the intrauterine canal and a ring (or ovoids) are placed against the cervix, against the vaginal fornices. Together, the tandem and ring/ovoids give rise to a 3D pear-shaped radiation dose distribution which ideally covers the extent of the cancer.

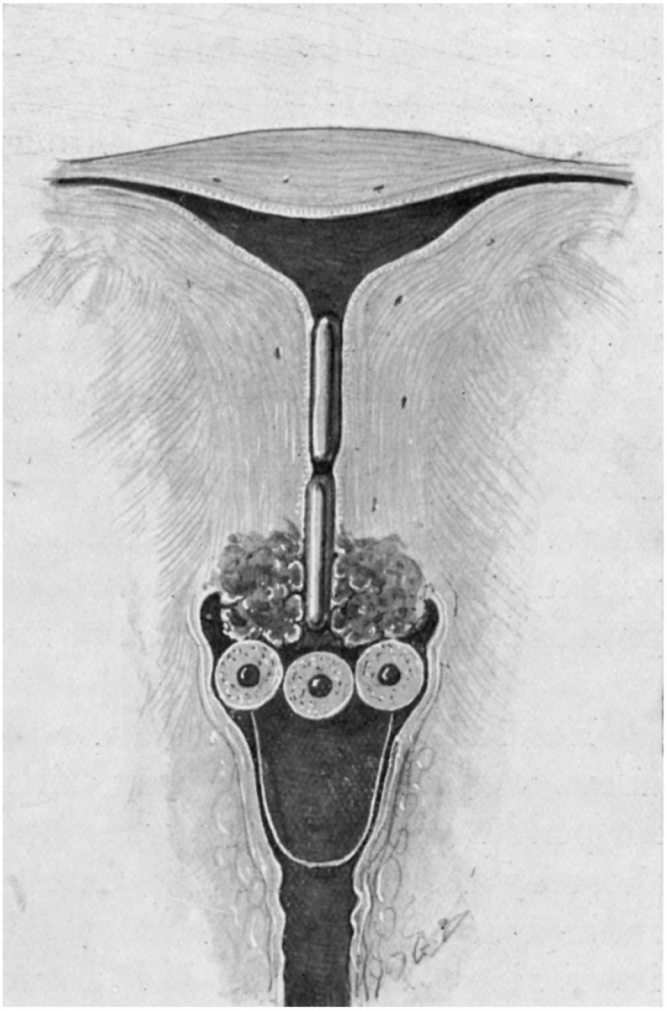

Figure 2.1: Classical placement of Radium tubes within the vaginal fornices and uterine canal for the treatment of cervical cancer. Figure reproduced from [4].

The use of Radium, although effective in the treatment of gynecological malignancies was prescribed entirely in an empirical fashion due to the lack of knowledge about (i) the precise dose rate distributions and (ii) the biological effects of radiation on the tumor and the nearby healthy OARs. Modern cervical cancer BT has been greatly shaped by the development of

dosimetry "systems". Dosimetric systems are a set of rules, specific to a radionuclide and its spatial dose distribution in a fixed geometry (i.e. intracavitary applicator). Classical dosing systems prescribed a specific activity (in Curies; Ci) for a specified application time (hours). One gram of Radium-226 undergoes 3.7 x $10^{10}$ disintegrations per second (37 Giga-Becquerel; 37 GBq) or, more traditionally, one Curie. A common prescription was in terms of milligram equivalents of Radium-226 for a given amount of time using the units of milligram-hours (mg-hours).

The three first historical systems were the Stockholm (1910), Paris (1919) and Manchester (1938) systems. In all three systems the specification of treatment was defined in terms of dose, length of time the radioactive source was in place and administration to achieve a reproducible prescription. The Stockholm system was fractionated in two to three fractions, which is to deliver the treatment in separate, individual sessions. Each fraction was treated with a 25-hour application of 100-200 mg of Radium-226. The total mg-hours of Radium used for treatment hovered around 7000 mg-hours, of which 4500 mg-hours were in the vagina and the remaining 2500 mg-hours were in the uterus. The Paris system was delivered in a single session (i.e. a single fraction), lasting 5 days to deliver 7200-8000 mg-hours to the cervix. Unlike the Stockholm system, the Paris system used equal amount of Radium in the uterus and vagina, .i.e, contributions of 3500 mg-hours from the uterine and vaginal loading's each. The intrauterine tandem, contained three Radium sources with activities (strengths) in the ratio of 1:1:0.5 with the 0.5 weighted source closest to the vagina.

The Stockholm and Paris systems suffered from two major problems. First, the dose prescription defined in terms of mg-hours (where 1 mg of Radium-226 corresponds to 1 mCi of activity, per definition) ignored anatomical targets such as the parametrium and the tolerance of healthy OARs such as the bladder and rectum. Second, when EBRT, whose dose is specified in terms of absorbed dose, was introduced into the initial treatment of the pelvis (prior to the BT boost), it become evident that the overall radiation treatment cannot be adequately combined. The Manchester system was a big step towards modern BT, which was the first system to define treatment in terms of absorbed dose to a point which is representative of the target and was approximately reproducible from patient to patient. In the search for a dose specification point, Tod and Meredith [5] began to calculate the absorbed dose to various points anatomically comparable from patient to patient. Instead of prescribing absorbed dose to a malignant region, absorbed dose was limited to the area in the medial edge of the broad ligament where the uterine vessels cross the ureter, a region more commonly referred to as the paracervical triangle. It was considered that the tolerance of the paracervical triangle is the main limiting factor in the

irradiation of the cervix. Prescribing a fixed dose to this point, known as Point-A, was thus a distinguishing feature of the Manchester system. The original Point-A was defined 2 cm from the mucous membrane of the lateral superior fornix of the vaginal/cervical interface and 2 cm laterally, perpendicular to the uterine canal (Figure 2.2).

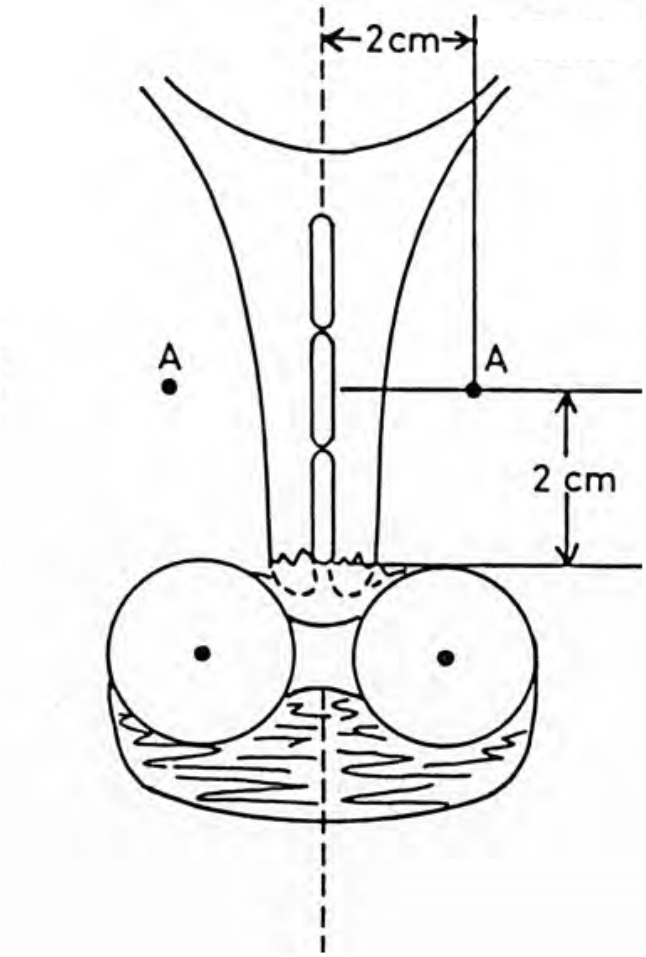


Figure 2.2: The International Commission on Radiation Units and Measurements report #89's definition of Point-A for classical BT point-based prescription. Figure reproduced from [6].

The dose specification in the Manchester system was defined as follows: a total dose (in Roentgens) to Point-A of 8000 R, delivered in 2 fractions with each fraction lasting approximately 3 days. In the Manchester system, the radioactive material was loaded such that about two-thirds of the absorbed dose to Point-A was delivered from the tandem. Point-A was slightly modified with the advent of x-ray based diagnostic radiography in a step towards definition Point-A based on imaging. The main challenge combining the x-ray based imaging and original

definition of Point-A was the definition of Point A related to soft-tissues (i.e. cervical os and uterine canal), which cannot be revealed on an x-ray radiograph. The modified Point-A, which is still used today, is defined relative to the implanted tandem-based applicator: 2 cm superiorly along the tandem starting from the top of the ovoid/ring which is anatomically located against the cervical os and vaginal fornices and 2 cm laterally from the tandem. This concept of absorbed dose to a single point (Point-A), made this system the most acceptable technique for the treatment of cervical cancer and has stood the test of time with approximately half of clinics still prescribing dose to Point-A according to a 2014 survey conducted by the American Brachytherapy Society (ABS) [7].

## 2.3 Image-guided brachytherapy

The popularity of image-guided BT (IGBT) in the last few decades has grown substantially with the introduction of use of 3D imaging (e.g. computed tomography (CT) & magnetic resonance imaging (MRI)) in day-to-day clinical operations. The replacement of Radium with artificially produced, high activity, radionuclides such as Ir-192 has enabled greater control of the dose delivery mechanism. Ir-192-based treatment units (HDR afterloaders) use source-stepping technology, wherein a single, cable-driven radiation source is stepped (i.e. in 1 mm increments) along the implanted IC and/or IS implant to deliver the treatment dose. With the source dwelling at various positions for various amounts of time to vary the amount of dose in a particular region. This basic modulated delivery can be tailored to achieve a custom 3D dose distribution within the patient.

IGBT enables clinicians to visualize the extent of tumor growth and the proximity of OARs. The introduction of volumetric based tumor targets and OARs has made it possible to move from prescription from Point-A to dose to 3D volumes in terms of dose-volume histogram (DVH) metrics. Coupled with computerized 3D dose calculation engines, the classical Point-A normalized, pear-shaped dose distribution can be optimized using patient-specific treatment plan to achieve a "sculpted-pear" which is tailored to the topology of the actual tumor; thereby increasing the dose the tumor receives and reduces unnecessary dose to healthy OARs.

Definitions for volume-based targets were established by The Groupe Européen de Curiethérapie and the European Society for Radiotherapy & Oncology (GEC-ESTRO) in 2005 and are summarized extensively in the International Commission on Radiation Units and Measurement's report #89 (ICRU-89) [6]. These include the gross tumor volume, intermediate-risk clinical target volume and the high-risk clinical target volume (HR-CTV or $CTV_HR$) - the

former two being option for IGBT treatment planning (Figure 2.3). The HR-CTV is defined

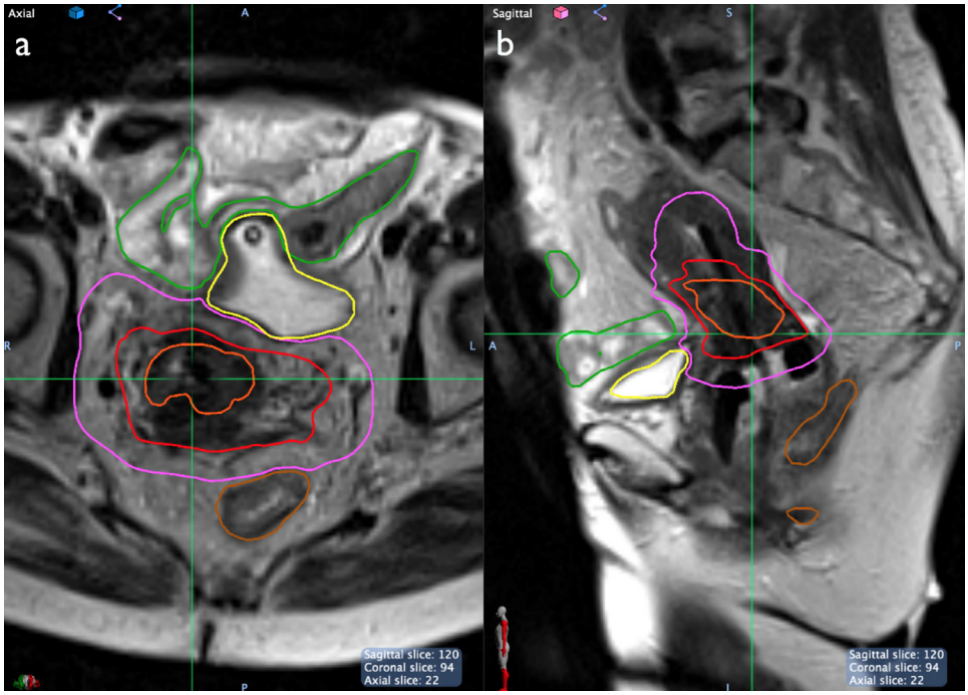


Figure 2.3: ICRU-89 definition of HR-CTV (red) and IR-CTV (purple) volumes in cervical cancer brachytherapy as seen on T2-weighted MR images. Bladder (yellow), rectum (brown) and bowel (green) are also shown in the axial (left) and sagittal (right) views. Figure reproduced from [8].

as the entire cervix, including the gross tumor volume and regions of potential involvement as seen on T2-weighted MRI known as the "gray zones". Validation of moving away from a strict Point-A prescription to a volume-based approach comes from multiple retrospective studies. The largest and most well known, retroEMBRACE found that women treated with IGBT has improved local control and reduced treatment-related toxicity compared to women treated with classical, x-ray radiography-based BT [9]. Prospective study results from the Soutien aux Techniques Innovantes et Couteuses (STIC) trial found a significant reduction of grade-3 and grade-4 toxicities when using 3D IGBT techniques (22.7% down to 2.6%, P<0.002). These two major findings are quite logical: by treating the extent of the tumor, no more and no less, we can improve local control and reduce major side-effects. It is no surprise that IGBT adoption has increased significantly over the past few decades. According to the ABS 2014 survey, in 2007, 43% of centers in the United States were performing BT treatment planning based on 2D

x-ray radiographs. In 2014, this number decreased 15% as about 50% of the centers adopted IGBT (CT and/or MRI) techniques.

## 2.4 Linear-quadratic model

The surviving fraction (SF) of irradiated cells follows a linear-quadratic (LQ) relationship with absorbed dose on a semi-logarithmic scale and is described by:

$$SF = e^{-(\alpha D + \beta D^2)} \tag{2.1}$$

where $D$ is the delivered dose in Gy, and $\alpha$ & $\beta$ are the linear and quadratic parameters, respectively, of the model. Different tissues respond differently to radiation damage in terms of seeing the effect early (acute) or late (chronic). Cell survival curves for late responding tissues tend to have a lower $\alpha/\beta$ ratio than early responding tissues. Generally tumors are assumed to have $\alpha/\beta$ ratio of 10 Gy and normal tissues have an $\alpha/\beta$ ratio of 3 Gy [6].

The biologically effective dose (BED) is a quantity based on the LQ-model that takes into consideration dose delivered in separate sessions (typically at least 6 hours apart), more commonly referred to as fractions. The BED is calculated as:

$$BED = D \times \left[ 1 + \frac{d}{\frac{\alpha}{\beta}} \right], \tag{2.2}$$

where $d$ is the absorbed dose per fraction. In the case of patients who receive two courses of radiation therapy of varying fractionation regimens we can use the BED to scale the doses such that they may be summed. One common method is calculating the BED in 2 Gy per fraction equivalents (EQD2). This is performed by setting the BED equation equal to a version of itself with $d$ equal to 2 Gy per fraction and solving for the total dose:

$$\text{EQD2} = D \, \frac{\left(1 + \frac{d}{\alpha/\beta}\right)}{\left(1 + \frac{2}{\alpha/\beta}\right)} \tag{2.3}$$

### 2.4.1 Optimal dose fractionation schedule

The most current clinical practice guideline for cervical cancer radiation therapy was published in 2020 by the Cervical Cancer Task Force of the American Society for Radiation Oncology

(ASTRO). For definitive radiotherapy, the cervix HR-CTV shall receive a total (EBRT + BT) dose of at least 80 Gy when converted to EQD2. The external beam component delivers a dose of 45 Gy in 1.8 Gy per fraction (25 fractions). BT delivers the remaining dose in typically 5 fractions of approximately 5.5 Gy per fraction.

## 2.5 Limitations of conventional brachytherapy

The radioactive source emits radiation with near-isotropic geometry. In the case of cervical cancer, the tandem-based applicator gives us a total distribution which is the cylindrically symmetric, pear-shaped dose distribution. The benefit of BT is touted as unrivaled in its ability to deliver a high dose of radiation to the tumor while minimizing exposure to OARs. However, this is only true if the tumor is small and contained within the uterus; in other words, in any direction, the closest OARs are further from the implant (radius) than the most distal extent of the tumor. For women with irregular and/or large cervix tumors which extend into the nearby paravaginal and parametrial regions, it is not possible to adequately treat the tumor extent without overdosing the OARs. In these frequent cases, the option is to either (i) underdose the tumor (at the detriment to local control) such that toxicity and side effects are tolerable, (ii) overdose the OARs and significantly reduce the patient's quality of life or (iii) to supplement the intracavitary tandem-based implant with interstitial needles to safely increase the dose to the tumor periphery.

The interstitial technique is not without issues. Firstly, practitioners of interstitial implantation are relatively rare due to the special surgical-like training which must be learned and maintained by radiation oncologists. Over the last ten years, the field of radiation oncology has published, ad nauseam, concerning the reality that BT utilization, interstitial BT in particular, is in decline [10–13]. The reasons for the decline are hypothesized to be multifaceted with a significant factor attributed to a lack of radiation oncologists with the necessary expertise and comfort in performing BT as demonstrated by the request from the American Board of Radiology to implement the "Focused Practice Recognition in Brachytherapy" as an element of its maintenance of certification [11]. One notable exception is the province of Quebec, which has maintained a steady use of BT from 2011 to 2019 [14]. Lecavalier-Barsoum *et al.* digress that despite the steady BT utilization in Quebec, many patients who might benefit from BT are never offered it as an option [14].

## 2.6 Limitations of brachytherapy dosimetry

### 2.6.1 Dose Calculation Methods in Brachytherapy

#### TG-43 dose protocol

Clinical BT dose distributions are calculated based on the AAPM Task Group #43 (TG-43) protocol. [15] TG-43 defines a 2D dose calculation formalism which specifies the dose rate (in water) from a BT source at a distance, $r$, away and at an angle, $\theta$, relative to the long axis of the BT source:

$$\dot{D}(r,\theta) = S_k \Lambda \frac{G_L(r,\theta)}{G_L(r_0,\theta_0)} g_L(r) F(r,\theta) \tag{2.4}$$

where $r_0, \theta_0$ is the reference distance at 1 cm from the center of the source perpendicular to the long axis of the source. Figure 2.4 illustrates the coordinate system used in the TG-43 protocol. $S_k$ is the air-kerma strength, which is defined as the air kerma rate at a distance d

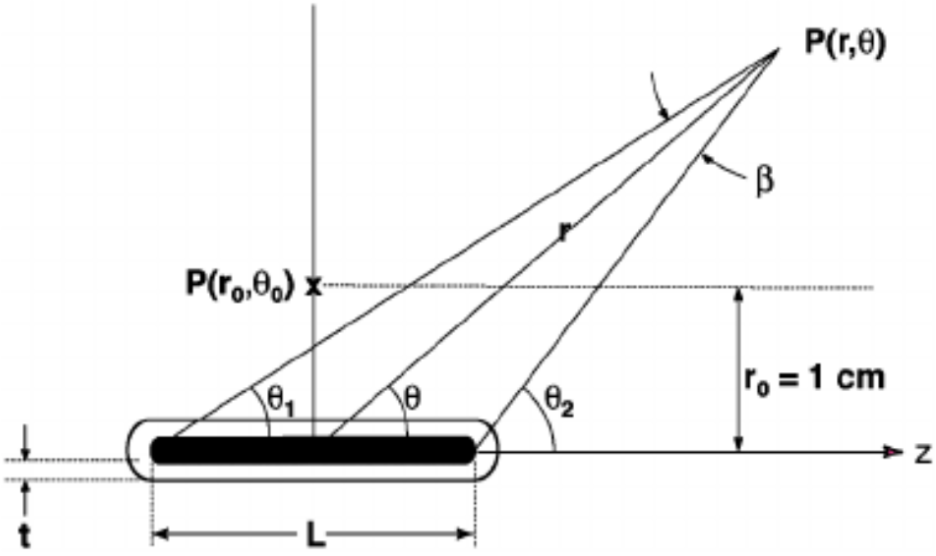


Figure 2.4: Coordinate system used for dose calculations using the TG-43 protocol. Figure reproduced from [15].

which excludes photons below an energy of 10 keV. The dose rate constant, $\Lambda$, converts the air kerma strength to dose rate in water. The geometry function $G_L(r,\theta)$ describes the dose rate fall-off due to geometry alone, ignoring dose fall-off due to attenuation and scatter. For a point-source, the geometry function follows the inverse square law ($\dot{D} \propto 1/r^2$). For a realistic

source with a length $L$, the geometry function is calculated using:

$$G_L(r,\theta) = \begin{cases} \frac{\beta}{Lr\,\sin\theta} & \text{if } \theta \neq 0^{\circ} \\ \frac{1}{r^2 - L^2/4} & \text{if } \theta = 0^{\circ} \end{cases}$$

where $\beta = 2\arctan\,(l/2r)$. TG-43's geometry function assumes that the source thickness is much smaller than its length ($L$) and can be treated as a line source.

The radial dose function $g_L(r)$ accounts for the dose rate fall-off due to scatter and attenuation in the absence of geometric dose fall-off. Finally the anisotropy function $F(r,\theta)$ describes the variation in dose rate as a function of polar angle $\theta$ and distance $r$ from the source center. Due to the long source construction which leads to photon self-attenuation and scattering, the dose rate at a fixed distance around the source is not perfectly isotropic and is corrected for by using the anisotropy function.

The TG-43 dose protocol makes two large assumptions; (1) the patient is composed entirely of water and (2) the patient is surrounded by water (the patient size is not finite; i.e. no air outside the patient). These two assumptions lead to valid dosimetric results if: (1) the patient and applicator materials are composed of water equivalent tissue types/material (in terms of radiation attenuation) in the photon energy region of the BT source emission and (2) the dose of interest is not being deposited near the patient surface. If the source is placed close to the patient's surface (breast cancer) or on the surface (skin cancer) the TG-43 formalist leads to an overestimation of the absorbed dose since in reality there is a lack of scatter material (air outside the patient body) but the TG-43 formalism assumes water. In the case of BT delivered with multiple radioactive seeds or high density shields, TG-43 would significantly overestimate the dose as it is not equipped to handle non-water equivalent materials. Specifically, TG-43 does not account for interseed attenuation in the case of multiple seed implants in BT (i.e. permanent seed implants). TG-43 remains the standard for clinical dosimetry to this day.

### Model-based dose calculation algorithms

Model-based dose calculation algorithms (MBDCAs) can handle patients and implanted devices of heterogeneous material composition and mass density such as metal, bone and air-filled cavities. They also take into consideration the finite patient dimensions and intersource/shield attenuation [16]. MBDCA-based dose calculations require volume element by volume element (voxel by voxel) assignment of tissue elemental composition (mass fraction of each element composing the tissue) and mass density. The patient 3D geometry is obtained via CT or

MR images in DICOM format, which is imported into the dose calculation engine where it is represented as a voxelized geometry (phantom). Tissue mass density also affects dose distributions and is readily obtained from CT images of the treated anatomy using a Hounsfield Unit (HU) to density calibration curve. In the case of MR or US images where mass density information is not available, density information can be user-defined on an organ by organ basis (structure-based). Similar information is required for the radiation source and the applicators (exact description of the source and applicator geometry and material composition).

Currently, there are three main MBDCAs used for BT dosimetry: (i) collapsed-cone superposition/convolution, (ii) Linear Boltzmann transport equation solvers and (iii) Monte Carlo method.

**Collapsed-Cone Superposition/Convolution**

The collapsed-cone superposition/convolution dose calculation method [17] separates the dose contributions into primary and secondary-scattered components. Direct superposition is computationally expensive and would lead to calculation times which are too long for the clinical time-frame. To speed this up, commercial implementations of this algorithm make sure of a collapsed-cone superposition method which uses a series of cones centers around the BT source. The energy released from each cone is attenuated and deposited along their respective axes. Discretizing the patient volume in this way leads to geometric discretization artifacts and ray-tracing artifacts in regions where scatter dominates over the primary fluence component. Increasing the resolution of the cones mitigates these negative impacts but at the cost of increasing computation time.

**Linear Boltzmann Transport Equation Solvers**

Grid-based Boltzmann equation solvers solve the linear Boltzmann transport equation (LBTE) for photon transport through discretized phase-space (position, direction and energy) on a Cartesian grid [18]. The algorithm solves the equation numerically by defining the LBTE at each voxel and solved iteratively over the entire volume. Grid-based solvers converge to the true dosimetric value in the limit of a very fine phase-space mesh resolution.

**Shortcomings of clinical MBDCAs**

Clinical implementations of MBDCAs such as collapsed-cone or LBTE-based dose engines share similar features such as their approach in separating the primary and scattered portions of the radiation, use of angular and spatial descretization, ray tracing and use of data pre-calculated

with the Monte Carlo method [19]. Clinical MBDCAs must make a compromise between accuracy and calculation time. As a clinical tool, many algorithm parameters such as the output dose grid resolution and extent are limited. The cost of being able to calculate dose with the push of a button and obtain a dose distribution in a clinical time-frame is the inability to handle many edge cases. One such example is breast BT, where the patient's breast is close to the extent of the CT image. As far as the clinical MBDCA is concerned, anything outside the CT image may be considered to be non-existent (i.e. particles transported to the edge of the image are killed). The impact of such a scenario would be a lack of backscatter, which would yield an erroneously overestimated dose.

**Monte Carlo method**

The Monte Carlo method stochastically solves the LBTE by randomly sampling the interaction probability distribution of particles interacting with the medium [20]. Fundamental physics processes are modeled to accurately simulate particle transport and energy deposition in medium under a variety of conditions (e.g. in the presence of a large magnetic field). In the past, Monte Carlo-based dose calculation methods were associated with very large computation times. This is due to the need to calculate all the interactions between the incoming radiation and irradiated medium until the energy of the simulated particles is entirely deposited or escapes the volume of interest. Monte Carlo has an error variance of the form $\sigma^2/n$. By increasing the number of initial radiation events simulated, $n$, we can reduce the variance. In other words, the required compute time still grows linearly with increasing simulated events, $n$. Using novel computing techniques such as taking advantage of the natively parallel compute architecture of GPU can reduce compute time significantly [21].

Another way to reduce the variance, is to construct the Monte Carlo simulation in a way which reduces the variance without affecting the output. Methods that achieve this are known as variance reduction techniques (VRTs). Examples include, range rejection, which discards an electron in motion if its residual range is smaller than the distance to the nearest boundary. Another example is the use of a pre-calculated phase-space file and contain the energy, direction and type of radiation of all particles in an arbitrary plane. This pre-calculated phase-space can be used for subsequent simulations by sampling from the phase-space file. Using a pre-calculated phase-space reusing or recycling particles is possible but care must be taken. If the phase-space's variance is large enough to introduce systematic bias then this will be propagated in the final dose calculation [22].

A common VRT in BT is the use of track-length estimation (TLE) in low-energy photon irradiation, such as BT. [23] In BT, TLE can be applied to speed up the local energy deposition of (secondary) electrons set in motion by photon interactions with the medium, more commonly referred to as kerma. In TLE , the electron interactions are not explicitly simulated. Instead, their entire energy is deposited locally (i.e. within the voxel). This approximation is valid if: (1) The electron range in medium, is smaller than the voxel dimension and (2) there is no significant radiative energy escaping the voxel (i.e. bremstrahlung or atomic de-excitation). For tissues with an effective atomic numbers less than 20 ($Z_{eff} < 20$), the relative difference between the linear energy absorption and energy transfer coefficients are effectively zero below energies of 1 MeV, far below the energy range of non-Cobalt-60-based BT.

**Monte Carlo dose calculation software for brachytherapy applications**

Currently there exists many Monte Carlo-based dose calculation packages for BT applications. BrachyDose and egs_brachy are based on the use of EGSnrc [24, 25]. ALGEBRA and RapidBrachyMC are based on Geant4 [26, 27], while MCPI29 and HDRMC are based on PTRAN and MCNP5 respectively [28, 29]. Inaccuracies in dose deposited in voxels where the radiation source or applicator overlap with the patient tissue were resolved by Yegin *et al.* in BrachyDose and Enger *et al.* in Geant4 [24, 30].

In most of the software packages mentioned above except for RapidBrachyMC, many parameters regarding the setup such as the isotope placed in the active core and spatial distribution of radioactivity are hard coded. In addition, the code packages are pure dose calculation software. RapidBrachyMC and RapidBrachyMCTPS are developed by our group and used in this thesis contains no hard-coded parameters. RapidBrachyMC is the Geant4-based dose calculation engine and is coupled to RapidBrachyMCTPS an interactive and user friendly graphical user interface equipped with catheter digitization, contouring tools and dose optimization algorithms. To our knowledge, RapidBrachyMCTPS is the sole open-source Monte Carlo-based treatment planning software for BT applications [27, 31].

### 2.6.2 Dose specification methods

Clinical BT dose calculations are based on TG-43's dose to water in water (radiation transport in water with dose scored in water, $D_{w,w}$). Regardless of tumor site inside the patient, applicator, shield dimensions and/or material composition/mass-densities, TG-43-based dosimetry assumes that the source is placed in a large spherical water phantom with uniform mass density. Despite

the advent of commercially available MBDCAs in the last couple of decades, $D_{w,w}$ is the standard reported dose due to the vast clinical experience with this quantity. MBDCAs inherently calculate dose to medium in medium (radiation transport through medium with dose scored in medium, $D_{m,m}$). $D_{m,m}$ is the natural choice for dose reporting. The professional societies of medical physics and radiation oncology (e.g. AAPM, ESTRO) have recommended that absorbed dose calculated with MBDCA should be documented but that $D_{w,w}$ remain the clinical standard for prescribing treatment until more experience with $D_{m,m}$ is obtained. An alternative, hybrid dose specification method is dose to water in medium (transport through medium but score dose to water, $D_{w,m}$). $D_{w,m}$ has the advantage of reporting dose to a small mass of water while properly transporting radiation through the heterogeneous medium. The rationale for using $D_{w,m}$ is that clinical knowledge is based on $D_{w,w}$.

## 2.7 Intensity modulated brachytherapy

Conventional BT is limited to the placement (dwell position) and timing (dwell time) of near-isotropically emitting radiation sources. In 2002, Martin Ebert proposed the theoretical concept of IMBT by using BT sources that provide anisotropic emissions to achieve intensity modulation [32]. If BT sources could be modified to provide a directional radiation beam, then the dose distribution can be modulated using the source emission direction as a third degree of freedom. The method of achieving anisotropic emission is by introducing attenuating material (shielding).

IMBT has regained interest in recent years for its ability to deliver asymmetric dose distributions which may help improve the therapeutic ratio of BT. In light of the surge of enthusiasm and promise of IMBT for impacting clinical care, the American Association of Physicists in Medicine (AAPM) formed, in 2019, task group #337 (TG337). TG337 has been tasked with defining the possibilities and limitations of improving conventional BT by using IMBT techniques and is actively working on the technological review and clinical recommendations which will be needed to translate IMBT into clinical use.

IMBT can be divided into static and dynamic shielding approaches. Static IMBT includes any technique in which the source does not move or rotate relative to the shield(s). Static IMBT approaches have been introduced into clinical practice since the early 1950s. Fletcher *et al.* developed a tandem-based cervix applicator with shielded ovoids to reduce bladder and rectal doses. [33] More modern shielded cervix applicators such as the updated Fletcher and Henschke models are rarely used due to uncertainties regarding true dosimetry. Endorectal mold

applicators with a static central shield have been used by a limited number of groups to spare the healthy contralateral rectum. [34] Rivard developed CivaSheet, a flexible implantable mesh containing $^{103}$Pd sources each shielded with a thin gold disk on one side [35]. The clinical use case for this device is for the irradiation of the a tumor bed after surgical resection. Seneviratne *et al.* reported on a 78-year-old man with persistent squamous cell carcinoma of the left axilla. Worry of radiation-induced toxicity to the nearby axillary structures discouraged the group from using EBRT to treat the axillary surgical bed post-resection. Using the CivaSheet static IMBT technique, a tumorcidal dose to the tumor bed was achieved without overdosing the nearby OARs which was unachievable using advanced EBRT techniques [36].

Dynamic shield IMBT on the other hand creates intensity modulation through the motion (i.e. rotation) of the shields relative to the source during the treatment. An appropriately designed dynamic IMBT shield has a low density region or window which allows photons to easily escape the applicator and a high density region which attenuates all other directions of emission.This results in a collimated beam which can be dynamically directed towards the tumor during the treatment. By limiting the time the low density emission window is directed towards OARs the dose distribution can be modulated to direct the dose away from OARs and towards the tumor. An example of this collimated beam geometry is shown in Figure 2.5.

In the context of cervical cancer BT, an IMBT device would need to be contained within the intracavitary tandem-based implant. The BT source itself has a diameter of 0.9 mm. The largest shield that could fit would be limited by the outer diameter of the tandem ( 6 mm). Another consideration, due to the adoption of MR-image-guided BT, is that the shielding material must be MR-safe. To satisfy these two constraints, the ideal shielding material would be of high-Z material (to maximize radiation attenuation) which exhibits a low magnetic susceptibility (MR safety).

Several groups have developed prototype IMBT systems for the treatment of cervical cancer. Han *et al.* investigated a static, six-grooved intrauterine shield. The directions of emission were limited to the six groove openings and dose modulation was accomplished by preferentially loading the source into the grooves which would improve tumor dose and reduce OAR dose. The static shield benefits from not requiring any rotational control but suffers from the fact that each groove reduces the amount of attenuating material available to achieve a highly anisotropic radiation emission, thereby limiting the modulation potential of the system. In an attempt to make the most of the attenuating material in the intrauterine tandem, Dadkhak *et al.* developed a dynamic multi-helix rotating shield which uses a small, low energy, electronic X-ray source instead of a radioactive isotope. The electronic X-ray source used emits a 50 kVp X-ray

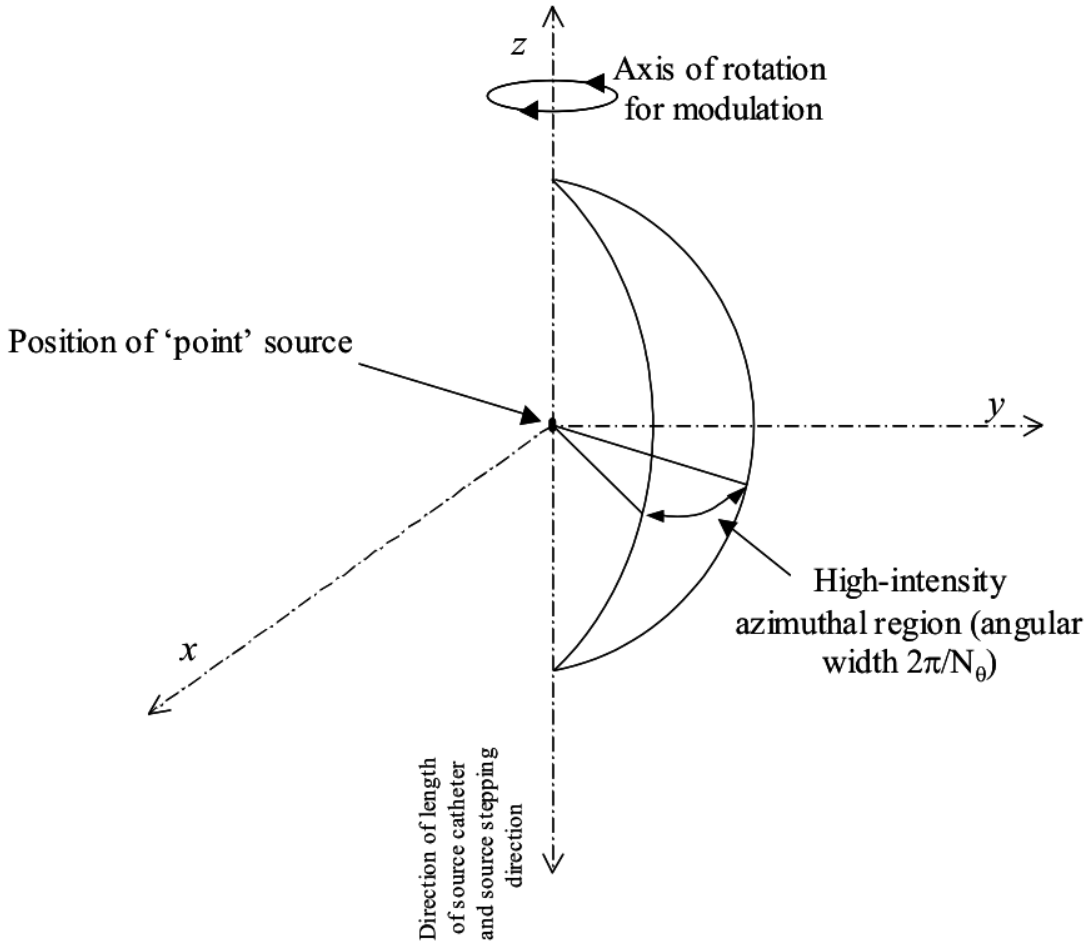


Figure 2.5: Coordinate system defining the high-intensity collimated beam emitted from a partial shielded source. Figure reproduced from Ebert [37].

spectrum ( 23 keV average energy), which is significantly easier to attenuate than Iridium-192 (380 keV average energy). A major limitation of using a 50 kVp source is in its ability to treat the portions of the cervical cancer which has spread into the paravagainal and parametrial tissues. Ytterbium-169 has been proposed as a potential alternative to Iridium-192 due to its lower average photon energy (93 keV), its higher than Iridium-192 radial dose function which would enable it to treat disease a few centimeters from the tandem, high practical specific activity and acceptable half-life (32 days versus 73.8 days for Iridium-192) [38]. Recently, an Ytterbium-169 source was proposed and manufactured in the dynamic shield IMBT prototype designed for interstitial prostate BT [38]. Famulari *et al.* demonstrated that their Ytterbium-169-based

IMBT delivery system was capable of producing highly anisotropic dose distributions using 0.8 mm-thick rotating Platinum shields (Figure 2.6.

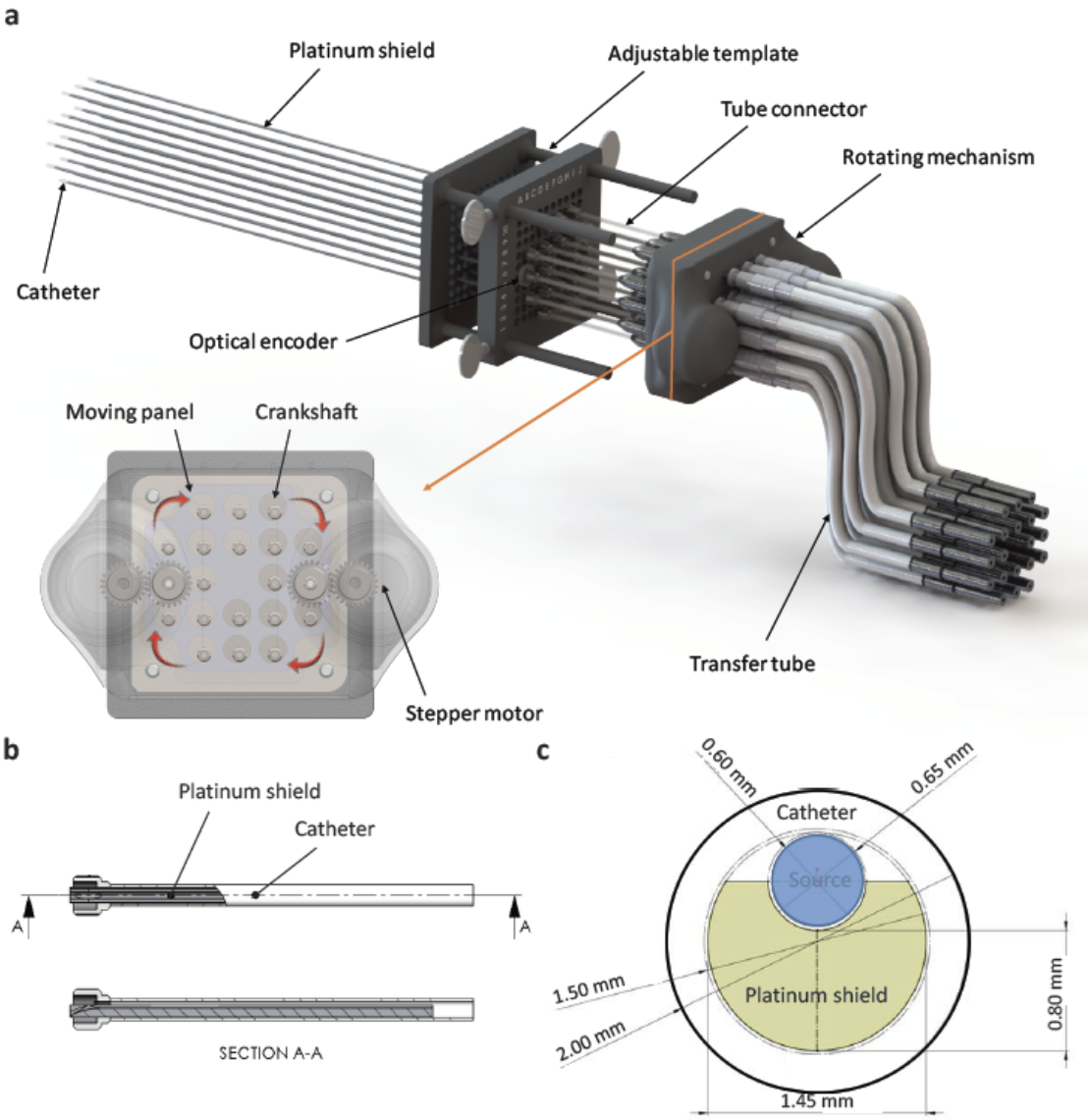


Figure 2.6: Famulari *et al*.'s dynamic shield IMBT prototype. The device makes use of thin Platinum shields which rotate around a custom Ytterbium-169 BT source for the treatment of prostate cancer. Figure reproduced from Famulari *et al*. [38]

Given that treatments with a shielded source will be longer than treatments with an unshielded source, another important consideration would be to use a source which can be produced with a large enough specific activity (i.e. Bq/kg) so as to keep treatment times

reasonable. Investigations towards the production of a Gadolinium-53 ($E_{\bar{\gamma}}$ = 60 keV) found that the specific activity was too low and radio-impurities too high to be used as a BT source [39]. Ytterbium-169 has resurfaced as a promising low energy radionuclide alternative with the gain in popularity of IMBT. Famulari *et al.* have successfully developed a Ytterbium-169 source for use in BT and IMBT [40]. A full evaluation of candidate radionuclides is described in Chapters 3 & 4.

## 2.8 Uncertainty estimation in the calculation of absorbed dose

Uncertainty is used to quantify the accuracy of calculations (i.e. dose from MBDCAs) and/or measurements (i.e. physical measurement of dose in an experiment). Additionally, having a detailed understanding of the uncertainty of two independent set of results can lead to a quantitative comparison of those results. Uncertainty can be split into random (Type-A) and systematic (Type-B) uncertainties. Type-A uncertainty is evaluated by statistical methods as the standard deviation of the mean of a series of measurements/observations. Unlike Type-A uncertainty which is calculated from a series of measurements or observations, Type-B uncertainty is estimated using the available information. Type-B uncertainties estimates usually come from calibration reports, journal articles or one's scientific judgement. The combined uncertainty is calculated by taking the square root of the sum of squares of the Type-A and Type-B components [41, 42].

### 2.8.1 Monte Carlo uncertainties in brachytherapy

Monte Carlo simulations report "statistically meaningful" averaged quantities produced from simulating millions to trillions of radiation histories. During the simulation, quantities of interest are tallied or scored in region(s) of interest. E.g.: simulating a beam of photons incident on a detector and scoring the deposited energy. Generally, the averaged quantities are reported, and it is customary to state the number of histories simulated. Uncertainty decreasing inversely with the square-root of the number of histories, where Poisson statistics apply, but it is not possible to reasonably estimate any statistical uncertainty from the number of histories alone.

### Scoring algorithms and uncertainties

Using the Monte Carlo method, the Type-A uncertainty, or variance, of a scored quantity (i.e. absorbed dose) may be estimated either batch-by-batch or history-by-history. The batch-by-batch technique estimates variance in a simple manner by splitting the simulation into smaller batches [43]. History-by-history estimates variance more accurately and can calculate variance on the fly as a simulation progresses with growing number of histories [44]. History-by-history techniques have been around since the 1980's however this method was computationally inefficient.

#### Batch-By-Batch

Batch-by-batch is realized by dividing the simulation into batches. Instead of running a single simulation, simulations are split into $N$ batches (typically 10 batches). Each of the $N$ batch simulations is made independent by applying unique random number seeds. At the completion of the simulation, the estimate of the uncertainty of the averaged scored quantity, $\bar{X}$, is:

$$s_{\bar{X}} = \sqrt{\frac{\sum_{i=i}^{N} (X_i - \bar{X})^2}{N(N-1)}} \tag{2.5}$$

where $N$ is the number of batches, $X_i$ is the value of X in batch $i$, and $\bar{X}$ is the mean value of $X$ evaluated over all the batches.

Since the contribution by the individual histories to $X_i$ is no longer recoverable, the standard deviation is not calculable for the completed simulation. Instead the standard error is used as an estimate for the standard deviation. However there will be significant fluctuations in this estimate since the sample size, $N$ is typically small.

Secondly, even though the batches are made "independent" by using different random seeds, this method ignores any correlations between primary particles when phase-space data is used as the source of particles.

#### History-By-History

Salvat is attributed with figuring out a clever method for efficiently implementing the history-by-history method for estimating uncertainty [43]. The following is from Walters *et al.*'s implementation of the history-by-history technique for BEAMnrc [44].

Going back to Eq. 2.5, let $X_i$ be the quantity scored in statistically independent history event $i$ (e.g. history $i$ instead of batch $i$). The equation is re-written as:

$$s_{\bar{X}} = \sqrt{\frac{1}{N-1}} \times \sqrt{\frac{\sum_{i=i}^{N} X_i{}^2}{N} - \left( \frac{\sum_{i=i}^{N} X_i}{N} \right)^2} \tag{2.6}$$

where $N$ is now the number of independent events i.e. histories.

If we keep track of $\sum_{i=i}^{N} X_i{}^2$ and $\sum_{i=i}^{N} X_i$ on the fly, then we can calculate uncertainty without the need to store the scored quantity in batches. This technique can be inefficient to evaluate $\sum_{i=i}^{N} X_i{}^2$ when there are large number of quantities being scores (i.e. voxelized patient made up of 1-2 mm$^3$ voxels). Sempau *et al.* outlined the following algorithm for quantity $X$:

```
IF  (nhist =X_last) THEN
   X_tmp = X_tmp + delta
ELSE
   X = X + X_tmp
   X2 = X2 + (X_tmp)^2
   X_tmp = delta
   X_last =nhist
ENDIF
```

where **X** stores $\sum_{i=i}^{N} X_i$ during the run, but at the end will store the quantity $\bar{X}$, **nhist** is the current history number, **X_last** is the number of the last history that contributes to **X**, **X_tmp** stores the sum of the contributions to **X** during the current step, and **X2** stores $\sum_{i=i}^{N} X_i{}^2$.

With this method:

1. The small sample size problem in the batch method is eliminated
2. Correlations when sampling from phase-space are handles (see Walters *et al.* for details [44]
3. Saved memory since we are no longer required to track the the value of $X$ in each batch

### Brachytherapy source geometry

The simulated BT source geometry is composed of the active radioactive core, encapsulation and only a portion of the drive cable which is practical to simulate (typically 5 mm of cable). The manufacturer provided source design provides nominal values which may vary from one produced source to another. The exact spatial distribution of the active core may also differ from the nominal design due to limitations in the production process. The dosimetric uncertainties associated with these effects should be estimated by simulating a realistic range of potential designs.

### Primary particle generation

The Monte Carlo simlulations which typically start from the radioactive decay process or by sampling from a known energy spectrum contain uncertainties related to the intensity, energy and directionality of emissions. Additionally, when comparing Monte Carlo-based BT simulations to experiments with physical sources, the dosimetrics impact due to the presence of trace radioactive contaminants should be evaluated depending on production process of the radionuclide.

### Patient geometry and composition

The patient extent as defined by medical imaging (e.g. CT, MR) may not fully capture the entire interaction space of interest. This effect could be significant if the edge of imaging is close to the patient tissue of interest, which would lead to a lack of scatter material in the Monte Carlo simulation, adding to the systematic dosimetric uncertainty. The uncertainties related to the elemental composition and mass densities (as well as electron densities) of the tissues should be considered in the uncertainty estimation [45]. The resulting material composition information is fed into the Monte Carlo framework for simulating the interaction of radiation with matter. The interaction and scoring cross section data which dictate the radiation interaction and energy deposition probabilities directly impact dose calculations. The influence of the cross section data's inherent uncertainties should be assessed in the uncertainty estimation.

## References

[1] Van Roosenbeek E, Shalek RJ, Moore EB. Safe encapsulation period for sealed medical radium sources. American Journal of Roentgenology. 1968;102(3):697–704.

[2] Curie M. Radium and the new concepts in chemistry. Nobel lecture. 1911.

[3] Abbe R. The use of radium in malignant disease. The Lancet. 1913;182(4695):524–527.

[4] Anne Woloshyn T. Soaking up the rays: Light therapy and visual culture in Britain, c. 1890–1940. Manchester University Press; 2017.

[5] Tod MC, Meredith WJ. A dosage system for use in the treatment of cancer of the uterine cervix. The British Journal of Radiology. 1938;11(132):809–824.

[6] ICRU. Prescribing, recording and reporting brachytherapy for cancer of the cervix. vol. ICRU Report 89. Bethesda, MD: International Commission on Radiation Units & Measurements; 2016.

[7] Grover S, Harkenrider MM, Cho LP, Erickson B, Small C, Small Jr W, et al. Image guided cervical brachytherapy: 2014 survey of the American Brachytherapy Society. International Journal of Radiation Oncology* Biology* Physics. 2016;94(3):598–604.

[8] Fields EC, Hazell S, Morcos M, Schmidt EJ, Chargari C, Viswanathan AN. Image-Guided Gynecologic Brachytherapy for Cervical Cancer. Seminars in Radiation Oncology. 2020;30(1):16–28. Advances in Brachytherapy. Available from: https://www.sciencedirect.com/science/article/pii/S1053429619300645.

[9] Sturdza A, Pötter R, Fokdal LU. Image guided brachytherapy in locally advanced cervical cancer: Improved pelvic control and survival in RetroEMBRACE, a multicenter cohort study. Radiother Oncol;120:428–433. Available from: https://doi.org/10.1016/j.radonc.2016.03.011.

[10] Han K, Milosevic M, Fyles A, Pintilie M, Viswanathan AN. Trends in the utilization of brachytherapy in cervical cancer in the United States. Int J Radiat Oncol Biol Phys;87:111–119. Available from: https://doi.org/10.1016/j.ijrobp.2013.05.033.

[11] Petereit DG, Frank SJ, Viswanathan AN. Brachytherapy: Where Has It Gone? J Clin Oncol;33:980–982. Available from: https://doi.org/10.1200/JCO.2014.59.8128.

[12] Orio PF, Nguyen PL, Buzurovic I, Cail DW, Chen YW. The decreased use of brachytherapy boost for intermediate and high-risk prostate cancer despite evidence supporting its effectiveness. Brachytherapy;15:701–706. Available from: https://doi.org/10.1016/j.brachy.2016.05.001.

[13] Andring L, Yoder A, Pezzi T, Tang C, Kumar R, Mahmood U, et al. PSA: Declining utilization of prostate brachytherapy. Brachytherapy. 2021. Available from: https://www.sciencedirect.com/science/article/pii/S1538472121004542.

[14] Lecavalier-Barsoum M, Khosrow-Khavar F, Asiev K, Popovic M, Vuong T, Enger SA. Utilization of brachytherapy in Quebec, Canada. Brachytherapy. 2021. Available from: https://www.sciencedirect.com/science/article/pii/S1538472121004529.

[15] Rivard MJ, Coursey BM, DeWerd LA, Hanson WF, Huq MS, Ibbott GS, et al. Update of AAPM Task Group No. 43 Report: A revised AAPM protocol for brachytherapy dose calculations. Med Phys. 2004;31(3):633–674.

[16] Enger SA, Vijande J, Rivard MJ. Model-based dose calculation algorithms for brachytherapy dosimetry. Semin Radiat Oncol. 2020;30:77–86.

[17] Ahnesjö A, van Veelen B, Carlsson-Tedgren A. Collapsed cone dose calculations for heterogeneous tissues in brachytherapy using primary and scatter separation source data. Comput Methods Programs Biomed. 1989;139:17–29.

[18] Gifford KA, Horton Jr JL, Wareing TA, Failla G, Mourtada F. Comparison of a finite-element multigroup discrete-ordinates code with Monte Carlo for radiotherapy calculations. Physics in Medicine & Biology. 2006;51(9):2253.

[19] Papagiannis P, Pantelis E, Karaiskos P. Current state of the art brachytherapy treatment planning dosimetry algorithms. The British journal of radiology. 2014;87(1041):20140163.

[20] Williamson JF. Monte Carlo and analytic calculation of absorbed dose near 137Cs intracavitary sources. International Journal of Radiation Oncology* Biology* Physics. 1988;15(1):227–237.

[21] Hissoiny S, D'Amours M, Ozell B, Després P, Beaulieu L. Sub-second high dose rate brachytherapy Monte Carlo dose calculations. Med Phys. 2012;39:7.

[22] Chetty IJ, Curran B, Cygler J, DeMarco J, Ezzell G, Faddegon B, et al. AAPM Task Group Report No. 105;"Issues associated with clinical implementation of Monte Carlo-based photon and electron external beam treatment planning,". Med Phys. 2007;34:4818–52.

[23] Williamson JF. Monte Carlo evaluation of kerma at a point for photon transport problems. Med Phys;14:567–576. Available from: https://doi.org/10.1118/1.596069.

[24] Yegin G, Taylor R, Rogers D. BrachyDose: A new fast Monte Carlo code for brachytherapy calculations. Med Phys. 2006;33(6):2074.

[25] Chamberland MJ, Taylor RE, Rogers D, Thomson RM. egs_brachy: a versatile and fast Monte Carlo code for brachytherapy. Physics in Medicine & Biology. 2016;61(23):8214.

[26] Afsharpour H, Landry G, D'Amours M, Enger S, Reniers B, Poon E, et al. ALGEBRA: ALgorithm for the heterogeneous dosimetry based on GEANT4 for BRAchytherapy. Physics in Medicine & Biology. 2012;57(11):3273.

[27] Famulari G, Renaud M, Poole CM, Evans MDC, Seuntjens J, Enger SA. RapidBrachyMCTPS: a Monte Carlo-based treatment planning system for brachytherapy applications. Phys Med Biol. 2018;63(17):175007.

[28] Chibani O, Williamson JF. M: A sub-minute Monte Carlo dose calculation engine for prostate implants. Medical physics. 2005;32(12):3688–3698.

[29] Chibani O, C-M Ma C. HDRMC, an accelerated Monte Carlo dose calculator for high dose rate brachytherapy with CT-compatible applicators. Medical physics. 2014;41(5):051712.

[30] Enger SA, Landry G, D'Amours M, Verhaegen F, L LB, Asai M, et al. Layered mass geometry: a novel technique to overlay seeds and applicators onto patient geometry in Geant4 brachytherapy simulations. Phys Med Biol. 2012;57(19):6269–6277.

[31] Glickman H, Antaki M, Deufel C, Enger SA. RapidBrachyMCTPS 2.0: a comprehensive and flexible Monte Carlo-based treatment planning system for brachytherapy applications; 2020. arXiv:2007.02902.

[32] Ebert MA. Possibilities for intensity-modulated brachytherapy: technical limitations on the use of non-isotropic sources. Phys Med Biol. 2002;47:2459–2509.

[33] Fletcher G, Shalek R, Wall J, Bloedorn F. A physical approach to the design of applicators in radium therapy of cancer of the cervix uteri. The American journal of roentgenology, radium therapy, and nuclear medicine. 1952;68(6):935–949.

[34] Poon E, Williamson JF, Vuong T, Verhaegen F. Patient-specific Monte Carlo dose calculations for high-dose-rate endorectal brachytherapy with shielded intracavitary applicator. Int J Radiat Oncol Biol Phys. 2008;72:1259–1266.

[35] Rivard MJ. A directional 103Pd brachytherapy device: Dosimetric characterization and practical aspects for clinical use. Brachytherapy. 2017;16(2):421–432.

[36] Seneviratne D, McLaughlin C, Todor D, Kaplan B, Fields EC. The CivaSheet: The new frontier of intraoperative radiation therapy or a pricier alternative to LDR brachytherapy? Advances in radiation oncology. 2018;3(1):87–91.

[37] Ebert MA. Potential dose-conformity advantages with multi-source intensity-modulated brachytherapy (IMBT). Australas Phys Eng Sc Med. 2006;29(2):165–171.

[38] Famulari G, Duclos M, Enger SA. A novel 169Yb-based dynamic-shield intensity modulated brachytherapy delivery system for prostate cancer. Med Phys;47:859–868. Available from: https://doi.org/10.1002/mp.13959.

[39] Famulari G, Urlich T, Armstrong A, Enger SA. Practical aspects of 153Gd as a radioactive source for use in brachytherapy. Applied Radiation and Isotopes. 2017;130:131–139.

[40] Famulari G, Linares Rosales HM, Dupere J, Medich DC, Beaulieu L, Enger SA. Monte Carlo dosimetric characterization of a new high dose rate Yb brachytherapy source and independent verification using a multipoint plastic scintillator detector. Medical Physics. 2020;47(9):4563–4573.

[41] DeWerd LA, Ibbott GS, Meigooni AS, Mitch MG, Rivard MJ, Stump KE, et al. A dosimetric uncertainty analysis for photon-emitting brachytherapy sources: Report of AAPM Task Group No. 138 and GEC-ESTRO. Medical physics. 2011;38(2):782–801.

[42] Castro P, García-Vicente F, Mínguez C, Floriano A, Sevillano D, Pérez L, et al. Study of the uncertainty in the determination of the absorbed dose to water during external beam radiotherapy calibration. Journal of Applied Clinical Medical Physics. 2008;9(1):70–86.

[43] Sempau J, Wilderman SJ, Bielajew AF. DPM, a fast, accurate Monte Carlo code optimized for photon and electron radiotherapy treatment planning dose calculations. Physics in Medicine & Biology. 2000;45(8):2263.

[44] Walters B, Kawrakow I, Rogers D. History by history statistical estimators in the BEAM code system. Medical physics. 2002;29(12):2745–2752.

[45] Mann-Krzisnik D, Verhaegen F, Enger SA. The influence of tissue composition uncertainty on dose distributions in brachytherapy. Radiother Oncol. 2018;126:394–410.

# Chapter 3

# Monte Carlo Dosimetry Study of Novel Rotating MRI-Compatible Shielded Tandems for Intensity Modulated Cervix Brachytherapy

**Morcos, M.** and Enger, S.A., 2020.
*Physica Medica*, 71, pp.178-184.
https://doi.org/10.1016/j.ejmp.2020.02.014

# Abstract

**Purpose:** Intensity modulated brachytherapy (IMBT) with rotating metal shields enables dose modulation that can better conform to the tumor while reducing OAR doses. In this work, we investigate novel rotating shields, compatible with MRI-compatible tandems used for cervix brachytherapy. Three unique shields were evaluated using the traditional $^{192}$Ir source. Additionally, $^{75}$Se and $^{169}$Yb isotopes were investigated as alternative sources.

**Materials and methods:** Three different IMBT shields were modeled and simulated in RapidBrachyMCTPS. Each tungsten shield was designed to fit inside a 6 mm-wide MRI-compatible tandem. The active core of the source was replaced with $^{192}$Ir, $^{75}$Se and $^{169}$Yb. Transmission factors (TFs) were calculated and defined as the dose ratio at 1 cm on opposite sides of the shielded tandem on the transverse plane. Polar and azimuthal anisotropy plots were extracted from simulations. Dose homogeneities ($\frac{V_{200\%}}{V_{100\%}}$) were calculated for all radionuclide-shield combinations.

**Results:** TFs are favorable for IMBT and ranged between 12.9%-32.2% for $^{192}$Ir, 4.0%-16.1% for $^{75}$Se and 1.2-6.4% for $^{169}$Yb for all shield designs. Average beam-widths in the polar and azimuthal directions were reduced to the range of 42°-112° and 27°-107°, respectively, for all shield-radionuclide combinations. Dose homogeneities for all radionuclide-shield combinations were all within 12% of the non-IMBT tandem.

**Conclusions:** This study has quantitatively assessed the influence of various rotating cervical cancer-specific IMBT tandem shields on dosimetry. The dynamic single-channel shields and narrow beam-widths in the polar and azimuthal direction maximize the modulation capacity of IMBT and pave the way for treating large and complex cervical cancer without interstitial needle implantation.

## 3.1 Introduction

The standard of care for women with unresectable cervical cancer includes external beam radiotherapy (EBRT) with chemotherapy followed by a brachytherapy (BT) boost [1]. EBRT which treats the pelvis and adjacent nodal regions provides approximately 50% of the total dose. BT provides the remaining course of radiation to destroy the residual tumor cells. Recent advances in magnetic resonance image (MRI) guided BT have significantly improved local control: 95-100% in limited stages (FIGO IB-IIB) and 85-90% in more advanced stages [2]. Intracavitary cervix BT provides a cylindrically symmetric pear-shaped dose distribution, adequate for treating small tumors contained within the uterine body. Large tumors which extend into the parametrial and/or paravaginal tissues cannot, in most cases, be safely treated without overdosing nearby organs at risk (OARs). In advanced cases, supplementing the intracavitary implant with interstitial BT needles enables conformal dose delivery to the tumor while reducing OAR doses [1]. Despite the excellent results achieved with BT, there are an increasing number of reports testifying on a systemic decline in BT utilization [3–5]. The reasons for the decline are multifaceted, however, a significant factor is related to a lack of radiation oncologists with the necessary expertise and comfort to perform BT as is evidenced by a request from the American Board of Radiology to implement the Focused Practice Recognition in BT as an element of its Maintenance of Certification [4]. Of the various BT techniques, the most complex and resource intensive is interstitial BT.

Static and dynamic intensity modulated BT (IMBT) techniques have become topics of great interest in the radiation oncology field since the concept of using radially asymmetric BT sources was first introduced by Ebert in 2002 [6]. By incorporating high-Z metallic shields into BT applicators, radiation can be directed towards the tumor and away from the OARs. According to a recent systematic review of IMBT literature, IMBT has been shown to decrease dose to OARs and increase tumor coverage [7]. Several groups have investigated theoretical feasibility of IMBT for treatment of cervical cancer. Han *et al*., presented a static, six-grooved tandem shield which controls the direction of emission by preferentially loading the source into the grooves [8]. The limitation with this shield model is that only emissions at every 60-degrees can be used. In addition, due to the use of six channels, less attenuating material can fit inside the tandem. Dadkhah *et al*., investigated a dynamic multi-helix rotating tandem shield which uses a 50 kVp electronic BT source [9]. A limitation of using a 50 kVp electronic BT source is its inability to treat disease that spreads laterally into the parametrium, as is often the case with

advanced cervix cancers, due to the low energy of these sources.

In intracavitary BT, the radiation source is placed in a specialized applicator inside a body cavity. To implement IMBT, the shield must be thick enough to significantly modify the intensity of the source and yet fit inside existing BT catheters and applicators. In addition, the emission spectrum from the source must be suitable for treatment of spread disease into the parametrium. Low-energy photon emitting, or electronic BT sources are not suitable since the dose distribution decreases rapidly with distance from the source due to strong attenuation in tissue. For this energy range photoelectric interactions are dominating and the decrease in absorbed dose with distance from the source is not compensated by scatter. For sources with spectra in intermediate and high-energy regions, photoelectric interactions are minimal in soft tissue and Compton scattering is the dominant photon interaction. The attenuation in tissue is compensated by single/multiple-photon scatter. While the dose distribution from intermediate energy sources and $^{192}$Ir are similar in this respect, the energy of scattered photons emitted from intermediate energy sources is much lower than that of $^{192}$Ir, with substantially lower shield thickness requirements. Several alternative radionuclides for high dose rate (HDR) BT have been investigated such as $^{75}$Se, 57Co, $^{169}$Yb and 153Gd [10–14]. Of particular interest are $^{75}$Se and $^{169}$Yb, which have average photon energies of 215 and 93 keV, respectively. $^{75}$Se and $^{169}$Yb have reasonably practical half-lives for HDR BT at 120 and 32 days, respectively. $^{192}$Ir, $^{75}$Se and $^{169}$Yb have specific activities of 9.2, 15 and 24 kCi/g, respectively [15]. Their relatively high specific activities indicate that the conventional source size can remain roughly the same and maintain a high enough dose rate [16].

In this work, we investigate the use of MRI-compatible, rotating intrauterine tandem shields through Monte Carlo (MC) simulations and evaluating clinically relevant dosimetric parameters. Our novel designs require only a single source channel, maximizing the amount of attenuating material in the intrauterine tandem and thereby maximizing the absorbed dose modulation capacity of the device. We investigate $^{75}$Se and $^{169}$Yb in addition to the conventional $^{192}$Ir BT source.

## 3.2 Materials and methods

### 3.2.1 IMBT Delivery System

The developed IMBT delivery system (Figure 3.1) is compatible with any commercial HDR afterloader as an add-on device which resides between the applicator and the afterloader [17, 18]. The device controls the rotation of the shields within the applicator while the afterloader independently controls the source position along the channel. The delivery system is compatible with both interstitial and intracavitary applicators and is divided into three systems: the rotating mechanism, joint assembly and shield assembly. Shield rotation is driven by a flexible luer that enable docking to the applicator at an angle. For this application, a stepper motor is equipped with a rotary encoder that provides closed loop feedback by tracking the angular position of the motor shaft. A second sensor is placed directly on the shield assembly that provides readout of the actual position of the shield with direct feedback to the controller.

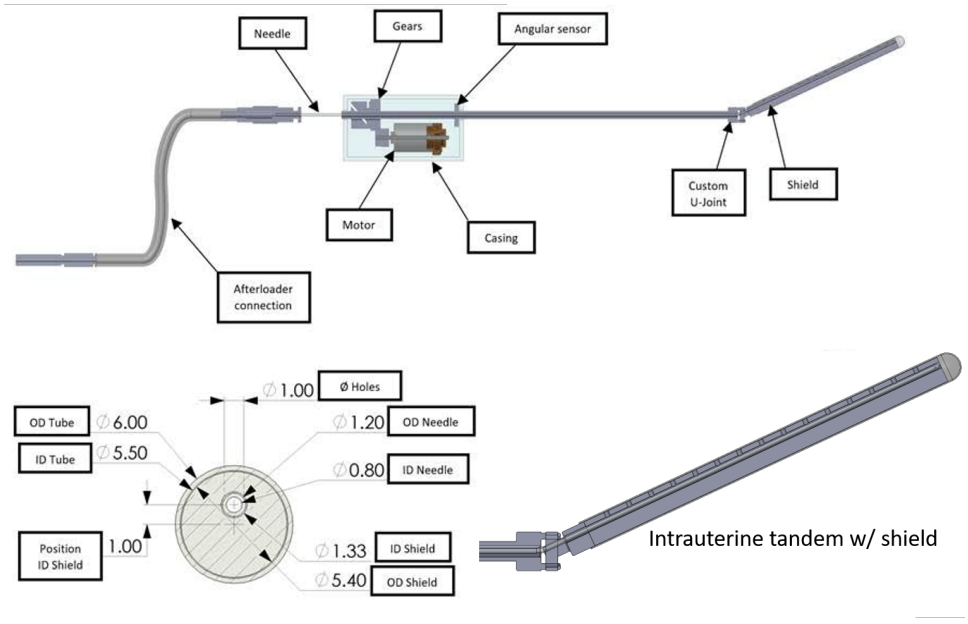


Figure 3.1: Prototype delivery system for IMBT compatible with clinical HDR afterloaders. Delivery system controls the rotation of the shield inside the tandem while the clinical afterloader controls the source position within the applicator.

### 3.2.2 IMBT Cervix Applicator

#### Applicator Design

The MRI/CT-compatible tandem and ring applicator (Elekta Brachytherapy, Veenendaal, The Netherlands) was redesigned to enable rotating shield IMBT. The clinical tandem has a 6 mm outer diameter and an inner diameter close to 3 mm. To maximize the amount of shielding material in the tandem, the applicator was redesigned with an inner diameter of 5.4 mm. The ring is unshielded and is left unchanged. For the purpose of this study, the tandem casing material (0.3 mm thick) is considered to be water equivalent.

#### Shield Design

Shields were modeled to fit inside the redesigned MRI/CT-compatible tandem (inner diameter 5.4 mm) and connect to the IMBT delivery system described in the previous section through a miniature joint, which enables the transfer of rotational force while maintaining the bend required for the angled tandem. Directional emission with a single channel maximizes the amount of attenuating material within the tandem and is possible due to the rotational IMBT delivery system. All shield designs are based on a solid cylinder as illustrated in Figure 3.2. The first design, Type A, is an offset cylinder (4.07 mm diameter) with the source channel on the surface and the two bodies rotate around each other within the tandem (Figure 3.2a). The Type B shield (Figure 3.2b) is a solid cylindrical shield (5.4 mm diameter) with a single groove etched on the surface which serves as the source channel. The third design, Type C, resembles a flute due to the beam collimations (1 mm diameter holes, spaced 10 mm apart) along the outer surface of a 5.4 mm diameter cylinder (Figure 3.2c). The Type C's source channel is bored 1 mm from the center. The source channel diameter for all shields is 1.33 mm (4-French). All shields are 8 cm long for compatibility with the longest tandem size. For the conventional, non-shielded tandem, the source channel was placed in the center.

#### Shield material selection

Tungsten was chosen as the candidate shield material due its relative high density and low magnetic susceptibility [19]. Tungsten and its non-iron alloys strike a balance between affordability and manufacturability. Static tungsten-based BT shields have been shown to exhibit minimal

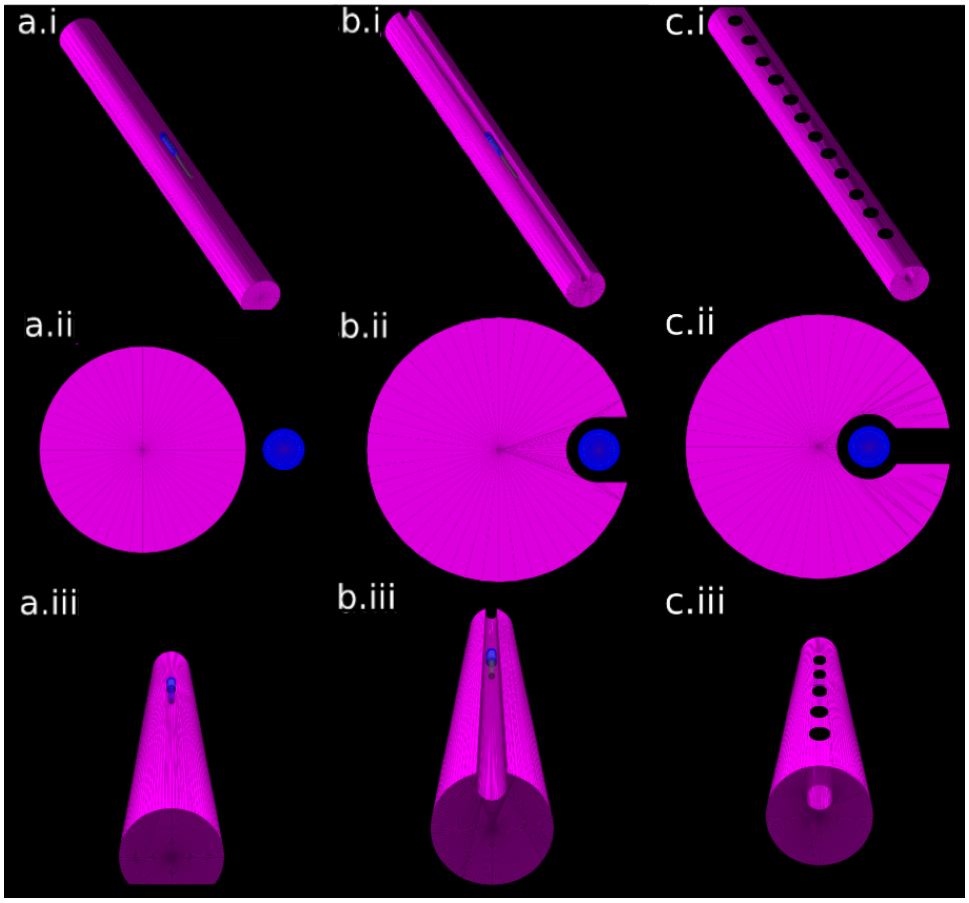


Figure 3.2: Design rendering for tandem shield model (a) Type-A, (b) Type-B and (c) Type-C. Isomeric (i), bottom (ii) and angled-top (iii) views. BT source is in blue and the source cable in gray.

magnetic susceptibility artifacts in MRI based BT [20], and clinically acceptable metal artifacts in CT imaging [21].

### HDR Source

The simulated HDR source was modeled after the Flexisource used in the Elekta Flexitron afterloader (Elekta Brachytherapy, Veenendaal, The Netherlands). The active core is a cylinder with 0.6 mm diameter and 3.5 mm length. The active core material was set to $^{192}$Ir, $^{75}$Se or $^{169}$Yb. The active core was encapsulated by stainless-steel-304 with outer dimensions of 4.6 mm length and 0.85 mm diameter. The drive cable is also composed of stainless-steel-304 and

is modeled with a length of 5 mm. Geometry details and material compositions are described at length in the published work of Granero *et al* [22].

### 3.2.3 Monte Carlo Simulations

Simulations were performed with RapidBrachyMCTPS [23], a benchmarked MC-based treatment planning software for BT applications built with the Geant4 MC toolkit [24]. The active core of the source was replaced with $^{192}$Ir, $^{75}$Se and $^{169}$Yb. In RapidBrachyMCTPS, particles can be generated through direct sampling of the decay scheme by utilizing Geant4 radioactive decay module [25] and photon decay spectra from the Evaluated Nuclear Structure Data File (ENSDF) [26]. In this work, 108 decay events were simulated for each radionuclide. $^{192}$Ir which has approximately 2.3 photons per decay event would lead to a simulation with 2.3 x 108 primary photons [27], similarly $^{75}$Se and $^{169}$Yb generate approximately 2.3 and 3.8 photons per decay, respectively. Penelope low-energy electromagnetic physics list was used to simulate electromagnetic interactions. Due to the low photon energies emitted from the simulated radionuclides, dose was approximated by the collisional kerma and scored using a track length estimator [28]. Parallel world formalism implemented in Geant4 was used for scoring with the resolution of the scoring grid being 1 mm3. The source-shield geometry was placed in the center of a (50 cm)3 water phantom. A single dwell position located half way up the 8 cm long intrauterine shield was simulated for all shield types and simulated radionuclides. The source was oriented in the positive-z direction. The tandem is centered at the origin.

The dynamic rotating shield IMBT system is best explained using a spherical coordinate system. In the spirit of TG-43 [29], the polar angle (also known as the zenith angle) measured from the z-axis is denoted as $\theta$. We define $\psi$ to be the azimuthal angle in the x-y plane and is the axis of rotation for dose modulation. The radius, r, is defined as the distance from the origin. The coordinate system is illustrated in Figure 3.3.

To quantitatively evaluate the attenuation capacity of each shield-radionuclide combination, the transmission factor, TF, is defined as:

$$TF = \frac{D(r = 1cm, \theta = 90^\circ, \psi = 180^\circ)}{D(r = 1cm, \theta = 90^\circ, \psi = 0^\circ)} \tag{3.1}$$

where TF is the ratio of the dose at 1 cm from the center of the tandem on the x-y plane of the shielded side to the unshielded side. The emission window is at $\psi = 0^\circ$.

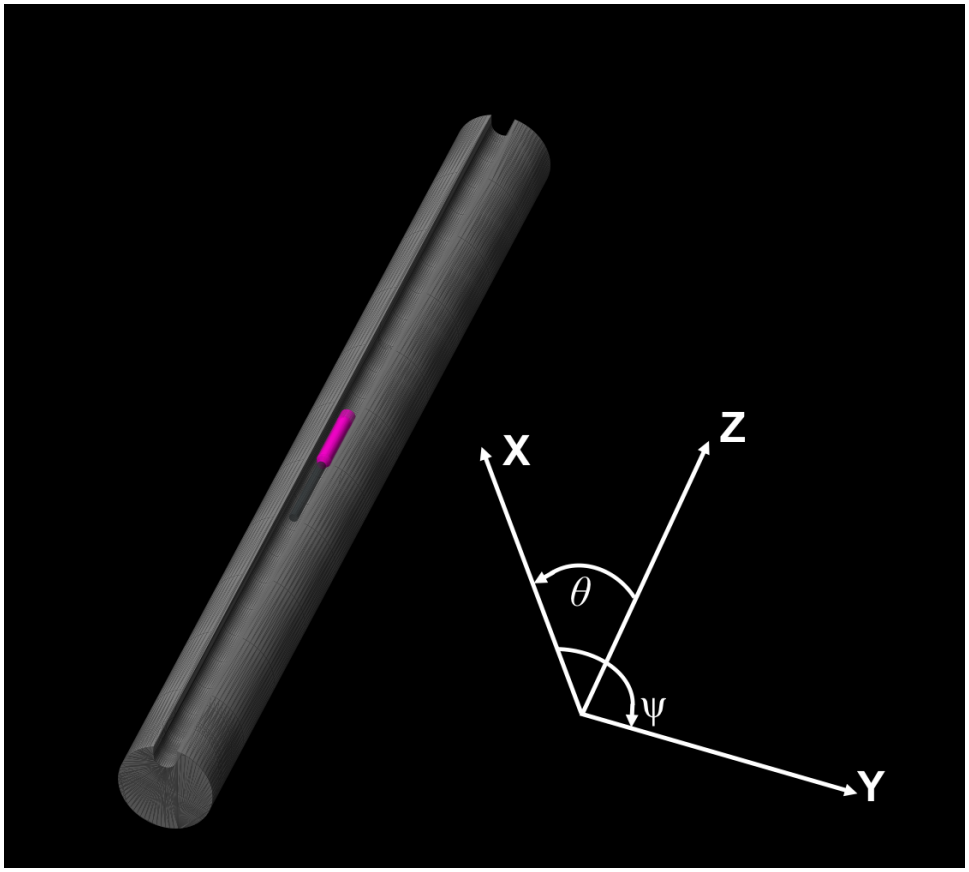


Figure 3.3: Source/shield combination oriented in positive-Z direction. The polar angle, $\theta$, is measured from the z-axis. The shield rotation of axis is defined as the rotation in the x-y plan and is denoted using $\psi$. The shield and source are shown in gunmetal and magenta, respectively.

## 3.3 Results

Dose distributions were normalized at $r = 1cm, \theta = 90^\circ, \psi = 0^\circ$. All simulations achieved a statistical uncertainty of <2%. Axial (x-y plane) and sagittal (z-x plane) views of normalized dose distributions are shown for all shield-radionuclide combinations in Figure 3.4 and Figure 3.5, respectively.

### 3.3.1 Transmission Factors

TFs are summarized in Table 3.1. Dose ratios, at 1 cm from tandem center, of the shielded side (back) of the tandems to the opposite, unshielded side (front) is useful in highlighting the attenuating differences between various shield-radionuclide combinations.

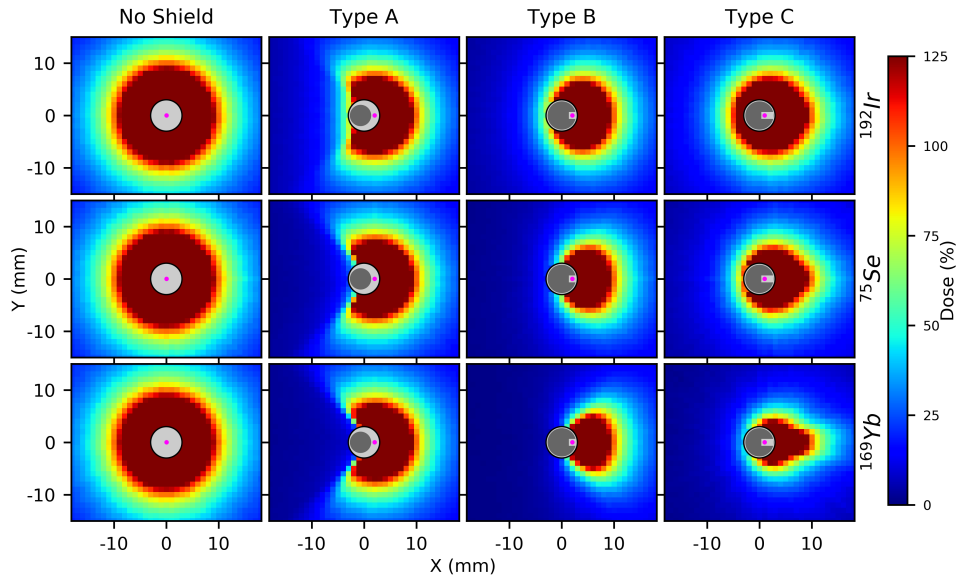


Figure 3.4: Axial cross-section of MC calculated doses for novel rotating shield Types-A, -B and -C and non-shielded tandem. From top to bottom are $^{192}$Ir, $^{75}$Se and $^{169}$Yb. Doses are normalized at 1 cm from the tandem center. The tandem, shield and source are illustrated in light gray, dark gray and magenta, respectively. Dose in the tandem is hidden for clarity.

### 3.3.2 Anisotropy and beam size

The normalized polar and azimuthal anisotropies are shown in Figure 3.6 and Figure 3.7. Beam widths, defined as the full width at 80% maximum in the polar direction (evaluated at $r = 1cm, \psi = 0°$) are annotated on the subplots of Figure 3.6. Similarly, beam widths in the azimuthal direction (evaluated at $r = 1cm, \theta = 90°$) are annotated in Figure 3.7.

### 3.3.3 Dose Homogeneity

To quantify dose homogeneity, which is the ratio of the volume receiving at least 200% of the prescribed dose to the volume receiving at least 100% of the prescribed dose is calculated for all cases. Dose in voxels which are inside the tandem are excluded to assess dose homogeneity the patient is exposed to. Dose homogeneities for all shield-radionuclide combinations are summarized in Table 3.2.

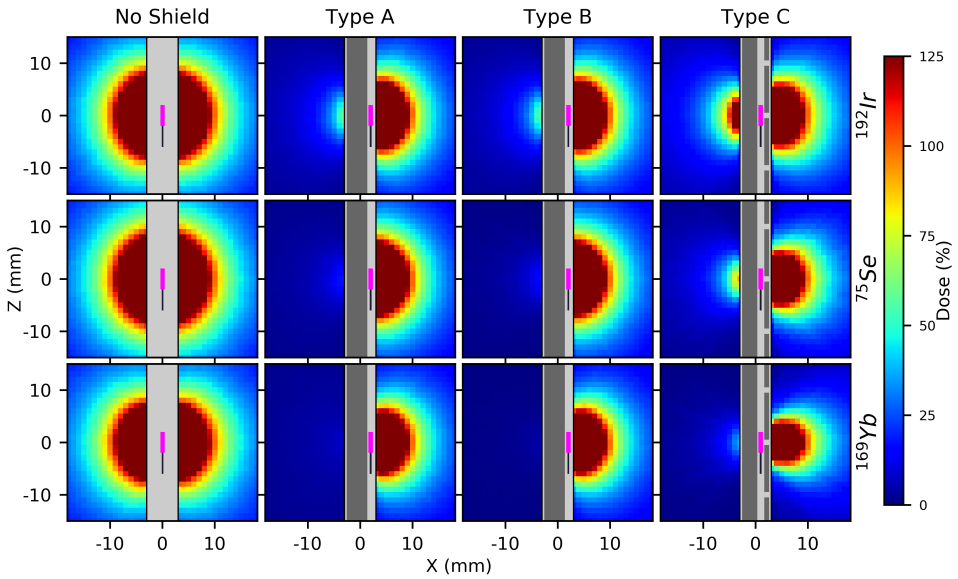


Figure 3.5: Sagittal cross-section of MC calculated doses for non-shielded tandem and novel rotating shield Types-A, -B and -C. From top to bottom are $^{192}$Ir, $^{75}$Se and $^{169}$Yb. Doses are normalized at 1 cm from the tandem center. The tandem, shield and source are illustrated in light gray, dark gray and magenta, respectively. Dose in the tandem is hidden for clarity.

## 3.4 Discussion

Conventional intracavitary cervix BT provides a radially symmetric pear-shaped dose distribution which is adequate for treating small tumors contained within the uterine body. For patients with large ($\geq 30\ cm^3$) tumors which spread to the parametrial and/or paravaginal tissues, interstitial BT has been shown to improve local control while reducing OAR doses [30]. By obviating the need for interstitial needle implantation, IMBT enables modulation of absorbed dose during the treatment by dynamically controlling an intracavitary rotating shield inside the applicator. IMBT has the potential to revolutionize BT in the way multi-leaf collimators have for external beam radiotherapy. Needle-less IMBT for treatment of cervical cancer and other tumor types treated with intracavitary BT would revitalize the field and increase adoption rates, thereby helping to reverse the declining BT utilization rates [3–5].

In this study, the dosimetric impact of replacing conventional cervix tandems with MR-compatible rotating shields were investigated. The modulation capacity of promising alternative

Table 3.1: TFs for all shield-radionuclide combinations. TF for no-shield is unity due to cylindrical symmetry.

| | Type A | Type B | Type C |
|---|---|---|---|
| $^{192}$Ir | 13.1% ± 0.4% | 12.9% ± 0.4% | 32.2% ± 0.4% |
| $^{75}$Se | 4.2% ± 0.7% | 4.0% ± 0.8% | 16.1% ± 0.6% |
| $^{169}$Yb | 1.8% ± 1.2% | 1.2% ± 1.5% | 6.4% ± 1.3% |

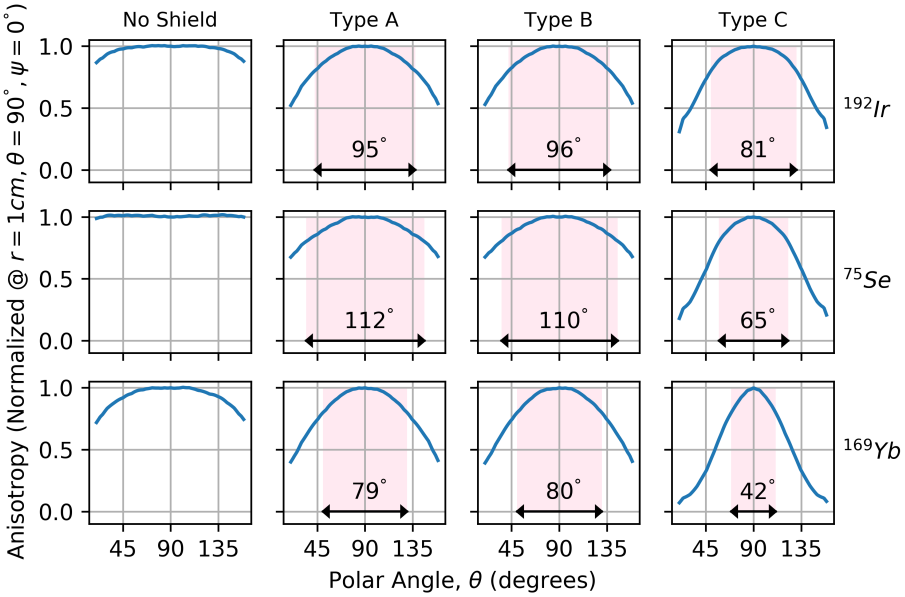


Figure 3.6: Polar anisotropy at a radial distance of 1 cm, normalized at $r = 1cm, \theta = 90°, \psi = 0°$. The source is oriented in the positive-z direction. Polar anisotropy is evaluated at $\psi = 0°$. Similar to TG-43, $\theta = 90°$, defines the source transverse plane. Beam widths in the superior-inferior direction, defined as the full-width at 80% of the maximum are annotated in the plots.

radionuclides, namely $^{75}$Se and $^{169}$Yb, was evaluated in addition to the conventional $^{192}$Ir HDR source. This study demonstrated that all three radionuclides are viable sources for rotating shield IMBT, achieving significantly anisotropic dose distributions, for all shield-radionuclide combinations evaluated. Han *et al.* reported on their static tandem shield with six grooves, separated by 60-degrees, which exhibited a reasonable shielding capacity and limited modulation control. Our rotating shield designs investigated in this study are not limited to 60-degree emission gaps and maximize the amount of shielding material inside the tandem since only

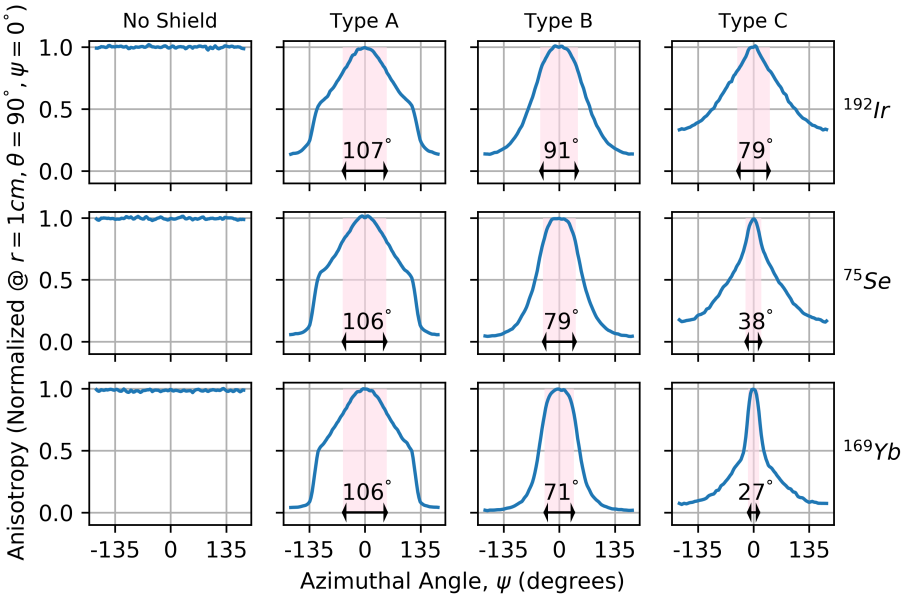


Figure 3.7: Azimuthal anisotropy at a radial distance of 1 cm, normalized at $r = 1cm, \theta = 90°, \psi = 0°$. The emission window is centered at $\psi = 0°$. Azimuthal anisotropy is evaluated at $\theta = 90°$. Beam widths in the axial plane, defined as the full-width at 80% of the maximum are annotated in the plots. Azimuthal anisotropy for no-shield is unity due to cylindrical symmetry.

single source channel is required.

Several investigations of a 50 kVp electronic BT source for treatment of cervical cancer have been reported [9, 31]. Although a very low energy beam is more easily shielded for IMBT, too low an energy may compromise the ability to treat patients with disease that has spread in the parametrium and paravaginal tissue. By comparison, $^{75}$Se and $^{169}$Yb make better alternative lower energy sources as is evident from the radial dose functions in Figure 3.8. In consideration of this clinically relevant discussion, the dose homogeneity, defined as $\frac{V_{200\%}}{V_{100\%}}$ in this study, was within 12% of the conventional tandem for all shield-radionuclide combinations. This result demonstrates that dose modulation can be achieved without introducing unacceptable hotspots in the patient.

The shields investigated in this study were designed sequentially, improving the design at every step by examining the simulated dose distributions. Despite its simple design, the Type A shield was capable of reducing the dose on the shielded side of the tandem, at 1 cm, to 13.1%,

Table 3.2: Dose homogeneity for all shield-radionuclide combinations. Voxels contained within the 6 mm-wide tandem are not used in the calculation.

| | No Shield | Type A | Type B | Type C |
|---|---|---|---|---|
| $^{192}$Ir | 0.31 | 0.33 | 0.33 | 0.29 |
| $^{75}$Se | 0.30 | 0.32 | 0.34 | 0.29 |
| $^{169}$Yb | 0.31 | 0.33 | 0.35 | 0.27 |

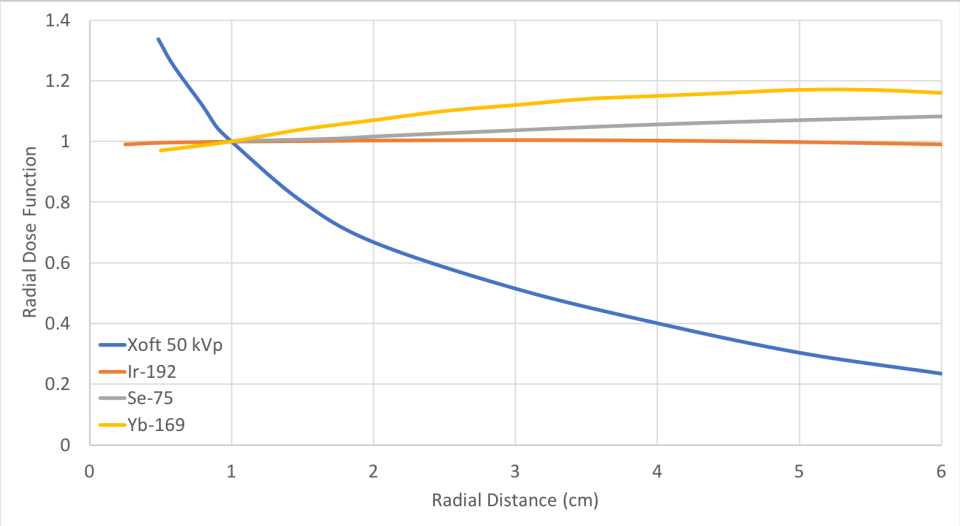


Figure 3.8: Radial dose function for various BT sources normalized at 1 cm. Data for $^{192}$Ir and $^{169}$Yb are from GEC-ESTRO BRAPHYQS32. Data for Xoft and $^{75}$Se are from our prior works [32].

4.2% and 1.8% for $^{192}$Ir, $^{75}$Se and $^{169}$Yb, respectively. The Type A design's shortcoming is its relatively large beam width ( 106°) in the azimuthal direction, which would limit its axial modulation capacity (Figure 3.7). The Type B (single grooved) shield improves upon Type A's design by filling the tandem with more attenuating material and simplifying the rotation mechanics (shield rotation is concentric with tandem). The key improvement is the narrower azimuthal beam width without sacrificing transmission on the posterior end. Type C's flute-style design achieves small beam widths in the azimuthal and polar directions. The resulting narrow beam comes at the expense of increasing posterior transmission. A tightly collimated beam in the azimuthal and polar directions has the potential benefit of treating distance parametrial disease without significantly increasing dose to nearby OARs in the superior-inferior direction.

## 3.5 Conclusions

This study has quantitatively evaluated the impact of various MRI-compatible tandem shield designs, combined with a previously investigated IMBT delivery system. The studied intrauterine IMBT shields maximize the shielding potential due to the single-channel dynamic rotating delivery system. The flute style shield is optimized for treating cervical cancers with extensive parametrial disease due to its dose modulation capacity in the superior-inferior direction in addition to the azimuthal direction. Retrospective patient simulations are the focus of our next investigation.

**Acknowledgements:** The project is funded by the Collaborative Health Research Projects (#248490) and the Natural Sciences and Engineering Research Council of Canada (#241018). Computations were made on the supercomputers MP2 and Graham managed by Calcul Québec and Compute Canada. The operation of these supercomputers are funded by the Canada Foundation for Innovation (CFI), the ministère de l'Économie, de la science et de l'innovation du Québec (MESI) and the Fonds de recherche du Québec - Nature et technologies (FRQ-NT).

**Conflict of interest:** None.

## References

[1] Viswanathan AN, Beriwal S, De Los Santos JF. American Brachytherapy Society consensus guidelines for locally advanced carcinoma of the cervix. Brachytherapy;11:47–52. Available from: https://doi.org/10.1016/J.BRACHY.2011.07.002.

[2] Sturdza A, Pötter R, Fokdal LU. Image guided brachytherapy in locally advanced cervical cancer: Improved pelvic control and survival in RetroEMBRACE, a multicenter cohort study. Radiother Oncol;120:428–433. Available from: https://doi.org/10.1016/j.radonc.2016.03.011.

[3] Han K, Milosevic M, Fyles A, Pintilie M, Viswanathan AN. Trends in the utilization of brachytherapy in cervical cancer in the United States. Int J Radiat Oncol Biol Phys;87:111–119. Available from: https://doi.org/10.1016/j.ijrobp.2013.05.033.

[4] Petereit DG, Frank SJ, Viswanathan AN. Brachytherapy: Where Has It Gone? J Clin Oncol;33:980–982. Available from: https://doi.org/10.1200/JCO.2014.59.8128.

[5] Orio PF, Nguyen PL, Buzurovic I, Cail DW, Chen YW. The decreased use of brachytherapy boost for intermediate and high-risk prostate cancer despite evidence supporting its effectiveness. Brachytherapy;15:701–706. Available from: https://doi.org/10.1016/j.brachy.2016.05.001.

[6] Ebert MA. Possibilities for intensity-modulated brachytherapy: Technical limitations on the use of non-isotropic sources. Phys Med Biol;47:2495–2509. Available from: https://doi.org/10.1088/0031-9155/47/14/309.

[7] Callaghan CM, Adams Q, Flynn RT, Wu X, Xu W, Kim Y. Systematic Review of Intensity-Modulated Brachytherapy (IMBT): Static and Dynamic Techniques. Int J Radiat Oncol;105:206–221. Available from: https://doi.org/10.1016/j.ijrobp.2019.04.009.

[8] D YH, MJ W, DJ S. Direction-Modulated Brachytherapy for High-Dose-Rate Treatment of Cervical Cancer. I: Theoretical Design Radiation Oncology. Int J Radiat Oncol Biol Phys;89:666–673. Available from: https://doi.org/10.1016/j.ijrobp.2014.02.039.

[9] Dadkhah H, Kim Y, Wu X, Flynn RT. Multihelix rotating shield brachytherapy for cervical cancer;. Available from: https://doi.org/10.1118/1.4933244.

[10] Granero D, Perez-Calatayud J, Ballester F, Bos AJJ, Venselaar J. Broad-beam transmission data for new brachytherapy sources, Tm-170 and Yb-169. Radiat Prot Dosimetry;118:11–15. Available from: https://doi.org/10.1093/rpd/nci322.

[11] Ballester F, Granero D, Perez-Calatayud J, Venselaar JLM, Rivard MJ. Study of encapsulated 170Tm sources for their potential use in brachytherapy. Med Phys;37:1629–1637. Available from: https://doi.org/10.1118/1.3360441.

[12] Enger SA, D'Amours M, Beaulieu L. Modeling a Hypothetical Tm-170 Source for Brachytherapy Applications. Med Phys;38:5307–5310. Available from: https://doi.org/10.1118/1.3626482.

[13] Enger SA, Fisher DR, Flynn RT. Gadolinium-153 as a brachytherapy isotope. Phys Med Biol;58:957–964. Available from: https://doi.org/10.1088/0031-9155/58/4/957.

[14] Shoemaker T, Vuong T, Glickman H, Kaifi S, Famulari G, Enger SA. Dosimetric Considerations for Ytterbium-169, Selenium-75, and Iridium-192 Radioisotopes in High-Dose-Rate Endorectal Brachytherapy. Int J Radiat Oncol;105:875–883. Available from: https://doi.org/10.1016/J.IJROBP.2019.07.003.

[15] Song WY, Tanderup K, Pieters BR. Emerging Technologies in Brachytherapy. Boca Raton: CRC Press;. Available from: https://doi.org/https://doi-org.proxy3.library.mcgill.ca/10.1201/9781315120966.

[16] V BA, AA B, GA K, AP C. Simulation of 75Se Encapsulated Sources for Their Potential Use in Brachytherapy. Moscow Univ Phys Bull;73:339–341. Available from: https://doi.org/10.3103/S0027134918030049.

[17] Famulari G, Enger SA. A Novel Intensity Modulated High Dose Rate Brachytherapy Delivery System with 169 Yb. Int J Radiat Oncol;99:E657. Available from: https://doi.org/10.1016/j.ijrobp.2017.06.2187.

[18] Famulari G, Enger SA. Intensity modulated brachytherapy system for dynamic modulation of shielded catheters. Radiother Oncol;127:S90.

[19] Lide DR. CRC Handbook of Chemistry and Physics. vol. 128. 86th ed. David R, editor. Boca Raton, FL: American Chemical Society;. Available from: https://doi.org/10.1021/ja059868l.

[20] Soliman AS, Elzibak A, Easton H. Quantitative MRI assessment of a novel direction modulated brachytherapy tandem applicator for cervical cancer at 1.5 T. Radiother Oncol;120:500–506. Available from: https://doi.org/10.1016/j.radonc.2016.07.006.

[21] Elzibak AH, Kager PM, Soliman A. Quantitative CT assessment of a novel direction-modulated brachytherapy tandem applicator. Brachytherapy;17:465–475. Available from: https://doi.org/10.1016/j.brachy.2017.10.006.

[22] Granero D, Perez-Calatayud J, Casal E, Ballester F, Venselaar J. A dosimetric study on the Ir-192 high dose rate Flexisource. Med Phys;33:4578–4582. Available from: https://doi.org/10.1118/1.2388154.

[23] Famulari G, Marc-AndréRenaud CMP, Evans MDC, Seuntjens J, Enger SA. Rapid-BrachyMCTPS: a Monte Carlo-based treatment planning system for brachytherapy applications. Phys Med Biol;63(175007). Available from: https://doi.org/10.1088/1361-6560/aad97a.

[24] Agostinelli S, Allison J, Amako K. Geant4—a simulation toolkit. Nucl Instruments Methods Phys Res Sect A Accel Spectrometers. Detect Assoc Equip;506:250–303. Available from: https://doi.org/10.1016/S0168-9002(03)01368-8.

[25] Pia MG, Bell ZW, Batic M. Radioactive Decays in Geant4. IEEE Trans Nucl Sci;60:2966–2983. Available from: https://doi.org/10.1109/tns.2013.2270894.

[26] File TJENSD;. Online]. Available:. Available from: http://www.nndc.bnl.gov/ensdf/.

[27] Borg J, Rogers DWO. Monte Carlo calculations of photon spectra in air from 192Ir sources;.

[28] Williamson JF. Monte Carlo evaluation of kerma at a point for photon transport problems. Med Phys;14:567–576. Available from: https://doi.org/10.1118/1.596069.

[29] Rivard MJ, Coursey BM, Dewerd LA. Update of AAPM Task Group;. Report: A revised AAPM protocol for brachytherapy dose calculations. 2004. Available from: https://doi.org/10.1118/1.1646040.

[30] Fokdal L, Sturdza A, Mazeron R. Image guided adaptive brachytherapy with combined intracavitary and interstitial technique improves the therapeutic ratio in locally advanced cervical cancer: Analysis from the retroEMBRACE study. Radiother Oncol;120:434–440. Available from: https://doi.org/10.1016/j.radonc.2016.03.020.

[31] Liu Y, Flynn RT, Kim Y. Paddle-based rotating-shield brachytherapy. Med Phys;42:5992–6003. Available from: https://doi.org/10.1118/1.4930807.

[32] Devic S, Liang L, Tomic N. Dose measurements nearby low energy electronic brachytherapy sources using radiochromic film. Phys Medica;64:40–44. Available from: https://doi.org/10.1016/J.EJMP.2019.05.017.

# Chapter 4

# A novel minimally invasive dynamic-shield, intensity-modulated brachytherapy system for the treatment of cervical cancer

**Morcos, M.**, Antaki, M., Viswanathan, A.N., Enger, S.A., 2021.
*Medical physics*, 48(1), pp.71-79.
https://doi.org/10.1002/mp.14459

# Abstract

**Purpose:** To present a novel, MRI-compatible dynamic-shield intensity modulated brachytherapy (IMBT) applicator and delivery system using $^{192}$Ir, $^{75}$Se and $^{169}$Yb radioisotopes for the treatment of locally advanced cervical cancer. Needle-free IMBT is a promising technique for improving target coverage and organ at risk (OAR) sparing.

**Materials and methods:** The IMBT delivery system dynamically controls the rotation of a novel tungsten shield placed inside an MRI-compatible, 6-mm wide intrauterine tandem. Using 36 cervical cancer cases, conventional intracavitary brachytherapy (IC-BT) and intracavitary/interstitial brachytherapy (IC/IS-BT) (10 Ci $^{192}$Ir) plans were compared to IMBT (10 Ci $^{192}$Ir; 11.5 Ci $^{75}$Se; 44 Ci $^{169}$Yb). All plans were generated using the Geant4-based Monte Carlo dose calculation engine, RapidBrachyMC. Treatment plans were optimized then normalized to the same HR-CTV D90 and the D2cc for bladder, rectum and sigmoid in the research brachytherapy planning system, RapidBrachyMCTPS. Plans were re-normalized until either of the three OARs reached dose limits to calculate the maximum achievable HR-CTV D90 and D98.

**Results:** Compared to IC-BT, IMBT with either of the three radionuclides significantly improves the HR-CTV D90 and D98 by up to 5.2% $\pm$ 0.3% (P<.001) and 6.7% $\pm$ 0.5% (P<.001), respectively, with the largest dosimetric enhancement when using $^{169}$Yb followed by $^{75}$Se and then $^{192}$Ir. Similarly, D2cc for all OARs improved with IMBT by up to 7.7% $\pm$ 0.6% (P<.001). For IC/IS-BT cases, needle-free IMBT achieved clinically acceptable plans with $^{169}$Yb-based IMBT further improving HR-CTV D98 by 1.5% $\pm$ 0.2% (P=.034) and decreasing sigmoid D2cc by 1.9% $\pm$ 0.4% (P=.048). Delivery times for IMBT are increased by a factor of 1.7, 3.3 and 2.3 for $^{192}$Ir, $^{75}$Se and $^{169}$Yb, respectively, relative to conventional $^{192}$Ir BT.

**Conclusions:** Dynamic shield IMBT provides a promising alternative to conventional IC- and IC/IS-BT techniques with significant dosimetric enhancements and even greater improvements with intermediate energy radionuclides. The ability to deliver a highly conformal, OAR-sparing dose without IS needles provides a simplified method for improving the therapeutic ratio less invasively and in a less resource intensive manner.

## 4.1 Introduction

Brachytherapy (BT) is capable of delivering a very high dose of conformal radiotherapy and is recommended for all cases of localized cervical cancer after external beam radiation. [1] The introduction of image-guided high dose rate (HDR) BT has significantly improved patient outcomes. Several groups have published results with image-guidance showing a 17% increase in local control of large tumors from 81% to 98% and an 11% decrease in rectal bleeding from 13% to 2%. [2, 3] However, even with these advanced planning techniques, target coverage may be compromised when using intracavitary BT (IC-BT) for large or irregularly shaped tumors due to the vicinity of organs at risk (OARs) and radially isotropic dose distribution from conventional HDR BT radiation sources. RetroEMBRACE demonstrated that hybrid intracavitary/interstitial BT (IC/IS-BT) significantly increased local control by 10% without increasing morbidity for larger tumors, compared to the intracavitary BT (IC-BT) group. [4] Despite the excellent results achieved with BT, there are many reports that a startling number of patients do not receive this state of the art treatment. [5] For cervical cancer, this translates to preventable disease-related deaths. Possible explanations for the reduction of BT utilization are inadequate training, especially with intrauterine tandem placement, interstitial needle implantation and the comfort of a physician with non-invasive techniques such as IMRT and SBRT. [5]

A limitation with conventional BT is its near-isotropic dose distributions, delivering high dose to the tumors but often with non-ideal dose conformity. Recent efforts in obtaining anisotropic dose distributions in HDR BT include incorporating metal shields inside the applicators during treatment to direct the radiation towards the tumor and away from the OARs. Examples include static directional modulated BT (DMBT) and dynamic shield intensity modulated BT (IMBT), referred to herein simply as IMBT. [6–9] With DMBT, a static metal alloy shield placed inside conventional applicators enable anisotropic dose distributions, which have been shown to decrease OARs doses in rectal and cervical cancer BT. [10, 11] The IMBT technique uses metallic shields which can rotate during the treatment, independent of the applicator that they are contained in, and allow for dynamic directional control of the radiation emission. IMBT with intermediate energy BT has been investigated. IMBT using 153Gd was proposed for interstitial prostate BT. [12] The proposed system reduced urethral D10 (dose to water in water, Dw,w) by 20-26%. However due to the low specific activity of 153Gd, 20 simultaneous HDR sources were required and treatment times were on the order of 2 hours. Electronic BT-based IMBT for cervical cancer uses a 50 kVp source which is more easily shielded, yet has limited

penetration depth and require a larger tandem, 9.4 mm in diameter. [7] An additional limitation of the aforementioned IMBT investigation is that the dose calculations were based on dose to water, an assumption which leads to dosimetric inaccuracies due to the non-water equivalence of mass energy absorption coefficient for metal and different tissues. [13, 14] The inaccuracies increase with decreasing photon energy where photoelectric interactions dominate. [15] $^{75}$Se and $^{169}$Yb have been hypothesized for HDR BT use for decades due to their high practical specific activities of 5.8 and 8.0 kCi/g, respectively compared to 3.9 kCi/g for $^{192}$Ir. [16, 17] Recently, $^{75}$Se and $^{169}$Yb are being considered once again due to the increased interest in IMBT and reduced production costs based on possible reactivation of sources. [9, 18] Famulari et al. recently reported on a miniature 18 Ci $^{169}$Yb-based IMBT delivery system for interstitial prostate BT capable of delivering a 15 Gy prostate treatment in 20 minutes with a single source and achieving urethral D10 (dose to medium in medium, Dm,m) sparing of 13.3% without affecting target coverage. [9]

The purpose of this study was to evaluate plan quality improvements using needle-free $^{192}$Ir-, $^{75}$Se- and $^{169}$Yb-based IMBT compared to conventional $^{192}$Ir IC-BT and IC/IS-BT for cervical cancer. The MRI-compatible IMBT delivery prototype system for treatment of cervical cancer used in this study builds on our prior work. [8, 19]

## 4.2 Materials and methods

### 4.2.1 IMBT cervix applicator and shield design

Tandem of the MRI/CT-compatible Venezia applicator (Elekta Brachytherapy, Veenendaal, The Netherlands) with an outer diameter of 4 mm and an inner diameter of approximately 2.5 mm was redesigned to enable IMBT. To maximize the amount of shielding material in the tandem, the applicator was redesigned with an outer diameter of 6 mm and inner diameter of 5.4 mm. The tandem shield with a thickness of 5.4 mm, resembles a flute due to the 1 mm diameter beam collimation holes spaced 10 mm apart along its outer surface which, in addition to collimation the beam laterally, help limit the dose to OARs above and below the dwell position. The shield is connected to the rotating IMBT delivery system through a custom miniature joint, which enables the transfer of rotational force while maintaining the bend required for the angled tandem. The lunar ovoids are unshielded and left unchanged. Directional emission with a single channel maximizes the amount of attenuating material within the tandem and is possible due

to the rotational delivery system. The tandem shield's source channel is bored 1 mm from the center. The source channel diameter is 1.33 mm (4-French). Tungsten was chosen as the candidate shield material due its relative high density and low magnetic susceptibility [20, 21] and clinically acceptable metal artifacts in CT imaging. [22] The IMBT delivery system is illustrated in Figure 4.1. The system is compatible with any clinical HDR afterloading systems as an add-on device, resides between the applicator and the afterloader [23, 24] and controls the rotation of the shield within the applicator tandem. Further details of the mechanical design of the IMBT delivery system are described in a previous publication. [8]

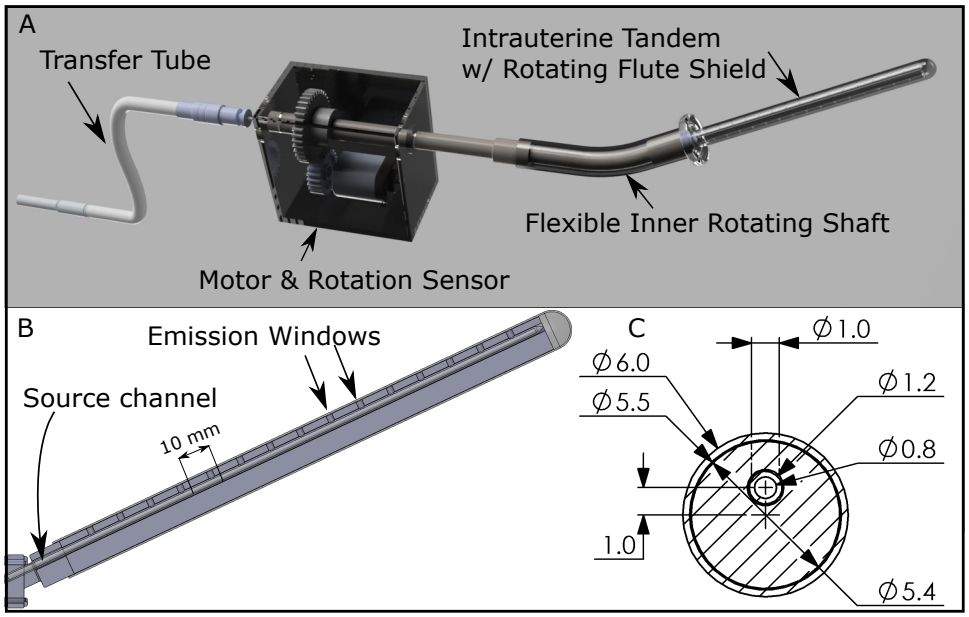


Figure 4.1: Prototype delivery system for intensity modulated brachytherapy compatible with clinical high dose rate afterloaders. Deliver y system controls the rotation of the shield inside the tandem while the clinical afterloader controls the source position within the applicator. (a) Overview of delivery system and rotating mechanism. (b) Cross-sectional side view of rotating flute shield. (c) Cross-sectional top-view of rotating flute shield

### 4.2.2 Patient dataset

Thirty-six cervical cancer implants with staging ranging from IB to IVA were considered in a retrospective Institutional Review Board approved study. High-risk CTV (HR-CTV) volumes ranged from 8.2 to 113.8 $cm^3$ (mean 29.5 $cm^3$, standard deviation 20.1 $cm^3$). 14 implants were performed with the Venezia hybrid applicator (Elekta Brachytherapy, Veenendaal, The

Netherlands). The Vienna-style hybrid Tandem and Ring applicator (Elekta Brachytherapy,, Veenendaal, The Netherlands) was used on the remaining 22 cases. All implants were performed under MR-guidance. For six of the cases, hybrid IC/IS-BT implants combined with between 3 and 6 needles (median, 5 needles) were used. The OARs and HR-CTV for all the cases were contoured by an experienced BT physician on high resolution 3D T2-weighted MR images. 14 of the 36 cases had supplemental CT imaging using 1 mm slice thickness. Per the American Brachytherapy Society (ABS) and American Society for Radiation Oncology (ASTRO) cervix guidelines, all patients received external beam radiation therapy (EBRT) in 25 fractions at 1.8 Gy/fraction followed by a 5 fraction HDR BT boost using 5.5 Gy/fraction. [25]

### 4.2.3 Monte Carlo dose calculation

Conventional HDR BT and IMBT plans were calculated using RapidBrachyMC, [26] a benchmarked Monte Carlo based dose calculation software for BT applications based on the Geant4 toolkit. [27] The simulated HDR source was modeled after the Flexisource (Elekta Brachytherapy, Veenendaal, The Netherlands). The active core material was set to $^{192}$Ir ($E_{\gamma,avg}$) = 380 keV) for the conventional HDR BT plans and to $^{192}$Ir, $^{75}$Se ($E_{\gamma,avg}$) = 210 keV) or $^{169}$Yb ($E_{\gamma,avg}$) = 93 keV) for the IMBT plans. For the calculation of total treatment times, the activity for $^{192}$Ir was set to the standard 10 Ci. Activities for $^{75}$Se and $^{169}$Yb were set to 11.5 and 44 Ci, respectively, using knowledge of the active core dimensions of the Flexisource and conservative estimates of practical specific activities for the $^{75}$Se and $^{169}$Yb sources. [9, 28] In this work, $10^8$ decay events per dwell position were simulated for each radionuclide to ensure type A uncertainties below 1% and 2% in the 100% and 50% isodose volumes, respectively. Photon decay spectra from the Evaluated Nuclear Structure Data File was used. [29] Penelope low-energy electromagnetic physics list was used to simulate electromagnetic interactions. [30] Due to the low photon energies emitted from the simulated radionuclides, dose was approximated by the collisional kerma and scored using a track length estimator. [31] Parallel world formalism implemented in Geant4 was used for scoring with a 1 mm3 voxel resolution. [32] To assess the conventional and IMBT Dw,w distributions, the tandem was placed in the center of a $(50\ \text{cm})^3$ water phantom. A single dwell position halfway up the 8 cm long intrauterine shield was simulated for all radionuclides.

### 4.2.4 Patient modeling

The anonymized patient data including MR images in DICOM format, contours from DICOM RT Structure Set files and dwell positions extracted from DICOM RT Plan files were imported into RapidBrachyMCTPS, [26, 33] an in-house comprehensive BT research treatment planning software. For each case, the images were converted to voxelized phantoms in the egsphant format, [34] with 1 x 1 x 1 mm3 voxel size. The MR image slice thickness was 3 mm. Tissue composition assignment was performed based on the recommendations of TG-186. [15] Elemental composition and densities for the applicator materials were taken from the manufacturer. [35] For cases with only MR imaging, tissue materials and nominal tissue mass densities were assigned to the contoured organs. For cases with supplemental CT imaging, voxel-wise mass densities were set using the CT's Hounsfield Unit (HU) to density calibration curve. Elemental composition for the simulated tissues and material with the corresponding nominal densities are provided in Table A.1. The HU to density calibration curve is presented in Table A.2.

### 4.2.5 Simulations

To prepare the IC-BT plans (n=30), the original clinical treatment plans were used to define the dwell positions and source path geometries for all the applicators. Similarly, IC/IS-BT plans (n=6) were setup to use the clinical dwell positions for the applicator and needles. All IMBT plans were generated by first removing any needles and the conventional tandem, while clinical ring dwells were kept. Secondly, the IMBT dwell positions were generated by fusing the IMBT tandem applicator model to the planning MRI. IMBT tandem dwell positions were spaced 10 mm apart. The IMBT tandem was set to rotate at 22.5° increments, increasing the number of IMBT tandem dwells by a factor of 16. Dm,m was scored for all (IC, IC/IS & IMBT) patient simulations. Each IMBT case was simulated using each of the three candidate radionuclides ($^{192}$Ir, $^{75}$Se & $^{169}$Yb).

### 4.2.6 Plan Evaluation

Plans were optimized in RapidBrachyMCTPS using a fast mixed integer optimization algorithm based on mixed-integer quadratic programming. [36] To remove planner bias, all plans were optimized using the same parameters with no post-optimization manual editing. For all plans, the ring dwells were used per clinical protocol based on the Vienna experience, which emulates the

classical Fletcher loading. [37] The optimizer's uniformity constraint was used which reduces hot/cold regions along the tandem and helps achieve the "sculpted pear" which is the cornerstone of modern image-guided cervix BT. [38] Optimized dose distributions were normalized such that HR-CTV D90 equals the prescription dose (5.5 Gy/fx) to allow for a fair comparison between the various modality-radionuclides combinations. For plan evaluations, EBRT and BT doses were converted to 2 Gy-equivalent fractions (EQD2) using the linear-quadratic model, [39] and assuming $\alpha/\beta$ of 3 and 10 Gy for the OARs ($Gy_3$) and HR-CTV ($Gy_{10}$), respectively. Once OAR doses were compared, difference in HR-CTV coverage were assessed by re-normalizing plans such that either of the OARs reaches GEC-ESTRO constraints. [40] To quantify dose homogeneities, we define the dose homogeneity index (DHIx), as follows: DHIx=(V100-Vx)/Vx, where V100 and Vx are the volumes receiving at least 100% and x% of the prescribed dose, respectively. DHI does not include dose to the applicator. Differences in dose-volume histogram (DVH) metrics were evaluated for statistical significance using a paired sample t-test with a criterion of $P < 0.05$.

## 4.3 Results

The relative dose distributions from a conventional tandem with $^{192}$Ir as the radiation source and the developed IMBT tandem combined with $^{192}$Ir, $^{75}$Se and $^{169}$Yb radiation sources simulated in a water phantom are shown in Figure 4.2. The IMBT tandem reduces the dose on the shielded side at 1 cm from the center of the tandem down to 32.2%, 16.1% and 6.4% for $^{192}$Ir, $^{75}$Se and $^{169}$Yb, respectively. Evaluated at a radial distance of 1 cm, the beam-widths in the axial plane (tandem shield axis of rotation) for the IMBT tandem are 79°, 38° and 27° for $^{192}$Ir, $^{75}$Se and $^{169}$Yb, respectively. The conventional tandem has a beam-width of 360° due to the cylindrically symmetric, non-shielded, distribution. A full characterization of this IMBT tandem has been investigated in detail in a previous study. [8]

Dm,m distributions for conventional tandem HDR BT with $^{192}$Ir as the radiation source and the IMBT tandem with $^{192}$Ir, $^{75}$Se and $^{169}$Yb as radiation sources are shown in Figure 4.3 for case #22. The isodose lines in Figure 4.3 were least conformal to the HR-CTV for the conventional tandem and most conformal for IMBT. The conformality of IMBT increased with decreasing radiation source photon energy ($^{192}$Ir$\rightarrow^{75}$Se$\rightarrow^{169}$Yb), the same trend was observed for bladder sparing. When re-normalizing the plans such that the dose-limiting bladder reaches GEC-ESTRO dose constraint (90 $Gy_3$), the HR-CTV D90 is 81.7 $Gy_{10}$ for conventional $^{192}$Ir

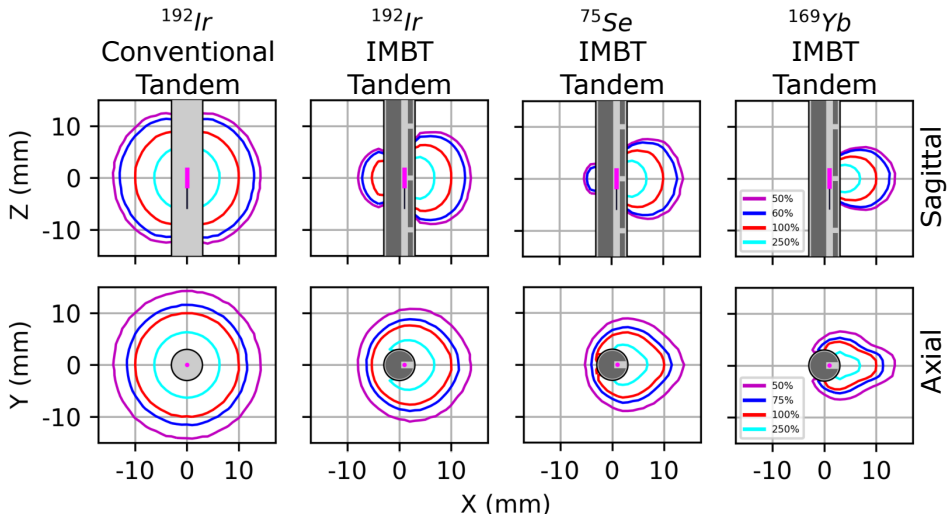


Figure 4.2: Relative Dw,w distributions, in a virtual water phantom, in the sagittal (top) and axial (bottom) planes of a conventional tandem (192Ir), intensity modulated brachytherapy tandem (192Ir, 75Se, 169Yb), from left to right. Dose distributions are normalized at 1 cm from the tandem center. The tandem, shield, and source are illustrated in light gray, dark gray, and magenta, respectively. Dose in the tandem is hidden for clarity.

BT and 87.6, 92.7 and 101.6 $Gy_{10}$ for $^{192}$Ir-, $^{75}$Se and $^{169}$Yb-based IMBT, respectively. For the simulated cohort of patients, the average total treatment times for conventional (10 Ci) $^{192}$Ir HDR BT was 6.0 $\pm$ 3.3 min compared to 10.3 $\pm$ 5.3 min, 19.9 $\pm$ 9.1 min and 14.0 $\pm$ 6.3 min for (10 Ci) $^{192}$Ir-, (11.5 Ci) $^{75}$Se- and (44 Ci) $^{169}$Yb-based IMBT, respectively.

Quantitative planning results of HR-CTV and OAR dose metrics for the reference $^{192}$Ir-based conventional IC-BT and $^{192}$Ir, $^{75}$Se and $^{169}$Yb-based IMBT are listed in Table 4.1. Overall, compared to conventional $^{192}$Ir IC-BT, the $^{192}$Ir, $^{75}$Se and $^{169}$Yb IMBT were significantly superior in terms of target coverage and OAR sparing. HR-CTV D98 and D90 were evaluated by renormalizing the plans up until either of the OARs reached GEC-ESTRO dose limits (bladder = 90 $Gy_3$, rectum/sigmoid = 75 $Gy_3$). HR-CTV D98 increased by 2.6%, 4.1% and 6.7% for IMBT with $^{192}$Ir, $^{75}$Se and $^{169}$Yb, respectively. Distributions of EQD2 DVH metrics (stratified by HR-CTV size) for IC-BT and IMBT techniques are shown in Figure 4.4. HR-CTV D90 was improved for $^{192}$Ir, $^{75}$Se and $^{169}$Yb IMBT plans by 2.2% (P=.002), 3.4% (P<.001) and 5.2% (P<.001), respectively, relative to IC-BT. IMBT HR-CTV D90 improves with increasing lateral extension relative to IC-BT with an average improvement of 4.5% as per Figure 4.4 (v). For equal HR-CTV D90 coverage, IMBT significantly (P<.001) reduced rectal D2cc relative to

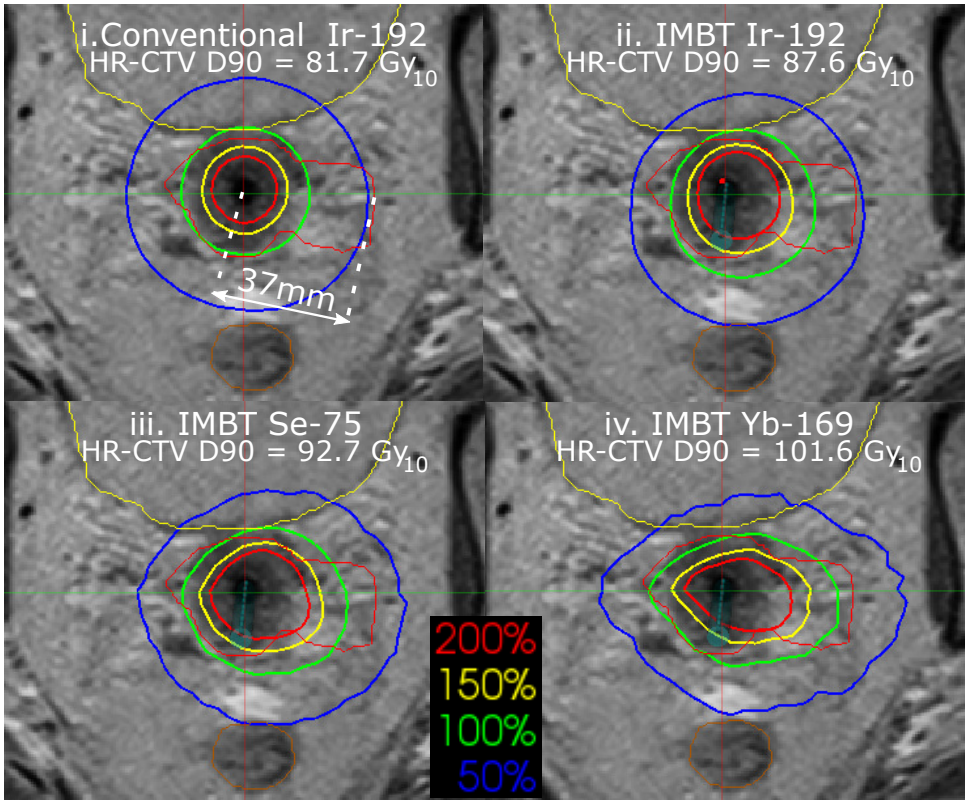


Figure 4.3: Optimized Dm,m distributions (limited to bladder constraint of 90 $Gy_3$) for (i) conventional BT with192Ir, (ii) intensity modulated brachytherapy (IMBT) with 192Ir, (iii) IMBT with 75Se, and (iv) IMBT with 169Yb. HR-CTV, bladder, and rectum and contoured in red, yellow and brown, respectively. The 100% isodose line is in green. Maximum achievable HR-CTV D90 (EQD2) is annotated in each panel and is calculated by setting bladder D2cc to 90 $Gy_3$ (GEC-ESTRO constraint). White arrow represents the HR-CTV's maximum transverse radius of 37 mm, measured from the center of the tandem. The IMBT tandem model is shown in teal in panels ii–iv.

IC-BT by 4.1%, 5.6% and 7.7% for $^{192}$Ir, $^{75}$Se and $^{169}$Yb-based IMBT, respectively. Sigmoid D2cc was significantly spared relative to IC-BT with a dose reduction of 1.4% (P=.032), 2.9% (P<.001) and 4.8% (P<.001) for $^{192}$Ir, $^{75}$Se and $^{169}$Yb-based IMBT, respectively. Similarly, bladder D2cc was reduced by 1.7%, 4.2% and 7.3% for $^{192}$Ir (P=.057), $^{75}$Se (P=.014) and $^{169}$Yb (P<.001) IMBT, respectively.

Table 4.2 lists the dosimetric indices for the subset of cases which had needles implanted (IC/IS-BT) and compares the conventional IC/IS-BT plans to needle-free IMBT. Additionally,

Table 4.1: DVH metrics for all IC-BT cases comparing conventional HDR BT (192Ir) to IMBT. OAR metrics are evaluated by setting HR-CTV D90 equal to the prescription. *HR-CTV metrics are evaluated by re-normalizing the plans until either of the three OARs hit their GEC-ESTRO dose constraint.

| Volume | Metric | Conv.192Ir IC-BT (Mean ± SD) | IMBT 192Ir (% change relative to Conv. IC-BT) | IMBT 75Se (% change relative to Conv. IC-BT) | IMBT 169Yb (% change relative to Conv. IC-BT) |
|---|---|---|---|---|---|
| HR-CTV | D98 | 83.4 ± 11.9 $Gy_{10}$ | 2.6% ± 0.3%<br>P = .002 | 4.1% ± 0.4%<br>P < .001 | 6.7% ± 0.5%<br>P < .001 |
| | D90 | 94.6 ± 11.2 $Gy_{10}$ | 2.2% ± 0.2%<br>P < .001 | 3.4% ± 0.3%<br>P < .001 | 5.2% ± 0.3%<br>P < .001 |
| Bladder | D2cc | 64.6 ± 11.6 $Gy_3$ | -1.7% ± 0.3%<br>P = .057 | -4.2% ± 0.7%<br>P = .014 | -7.3% ± 1.0%<br>P <.001 |
| Rectum | D2cc | 56.4 ± 9.5 $Gy_3$ | -4.1% ± 0.5%<br>P < .001 | -5.6% ± 0.5%<br>P < .001 | -7.7% ± 0.6%<br>P < .001 |
| Sigmoid | D2cc | 55.7 ± 9.4 $Gy_3$ | -1.4% ± 0.2%<br>P = .032 | -2.9% ± 0.4%<br>P < .001 | -4.8% ± 0.6%<br>P < .001 |

IC/IS plans were re-planned with the needles removed using the conventional IC-BT technique for comparison purposes. Relative to IC/IS-BT, conventional BT with the needles removed causes the plans to degrade with a 6.1% and 4.6% reduction in HR-CTV D98 and D90 coverage, and a 9.7% increase to bladder D2cc. Overall, needle-free $^{192}$Ir- and $^{75}$Se-based IMBT were not significantly different to IC/IS-BT aside from bladder D2cc which was increased by 8.1%. However, a 44% increase would be required to exceed GEC-ESTRO dose constraint for bladder. Needle-free IMBT with $^{169}$Yb lead to significantly improved plans relative to IC/IS-BT by reducing sigmoid D2cc by 1.9% and increasing HR-CTV D98 by 1.5%.

Dose homogeneities relative to conventional BT are summarized in Table 4.3. Changes to DHI150 were only significant for $^{169}$Yb-based IMBT with a minor change from 0.39 to 0.37 (P = .001). DHI200 decreased by 0.03 (P = .007) and 0.05 (P < .001) for $^{75}$Se- and $^{169}$Yb-based IMBT, respectively.

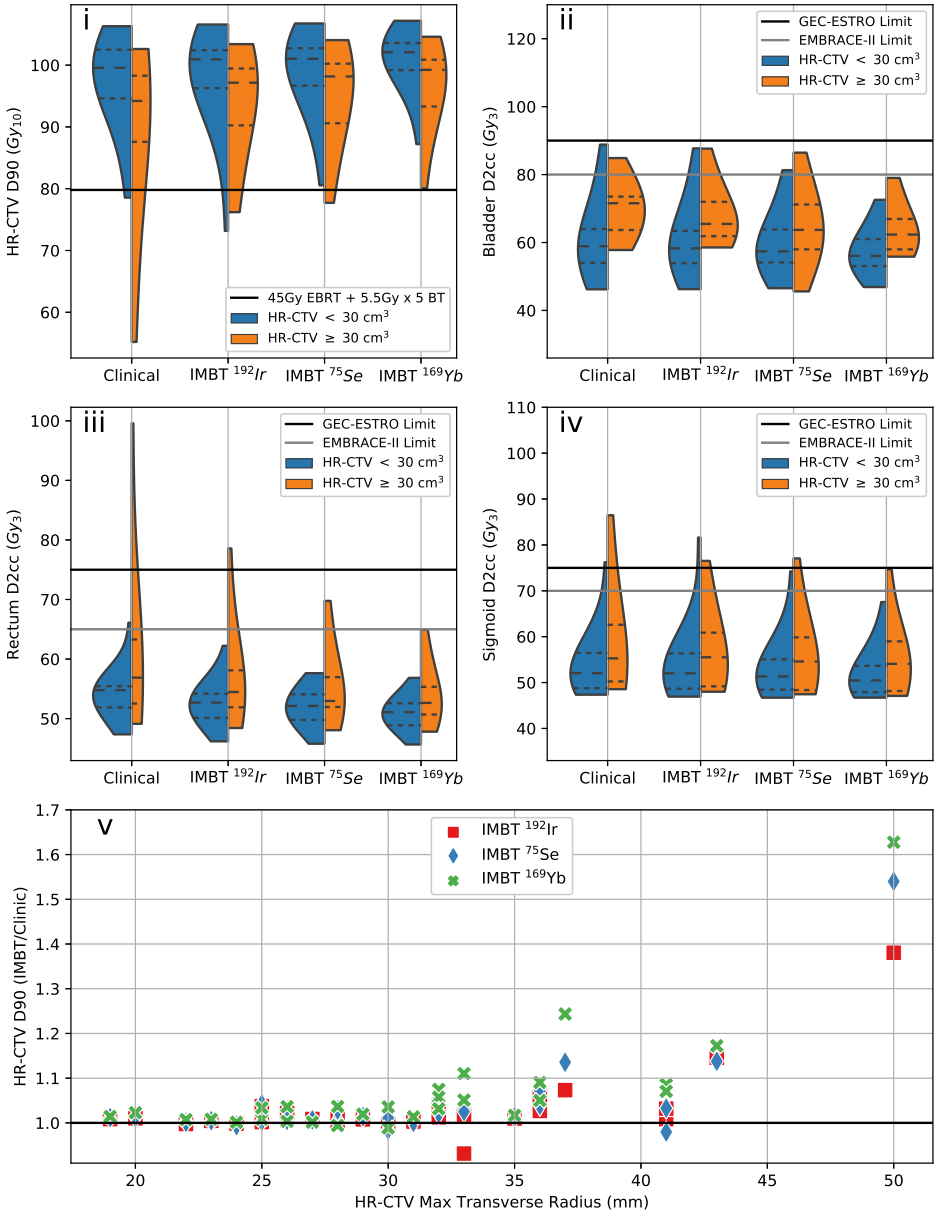


Figure 4.4: Distribution of EQD2 DVH metrics for conventional IC-BT and IMBT plans (i-iv). For each treatment type, distributions are split into large ($\geq$ 30 cm$^3$) and small ($<$ 30 cm$^3$) HR-CTV groups. Dashed lines are the distribution quartiles. Scatter plots of HR-CTV D90 IMBT/Clinical ratios for each radionuclide as a function of HR-CTV maximum transverse radius while respecting OAR dose constraints (v).

Table 4.2: DVH metrics for IC/IS-BT cases only. Conventional (IC/IS-BT) cases are compared to IMBT (192Ir, 75Se and 169Yb). Conventional cases were also re-planned with needles removed. OAR metrics are evaluated by setting HR-CTV D90 equal to the prescription. *HR-CTV metrics are evaluated by re-normalizing the plans until either of the three OARs hit their GEC-ESTRO dose constraint.

| Volume | Metric | Conv.192Ir IC/IS-BT (Mean ± SD) | Conv. 192Ir | IMBT 192Ir | IMBT 75Se | IMBT 169Yb |
|---|---|---|---|---|---|---|
| | | | Needles Removed (% change relative to Conv. IC/BT-BT) | | | |
| HR-CTV | D98* | 87.5 ± 11.3 $Gy_{10}$ | -6.1% ± 1.0% P = .038 | -2.6% ± 0.3% P = .112 | -1.1% ± 0.2% P = .099 | 1.5% ± 0.2% P = .034 |
| | D90* | 98.0 ± 10.4 $Gy_{10}$ | -4.6% ± 0.7% P= .044 | 1.5% ± 0.2% P= .161 | -0.6% ± 0.1% P = .272 | 0.7% ± 0.1% P = .274 |
| Bladder | D2cc | 62.4 ± 7.6 $Gy_3$ | 9.7% ± 1.6% P = .032 | 8.1% ± 1.4% P = .046 | 1.1% ± 0.2% P = .193 | 0.4% ± 0.1% P = .626 |
| Rectum | D2cc | 51.5 ± 2.2 $Gy_3$ | 7.1% ± 0.7% P = .052 | 3.1% ± 0.2% P = .084 | 1.6% ± 0.1% P = .266 | -0.7% ± 0.1% P = .631 |
| Sigmoid | D2cc | 54.9 ± 11.5 $Gy_3$ | 4.6% ± 1.2% P = .121 | 0.6% ± 0.1% P = .420 | -0.1% ± 0.1% P = .684 | -1.9% ± 0.4% P = .048 |

## 4.4 Discussion

An MRI-compatible IMBT delivery system has been realized in a practical tandem-based cervical applicator. To evaluate treatment plan dosimetry, the novel system was combined with the standardly available $^{192}$Ir source and two promising radionuclides in the high energy to intermediate range ($^{75}$Se, $^{169}$Yb). The study demonstrated that the IMBT tandem with either of the three investigated radionuclides ($^{192}$Ir, $^{75}$Se or $^{169}$Yb) achieves superior plans to conventional IC-BT over a wide range of HR-CTV volumes (8.2 to 113.8 $cm^3$). Compared to conventional IC-BT, IMBT improves the HR-CTV D90 and D98 by 2.2% to 5.2% and 2.6% to 6.7%, respectively, with the largest dosimetric enhancement when using $^{169}$Yb, followed by $^{75}$Se and then $^{192}$Ir.

Due to its lower average photon energy, $^{169}$Yb-based IMBT has the greatest modulation potential with a dose reduction of 93.6% at 1 cm from the tandem center on the shielded side and a narrow beam-width of 27° (Figure 4.2). $^{169}$Yb-based IMBT reduces the bladder D2cc by

Table 4.3: Dose homogeneity indices for conventional BT and IMBT.

| Metric | Conv. 192Ir | IMBT 192Ir | IMBT 75Se | IMBT 169Yb |
|---|---|---|---|---|
| DHI150 | 0.39 ± 0.05 | 0.39 ± 0.06<br>P = .878 | 0.38 ± 0.05<br>P = .209 | 0.37 ± 0.06<br>P = .001 |
| DHI200 | 0.63 ± 0.05 | 0.63 ± 0.06<br>P = .547 | 0.60 ± 0.05<br>P = .007 | 0.58 ± 0.07<br>P < .001 |

7% despite its frequent proximity to the target as demonstrated in Table 4.1 and Figure 4.3.

The developed IMBT tandem can deliver a highly conformal dose distribution with only a single tandem channel due to its novel rotating shield design. Safigholi et al. reported on a static DMBT tandem with 6 channels combined with two of the same radionuclides as this work, namely $^{192}$Ir and $^{169}$Yb, and observed that for HR-CTV volumes $\leq$ 30 cm$^3$, the OAR sparing potential of static DMBT showed little dependence on the source energy. [11] Their results are in contrast with our findings using the subset of cases with HR-CTV volumes $\leq$ 30 cm$^3$: Relative to $^{192}$Ir-based IMBT, $^{169}$Yb-based IMBT was capable of further reducing bladder, rectum and sigmoid D2cc by 5.8% (P=.002), 2.8% (P<.001) and 3.3% (P=.001), respectively. The superior results in this study are due to the single-channel rotating shield design which increases the amount of shielding material that can fit inside a 6 mm diameter tandem and is not limited to fixed emission directions.

Our applicator can generate highly anisotropic dose distributions and is not limited to lower energy radionuclides. Due to its design capabilities of housing a 5.4 mm diameter shield, even $^{192}$Ir-based IMBT can improve tumor coverage and OAR sparing. Hopfensperger et al. reported on a rotating helical multi-shielded tandem applicator capable of housing a pair of 1.25 mm thick platinum shields and requires a custom 0.6 mm diameter $^{169}$Yb source for appreciable dose modulation. [41] The authors did not report statistical significance for differences in dose but showed that 86% of their plans met constraints compared to 84% for IC/IS-BT plans. By comparison, our IMBT system with $^{169}$Yb, led to 100% of the evaluated cases meeting dose constraints, an 11% improvement relative to non-IMBT. In this work, we use fixed optimization parameters for all cases and prohibit further fine-tuning. This leads to plans which may not be optimal but avoids introducing planner bias. To the best of our knowledge, this study is the first to investigate the dosimetric impact of tandem-based IMBT while taking into consideration

patient heterogeneities and attenuation of ring/ovoid dwells due to the nearby shielded tandem.

Our IMBT delivery system combined with $^{169}$Yb was capable of significantly increasing the HR-CTV D98 by 1.5% and reducing sigmoid D2cc by 1.9% for IC/IS-BT cases. All other metrics were non-inferior to conventional IC/IS-BT, without using a single needle (Table 4.2). $^{192}$Ir- and $^{75}$Se- based IMBT were non-inferior to conventional IC/IS-BT except for $^{192}$Ir-based IMBT, which increased bladder D2cc by 8.1%. In the case of $^{192}$Ir-based IMBT, dose increase to the bladder would have brought the cohort mean total EQD2 bladder D2cc to 67.5 $Gy_3$, which is still 22.5 $Gy_3$ and 12.5 $Gy_3$ below GEC-ESTRO and EMBRACE-II dose limits, respectively. Given infinite time and resources, large samples are always preferred. However, it should come as no surprise to the informed reader that the paired t-test functions properly for modest sample sizes. In fact, the t-test was develop specifically for working with small sample sizes. [42] Despite the reduced statistical power, meaningful differences between IC/IS-BT and IC-BT or IMBT were still detected. The potential to replace IC/IS-BT with IMBT would obviate the need for complex implantation, reducing anesthesia and procedure times, and organ and/or blood vessel perforation. This novel BT modality could transform advanced IC/IS-BT into a minimally invasive out-patient procedure and supports a prospective clinical trial for carefully selected patients.

Patients with lateral extension greater than a radius of 30 mm benefitted most from $^{169}$Yb IMBT. Despite the lower energy of $^{169}$Yb, the modest decrease in DHI150 and DHI200 (0.02 and 0.05, relative to conventional $^{192}$Ir-based BT) is due to its favorable radial dose function. [8] It is important to note that due to the absence of needles, the IMBT dose is hottest in the center of the cervix and not in normal tissue. To put this in perspective, Kirisits et al. noted an increase to the 200% isodose volume from 25 to 33 $cm^3$, a 32% change, when adding interstitial needles to the tandem and ring. [43]

MRI-based dosimetry was used in this study. However, Shoemaker et al. showed in a previous study that when performing MRI-based planning, the loss of CT-density data will not have a clinically significant effect on dosimetry, as long as material elemental compositions and nominal mass densities are correctly assigned to each contoured structure and implanted objects such as shields and applicators. [13]

Treatment times with $^{192}$Ir-based IMBT would increase by a factor of 1.7, from 6.0 mins to 10.3 mins. For $^{75}$Se and $^{169}$Yb, treatments would be delivered in 19.9 mins and 14.0 mins

respectively, due to the high specific activity of these sources despite their lower energies. $^{75}$Se has a half-life of 118.5 days, more than 1.5 times that of $^{192}$Ir, making it a very attractive source from a financial and logistic perspective. $^{169}$Yb suffers from a shorter half-life (32 days) and may require more frequent source changes. For a clinic with high BT load, the dosimetric benefits of $^{169}$Yb could very well outweigh the costs of monthly source changes due to the ability to treat patients needle-free, on an out-patient basis. Delivery times can be reduced by using dual-source delivery (simultaneous ring and tandem delivery), which in theory, is possible with the Flexitron (Elekta Brachytherapy, Veenendaal, The Netherlands) afterloader. However, significant time savings would only be substantial for either patients with a short tandem (ring contribution increases) or patients with symmetric tumors requiring minimal IMBT modulation. Dual-source IMBT with two different radionuclides could provide another benefit in the form of energy modulation and will be the focus of a separate work.

## 4.5 Conclusions

$^{192}$Ir- and $^{75}$Se-based IMBT represents a superior alternative to conventional IC-BT with even greater improvements with $^{169}$Yb. Compared to IC/IS-BT, needle-free IMBT with $^{169}$Yb improve tumor coverage and OAR sparing;$^{75}$Se proved non-inferior; and $^{192}$Ir lead to clinically acceptable plans. The ability to deliver a conformal, OAR-sparing dose without a single interstitial needle is an exciting avenue towards improving local control and reducing morbidity in cervical cancer patients. IMBT could be the technological breakthrough that could revolutionize BT in the way multi-leaf collimators did for EBRT. This novel technology may aid in reversing the declining BT utilization rates and revitalize this life-saving modality.

**Acknowledgements:** The project is funded by the Collaborative Health Research Projects (#248490) and the Natural Sciences and Engineering Research Council of Canada (#241018). Computations were made on the supercomputers MP2 and Graham managed by Calcul Québec and Compute Canada. The operation of these supercomputers are funded by the Canada Foundation for Innovation (CFI), the ministère de l'Économie, de la science et de l'innovation du Québec (MESI) and the Fonds de recherche du Québec - Nature et technologies (FRQ-NT)
**Conflict of interest:** None.
**Supplementary material:** Supplementary material for this article can be found in Appendix A.

# References

[1] Holschneider CH, Petereit DG, Chu C. Brachytherapy: A critical component of primary radiation therapy for cervical cancer: From the Society of Gynecologic Oncology (SGO) and the American Brachytherapy Society (ABS. Brachytherapy;18:123–132. Available from: https://doi.org/10.1016/J.BRACHY.2018.11.009.

[2] Cho LP, Manuel M, Catalano P. Outcomes with volume-based dose specification in CT-planned high-dose-rate brachytherapy for stage I-II cervical carcinoma: A 10-year institutional experience. Gynecol Oncol;143:545–551. Available from: https://doi.org/10.1016/J.YGYNO.2016.09.017.

[3] Kang HC, Shin KH, Park SY, Kim JY. 3D CT-based high-dose-rate brachytherapy for cervical cancer: Clinical impact on late rectal bleeding and local control. Radiother Oncol;97:507–513. Available from: https://doi.org/10.1016/J.RADONC.2010.10.002.

[4] Tanderup K, Fokdal LU, Sturdza A. Effect of tumor dose, volume and overall treatment time on local control after radiochemotherapy including MRI guided brachytherapy of locally advanced cervical cancer. Radiother Oncol;120:441–446. Available from: https://doi.org/10.1016/j.radonc.2016.05.014.

[5] Petereit DG, Frank SJ, Viswanathan AN. Brachytherapy: Where Has It Gone? J Clin Oncol;33:980–982. Available from: https://doi.org/10.1200/JCO.2014.59.8128.

[6] Safigholi H, Han DY, Soliman A, Song WY. Direction modulated brachytherapy (DMBT) tandem applicator for cervical cancer treatment: Choosing the optimal shielding material. Med Phys;45:3524–3533. Available from: https://doi.org/10.1002/mp.13030.

[7] Dadkhah H, Kim Y, Wu X, Flynn RT. Multihelix rotating shield brachytherapy for cervical cancer. Med Phys;42:6579–6588. Available from: https://doi.org/10.1118/1.4933244.

[8] Morcos M, Enger SA. Monte Carlo dosimetry study of novel rotating MRI-compatible shielded tandems for intensity modulated cervix brachytherapy. Phys Medica;71:178–184. Available from: https://doi.org/10.1016/j.ejmp.2020.02.014.

[9] Famulari G, Duclos M, Enger SA. A novel 169Yb-based dynamic-shield intensity modulated brachytherapy delivery system for prostate cancer. Med Phys;47:859–868. Available from: https://doi.org/10.1002/mp.13959.

[10] Webster MJ, Devic S, Vuong T. Dynamic modulated brachytherapy (DMBT) for rectal cancer. Med Phys;40. Available from: https://doi.org/10.1118/1.4769416.

[11] Safigholi H, Yup Han D, Mashouf S. Direction modulated brachytherapy (DMBT) for treatment of cervical cancer: A planning study with 192 Ir, 60 Co, and 169 Yb HDR sources;. Available from: https://doi.org/10.1002/mp.12598.

[12] Adams QE, Xu J, Breitbach EK. Interstitial rotating shield brachytherapy for prostate cancer. Med Phys;41(051703). Available from: https://doi.org/10.1118/1.4870441.

[13] Shoemaker T, Vuong T, Glickman H, Kaifi S, Famulari G, Enger SA. Dosimetric Considerations for Ytterbium-169, Selenium-75, and Iridium-192 Radioisotopes in High-Dose-Rate Endorectal Brachytherapy. Int J Radiat Oncol;105:875–883. Available from: https://doi.org/10.1016/J.IJROBP.2019.07.003.

[14] Famulari G, Alfieri J, Duclos M, Vuong T, Enger SA. Can intermediate-energy sources lead to elevated bone doses for prostate and head & neck high-dose-rate brachytherapy? Brachytherapy;19:255–263. Available from: https://doi.org/10.1016/j.brachy.2019.12.004.

[15] Beaulieu L, Carlsson-Tedgren A, Carrier JF. Report of the Task Group 186 on model-based dose calculation methods in brachytherapy beyond the TG-43 formalism: Current status and recommendations for clinical implementation. Med Phys;39:6208–6236. Available from: https://doi.org/10.1118/1.4747264.

[16] Reynolds SA. Theoretical and Practical Specific Activities and Other Properties of Common Radionuclides. Oak Ridge;. TN (United States); 1973. Available from: https://doi.org/10.2172/4535530.

[17] Hetherington ELR, Wood NR. Australian Atomic Energy Commission. Research Establishment. The Production of Ytterbium-169 Radiography Sources in a High Flux Reactor. Australian Atomic Energy Commission Research Establishment.

[18] Flynn RT, Adams QE, Hopfensperger KM, Wu X, Xu W, Kim Y. Efficient 169 Yb high-dose-rate brachytherapy source production using reactivation. Med Phys;46:mp.13563. Available from: https://doi.org/10.1002/mp.13563.

[19] Morcos M, Enger SA. MR-Compatible Intensity Modulated Brachytherapy Applicator for Cervical Cancer. Brachytherapy;18:S21–S22. Available from: https://doi.org/10.1016/j.brachy.2019.04.049.

[20] Lide DR. CRC Handbook of Chemistry and Physics. vol. 128. 86th ed. David R, editor. Boca Raton, FL: American Chemical Society;. Available from: https://doi.org/10.1021/ja059868l.

[21] Soliman AS, Elzibak A, Easton H. Quantitative MRI assessment of a novel direction modulated brachytherapy tandem applicator for cervical cancer at 1.5 T. Radiother Oncol;120:500–506. Available from: https://doi.org/10.1016/j.radonc.2016.07.006.

[22] Elzibak AH, Kager PM, Soliman A. Quantitative CT assessment of a novel direction-modulated brachytherapy tandem applicator. Brachytherapy;17:465–475. Available from: https://doi.org/10.1016/j.brachy.2017.10.006.

[23] Famulari G, Enger SA. A Novel Intensity Modulated High Dose Rate Brachytherapy Delivery System with 169 Yb. Int J Radiat Oncol;99:E657. Available from: https://doi.org/10.1016/j.ijrobp.2017.06.2187.

[24] Famulari G, Enger SA. Intensity modulated brachytherapy system for dynamic modulation of shielded catheters. Radiother Oncol;127:S90.

[25] Viswanathan AN, Beriwal S, De Los Santos JF. American Brachytherapy Society consensus guidelines for locally advanced carcinoma of the cervix. Brachytherapy;11:47–52. Available from: https://doi.org/10.1016/J.BRACHY.2011.07.002.

[26] Famulari G, Marc-AndréRenaud CMP, Evans MDC, Seuntjens J, Enger SA. RapidBrachyMCTPS: a Monte Carlo-based treatment planning system for brachytherapy applications. Phys Med Biol;63(175007). Available from: https://doi.org/10.1088/1361-6560/aad97a.

[27] Agostinelli S, Allison J, Amako K. Geant4—a simulation toolkit. Nucl Instruments Methods Phys Res Sect A Accel Spectrometers. Detect Assoc Equip;506:250–303. Available from: https://doi.org/10.1016/S0168-9002(03)01368-8.

[28] Weeks KJ, Schulz RJ. Selenium-75 : A potential source for use in high-activity brachytherapy irradiator. Med Phys;13:728–731.

[29] File TJENSD;. Online]. Available:. Available from: http://www.nndc.bnl.gov/ensdf/.

[30] Geant4 Collaboration Physics lists for electromagnetic processes;. Available at. Available from: http://geant4.web.cern.ch/geant4/collaboration/workinggroups/electromagnetic/physlist.shtml.

[31] Williamson JF. Monte Carlo evaluation of kerma at a point for photon transport problems. Med Phys;14:567–576. Available from: https://doi.org/10.1118/1.596069.

[32] Enger SA, Landry G, D'Amours M. Layered mass geometry: A novel technique to overlay seeds and applicators onto patient geometry in Geant4 brachytherapy simulations. Phys Med Biol;57:6269–6277. Available from: https://doi.org/10.1088/0031-9155/57/19/6269.

[33] Glickman H, Antaki M, Deufel C, Enger SA. RapidBrachyMCTPS 2.0: A Comprehensive and Flexible Monte Carlo-Based Treatment Planning System for Brachytherapy Applications;. ArXiv Prepr arXiv200702902 2020.

[34] Walters B, Kawrakow I, Rogers DWO, et al. DOSXYZnrc users manual. Nrc Rep Pirs;794:1–125.

[35] E ABNBVS. Oncentra Brachy v4.6. Physics and Algorithms;.

[36] Antaki M, Deufel C, Enger SA. Fast mixed integer optimization (FMIO) for high dose rate brachytherapy. Phys Med & Biol.

[37] Kirisits C, Pötter R, Lang S, Dimopoulos J, Wachter-Gerstner N, Georg D. Dose and volume parameters for MRI-based treatment planning in intracavitary brachytherapy for cervical cancer. Int J Radiat Oncol Biol Phys;62:901–911. Available from: https://doi.org/10.1016/j.ijrobp.2005.02.040.

[38] Viswanathan AN, Erickson BA. Seeing is saving: The benefit of 3D imaging in gynecologic brachytherapy;. Available from: https://doi.org/10.1016/j.ygyno.2015.02.025.

[39] Dale RG. The application of the linear-quadratic dose-effect equation to fractionated and protracted radiotherapy. Br J Radiol;58:515–528. Available from: https://doi.org/10.1259/0007-1285-58-690-515.

[40] Haie-Meder C, Pötter R, Van Limbergen E. Recommendations from Gynaecological (GYN) GEC-ESTRO Working Group (I): concepts and terms in 3D image based 3D treatment planning in cervix cancer brachytherapy with emphasis on MRI assessment of

GTV and CTV. Radiother Oncol;74:235–245. Available from: https://doi.org/10.1016/J.RADONC.2004.12.015.

[41] Hopfensperger KM, Adams Q, Kim Y. Needle-Free Cervical Cancer Treatment Using Helical Multi-Shield Intracavitary Rotating Shield Brachytherapy with the 169;. Yb Isotope. Med Phys February 2020. Available from: https://doi.org/10.1002/mp.14101.

[42] Lehmann EL. Student" and Small-Sample Theory. In: Selected Works of E;. Available from: https://doi.org/10.1007/978-1-4614-1412-4_83.

[43] Kirisits C, Lang S, Dimopoulos J, Berger D, Georg D, Pötter R. The Vienna applicator for combined intracavitary and interstitial brachytherapy of cervical cancer: Design, application, treatment planning, and dosimetric results. Int J Radiat Oncol;65:624–630. Available from: https://doi.org/10.1016/J.IJROBP.2006.01.036.

# Chapter 5

# On the impact of absorbed dose specification, tissue heterogeneities and applicator heterogeneities on Monte Carlo-based dosimetry of Ir-192, Se-75 and Yb-169 in conventional and intensity modulated brachytherapy for the treatment of cervical cancer

**Morcos, M.**, Viswanathan, A.N., Enger, S.A., 2021.
*Medical physics*, 48(5), pp.2604-2613.
https://doi.org/10.1002/mp.14802

# Abstract

**Purpose:** The purpose of this study was to evaluate the impact of dose reporting schemes and tissue/applicator heterogeneities for $^{192}$Ir-, $^{75}$Se- and $^{169}$Yb-based MRI guided conventional and intensity modulated brachytherapy.

**Materials and methods:** Treatment plans using a variety of dose reporting and tissue/applicator segmentation schemes were generated for a cohort (n = 10) of cervical cancer patients treated with $^{192}$Ir-based Venezia brachytherapy. Dose calculations were performed using RapidBrachyMCTPS, a Geant4-based research Monte Carlo treatment planning system. Ultimately, five dose calculation scenarios were evaluated: (1) dose to water in water (Dw,w); (2) Dw,w taking the applicator material into consideration (Dw,wApp); (3) dose to water in medium (Dw,m); (4,5) dose to medium in medium with mass-densities assigned either nominally per structure (Dm,m (Nom)) or voxel-by-voxel (Dm,m).

**Results:** Ignoring the plastic Venezia applicator (Dw,wApp) overestimates Dm,m by up to 1% (average) with high energy source ($^{192}$Ir and $^{75}$Se) and up to 2% with $^{169}$Yb. Scoring dose to water (Dw,wApp or Dw,m) generally overestimates dose and this effect increases with decreasing photon energy. Reporting dose other than Dm,m (or Dm,m Nom) for $^{169}$Yb-based conventional and intensity modulated brachytherapy leads to a simultaneous overestimation (up to 4%) of CTVHR D90 and underestimation (up to 2%) of bladder D2cc due to a significant dip in the mass-energy absorption ratios at the depths of nearby targets and OARs. Using a nominal mass-density assignment per structure, rather than a CT-derived voxel-by-voxel assignment for MRI guided brachytherapy amounts to a dose error up to 1% for all radionuclides considered.

**Conclusions:** The effects of the considered dose reporting schemes trend correspondingly between conventional and intensity modulated brachytherapy. In the absence of CT-derived mass-densities, MRI-only based dosimetry can adequately approximate Dm,m by assigning nominal mass-densities to structures. Tissue and applicator heterogeneities do not significantly impact dosimetry for $^{192}$Ir and $^{75}$Se, but do for $^{169}$Yb, dose reporting must be explicitly defined since Dw,m and Dw,w may overstate the dosimetric benefits.

## 5.1 Introduction

Despite it being close to a decade since the American Association of Physicists in Medicine (AAPM) Task Group (TG)-186 [1] on model-based dose calculation algorithms (MBDCAs) in brachytherapy was published, adoption of these algorithms is still limited to documentation in parallel to the clinically used TG-43 [2] calculated dose. The TG-43 formalism describes the absorbed dose around a single source placed at the center of a water phantom with uniform density reported as the dose to water in water, herein referred to as Dw,w, where radiation transport occurs in water and absorbed dose is scored to a small water volume surrounded by water. In brachytherapy, clinical experience is based on the Dw,w dose reporting scheme, which ignores the influence of patient and applicator heterogeneities, intersource attenuation and finite patient dimensions. MBDCAs, which can handle the aforementioned effects are likely to correlate better with clinical outcomes. MBDCAs require voxel-by-voxel assignment of tissue mass-densities and elemental compositions to obtain interaction cross-sections and inherently calculate dose to medium in medium herein referred to as Dm,m, where radiation transport occurs in the medium and absorbed dose is scored to a small volume of the medium surrounded by medium.

An active area of research and innovation in brachytherapy is the use of static and dynamic high Z metal shields for intensity modulated brachytherapy (IMBT) [3–6]. In addition to the ubiquitous $^{192}$Ir high dose rate (HDR) brachytherapy source with an average photon energy ($E_{\gamma,avg}$) of 380 keV, alternative lower energy sources such as $^{75}$Se ($E_{\gamma,avg}$ = 210 keV) and $^{169}$Yb ($E_{\gamma,avg}$ = 93 keV) have been investigated due to their potential to maximize the modulation capabilities of IMBT due to their lower photon energies [3, 4, 7, 8]. The impact of tissue/applicator heterogeneities and dose reporting schemes (Dw,w vs. Dm,m) on gynecologic brachytherapy have only been investigated for high energy sources. Desbiens et al. showed that taking tissue and applicator heterogeneities into account have little (1%) impact on target and OAR DVH metrics for patients treated with $^{192}$Ir-based Syed-Neblett implants [9]. To the best of our knowledge, there have been no investigations bridging the gap between TG-43 and MBDCAs for cervical cancer patients treated with brachytherapy using high Z shield or intermediate energy sources such as $^{169}$Yb.

MBDCAs are also capable of reporting absorbed dose to water in medium, Dw,m, where radiation transport occurs in the medium but absorbed dose is scored to a small water volume

surrounded by the medium. Dw,m is a theoretical construct derived from an appropriate cavity theory [10, 11]. In external beam radiotherapy (EBRT), the arguments in favor of Dw,m are that current clinical knowledge is based on dose to water and that it is a simple surrogate for the cell nucleus dose [12]. In brachytherapy, however, the differences in tissue types relative to water in terms of mass-energy absorption coefficients can lead to significant differences between Dm,m and Dw,m due to the increasing importance of the photoelectric effect and merit site-specific investigations [1].

The aim of this study was to evaluate the calculated dose in $^{192}$Ir, $^{75}$Se and $^{169}$Yb based MR image guided conventional HDR brachytherapy as well as dynamic shield IMBT for treatment of cervical cancer by investigating the influence of source decay spectra and patient/applicator material heterogeneities on dosimetry using a variety dose calculation methods, dose reporting and tissue segmentation schemes.

## 5.2 Materials and methods

### 5.2.1 Clinical Protocol

Ten cervical cancer patients treated with intracavitary brachytherapy using the Venezia hybrid applicator (Elekta Brachytherapy, Veenendaal, The Netherlands) were used for this retrospective study. The median high-risk clinical target volume (CTVHR) was 31.5 cm3 (range: 19.9-76.0 cm3). The organs at risk (OAR) and CTVHR were contoured by an experienced brachytherapy physician on high resolution 3D T2-weighted MR images. Tissue densities were determined using CT images, which were acquired with the patient on a transfer system (Zephyr XL; Diacor, Inc., Salt Lake City, UT) used in our practice and described in detail along with the rest of the clinical workflow elsewhere [13]. Per the American Society for Radiation Oncology (ASTRO) cervix guidelines, all patients received EBRT in 25 fractions at 1.8 Gy/fraction followed by a 5 fraction HDR brachytherapy boost using 5.5 Gy/fraction [14].

### 5.2.2 Monte Carlo Simulations

Plans were calculated using RapidBrachyMC [15], an open-source and benchmarked Monte Carlo based dose calculation software for brachytherapy applications based on the Geant4 toolkit [16]. Conventional HDR brachytherapy plans were prepared by first aligning the Venezia

applicator model to the image set. IMBT plans contain a 5.4 mm diameter MR-compatible rotating pure tungsten shield embedded inside a modified, 6 mm wide, Venezia tandem (ring/lunar ovoids were unmodified) [3, 17]. The simulated HDR source was modeled after the clinically used Flexisource (Elekta Brachytherapy, Veenendaal, The Netherlands) and implemented into RapidBrachyMC using layered mass geometry [18]. The active core material was set to either $^{192}$Ir, $^{75}$Se or $^{169}$Yb for all plans. In this work, 108 decay events per dwell position were simulated for each radionuclide to ensure type A uncertainties between 0.3% and 1% for most voxels of interest (used for calculating dose-volume metrics of interest). Up to 2% uncertainty was observed for cases where the OAR was further than the implant (e.g. bowel, bone). The Monte Carlo simulation methods are summarized in Table B.3 as recommended by TG-268 [19]. A detailed uncertainty analysis for the voxels used for calculating dose-volume metrics are presented in Table B.4. Photon decay spectra from the Evaluated Nuclear Structure Data File were used [20]. Penelope low-energy electromagnetic physics list was used to simulate electromagnetic interactions [21]. Dose was approximated as collision kerma and track length estimation was used [22].

### 5.2.3 Patient & Applicator Modeling

The anonymized patient DICOM data were imported into RapidBrachyMCTPS [15, 23, 24], an in-house comprehensive brachytherapy research treatment planning software. Physician-defined contours were assigned a tissue composition according to ICRU 46 [25] and either a nominal or voxel-by-voxel mass-density was assigned using the segmentation schemes described in Table 5.1. All contours were post-processed to remove any overlap with the applicator as suggested by Desbiens et al. [9]. For each segmentation scheme, images were converted to voxelized phantoms in the egsphant format [26], with 1 x 1 x 1 mm$^3$ voxel size.

The first segmentation scheme (Seg-1) assumes that all voxels are water with unit density, calculations using Seg-1 naturally yield Dw,w. Seg-2 still assumes the patient is unit-density water but takes into consideration the applicator (Dw,w-App) material by using manufacturer supplied material and nominal density. In the case of conventional BT, the applicator contains no shielding. In the case of IMBT the intra-tandem tungsten shield is assigned as tungsten with a nominal density. Seg-3 is used to obtain Dm,m and Dw,m by assigning tissue, applicator and shield materials and by using a nominal density ($\rho$Nom) for the entire structure. In Seg-4,

Table 5.1: Material and density assignments for the different dose reporting/segmentation schemes (detailed elemental composition and density values included in the supplementary materials Table B.1).

| | Seg-1 (Dw,w) | | Seg-2 (Dw,w-App) | | Seg-3 (Dm/w,m $\rho$Nom) | | Seg-4 (Dm/w,m $\rho$CT) | |
|---|---|---|---|---|---|---|---|---|
| Contour | Material | Density (g/cm3) | Material | Density (g/cm3) | Material | Density (g/cm3) | Material | Density interquartile range, (g/cm3) |
| Body | Water | 0.998 | Water | 0.998 | FST | 1.02 | FST | 0.94-1.04 |
| CTVHR | Water | 0.998 | Water | 0.998 | FST | 1.02 | FST | 0.93-1.04 |
| Bladder | Water | 0.998 | Water | 0.998 | Bl | 1.03 | Bl | 0.95-1.01 |
| Rectum | Water | 0.998 | Water | 0.998 | Rc | 1.03 | Rc | 0.91-1.04 |
| Sigmoid | Water | 0.998 | Water | 0.998 | Rc | 1.03 | Rc | 0.93-1.05 |
| Bowel | Water | 0.998 | Water | 0.998 | Rc | 1.03 | Rc | 0.95-1.05 |
| Bone | Water | 0.998 | Water | 0.998 | CB | 1.92 | CB | 1.17-1.41 |
| Venezia | Water | 0.998 | PPSU/FG | 1.29/2.10 | PPSU/FG | 1.29/2.10 | PPSU/FG | 1.29/2.10 |
| IMBT Shield | N/A | N/A | Tungsten | 19.3 | Tungsten | 19.3 | Tungsten | 19.3 |

FST = Female Soft Tissue; Bl = Bladder; Rc = Rectum; CB = Cortical Bone
$\rho$Nom = Nominal density; $\rho$CT = CT-derived density; PPSU = Polysulfone; FG = Fiberglass; N/A = Not Applicable

materials are specified as per Seg-3, but mass-densities are derived from a CT Hounsfield unit (HU) to density calibration curve and assigned voxel-by-voxel ($\rho$CT). Mass-energy absorption coefficients ($\mu_{en}/\rho$) were generated using the "g" usercode developed by the National Research Council of Canada, EGSnrc [27], and is described in further detail elsewhere [28]. Specific elemental compositions, nominal tissue densities and the HU calibration curve are presented in the supplementary materials (Table B.1).

### 5.2.4 Dosimetric Evaluation

Dose-volume-histogram (DVH) indices recommended by ASTRO [14] were calculated for all treatment plans. For DVH calculation, RapidBrachyMCTPS considers voxels inside the polygon contour and doses are binned by 0.1 Gy increments [23]. For the conventional brachytherapy plans, the clinical plan dwell weights were used. For the IMBT version of those plans, the tandem shield rotated at 22.5° increments, and a simple pear-shaped distribution was achieved. D98 and D90 for CTVHR and D2cc for all OAR (bladder, rectum, sigmoid, bowel, pelvic bone) were taken from DVHs where Dx is defined as the minimum dose received by x% of the structure volume and Dvcc is the minimum dose to the most irradiated v cm3 of the structure.

To evaluate dosimetric changes resulting from the presence of the applicator in conventional brachytherapy, the percent difference between Dw,w and Dw,w-App was calculated. The comparison between Dw,w and Dw,w-App was not evaluated for IMBT since the radiation is attenuated and/or collimated in all directions. This is in contrast with static shielding techniques used in endorectal brachytherapy where calculating Dw,w to the CTV and ignoring the contra-

lateral tungsten shield leads to only 4% difference relative to and Dw,w-App. [29] Taking the applicator into account, the effect of ignoring the patient heterogeneities was studied by looking at the percent difference between Dm,m ($\rho$CT) and Dw,w-App. The effect of scoring dose to a small mass of water as opposed to medium was quantified by taking the percent difference between Dw,m ($\rho$CT) and Dm,m ($\rho$CT). Similarly, to isolate the effect of using a nominal versus CT-derived density, Dm,m ($\rho$Nom) was compared to Dm,m ($\rho$CT). Statistical significance was determined using a paired t-test using a criterion of P<.05.

## 5.3 Results

Figures 1 and 2 present box plots of dose reporting comparisons CTVHR and OAR, respectively, stratified by radionuclide and by delivery technique i.e. conventional brachytherapy and IMBT. All box plots are relative to Dm,m ($\rho$Nom). Tables 5.2 to 5.5 summarize key results highlighting the effects of various dose reporting and mass density assignment schemes on CTVHR and OAR dosimetric indices. Figures 3 and 4 illustrate the impact of the various absorbed dose specification, tissue/applicator heterogeneities methods in combination with $^{192}$Ir, $^{75}$Se and $^{169}$Yb for conventional and IMBT, respectively.

The effects of ignoring the Venezia applicator material are presented in Table 5.2. Ignoring the applicator material overestimates CTVHR D90 coverage by 0.2±0.0%, 0.2±0.0% and 0.7±0.1% for $^{192}$Ir, $^{75}$Se and $^{169}$Yb, respectively (P<.001). A similar trend for OAR is observed with D2cc being overestimated by up to 1.9% and the largest affect occurring when using $^{169}$Yb, which is the lowest energy radionuclide simulated.

The effect of ignoring patient heterogeneities (Dw,w-App) overestimates Dm,m by up to 1% and 2% to non-bone tissues for $^{192}$Ir- and $^{75}$Se-based brachytherapy, respectively (Table 5.3). With the exception of bladder, Dw,w-App overestimates non-bone tissues by up to 4% when using $^{169}$Yb. Dose to bone is underestimated by up to 7% (P=.004), 29% (P<.001) and 63% (P<.001) for $^{192}$Ir, $^{75}$Se and $^{169}$Yb, respectively. By comparison, dose to bone for IMBT cases is underestimated by up to 5% (P=.019), 23% (P<.001) and 56% (P=.001) for $^{192}$Ir, $^{75}$Se and $^{169}$Yb, respectively.

The differences between the dose reporting schemes Dw,m and Dm,m are summarized in Table 5.4. Dw,m underestimates Dm,m to bone by approximately 7% for $^{192}$Ir and up to

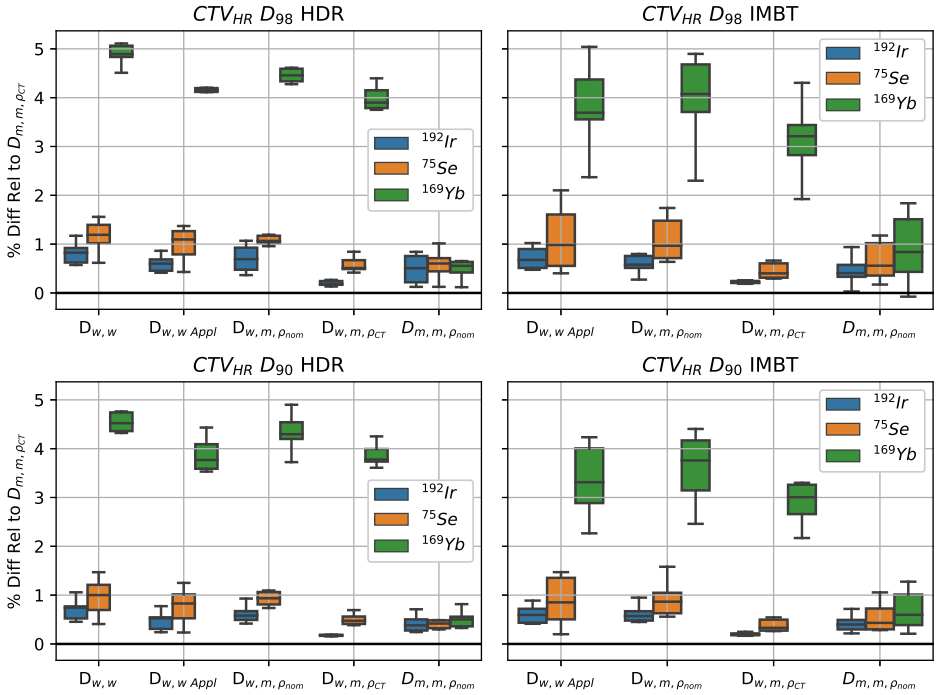


Figure 5.1: Dose reporting comparisons for CTVHR for conventional brachytherapy (left) and IMBT (right); box plots are stratified by radionuclide. All metrics are presented as a percent difference relative to the dose-to-medium in medium with CT-derived mass-densities (Dm,m ($\rho$CT)).

29% and 63% for $^{75}$Se and $^{169}$Yb, respectively. Dw,m and Dm,m for CTVHR and soft tissue OAR are indistinguishable for $^{192}$Ir and $^{75}$Se. For conventional brachytherapy with $^{169}$Yb, Dw,m overestimates Dm,m by 3.9±0.2% (P<.001) for CTVHR and underestimates by 1.7±0.1% (P=.001) for bladder. Similarly, reporting Dw,m for $^{169}$Yb-based IMBT overestimates Dm,m by 2.9 ± 0.5% (P=.003) for CTVHR and underestimates by 1.5 ± 0.1% (P<.001) for bladder.

Figure 4 illustrates the results from simulations of a $^{169}$Yb source centered in a spherical water phantom with 30 cm radius. Energy fluence as a function of depth in water, mass-energy absorption ratios relative to water as a function of photon energy and effective mass-energy absorption ratios as a function of depth are presented to show the reason why Dw,m (and Dw,w-App) simultaneously overestimate CTVHR D90 and underestimate bladder D2cc, relative to Dm,m, when using $^{169}$Yb.

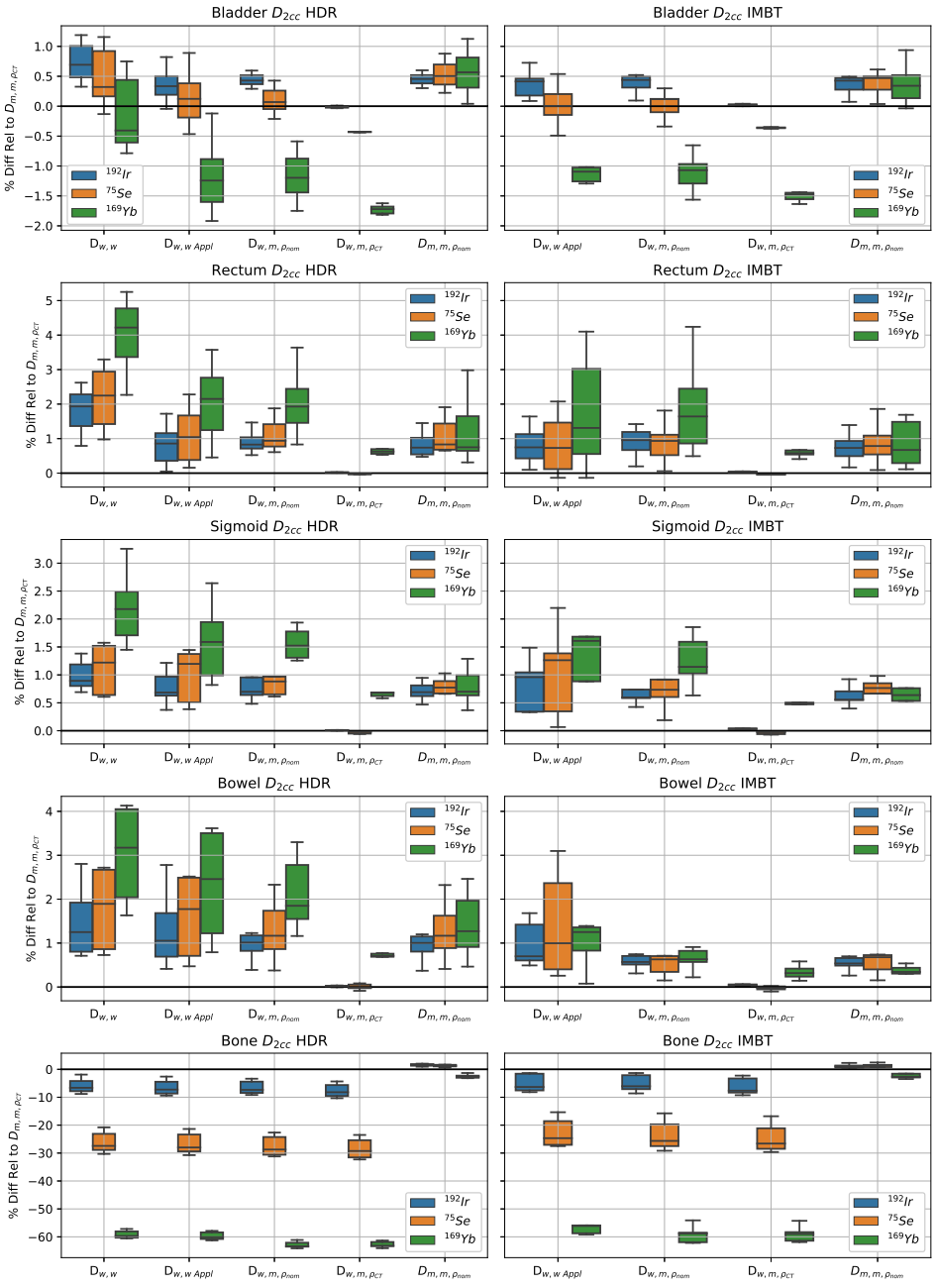


Figure 5.2: Dose reporting comparisons for OAR for conventional brachytherapy (left) and IMBT (right); box plots are stratified by radionuclide. All metrics are presented as a percent difference relative to the dose-to-medium in medium with CT-derived mass-densities (Dm,m($\rho$CT)).

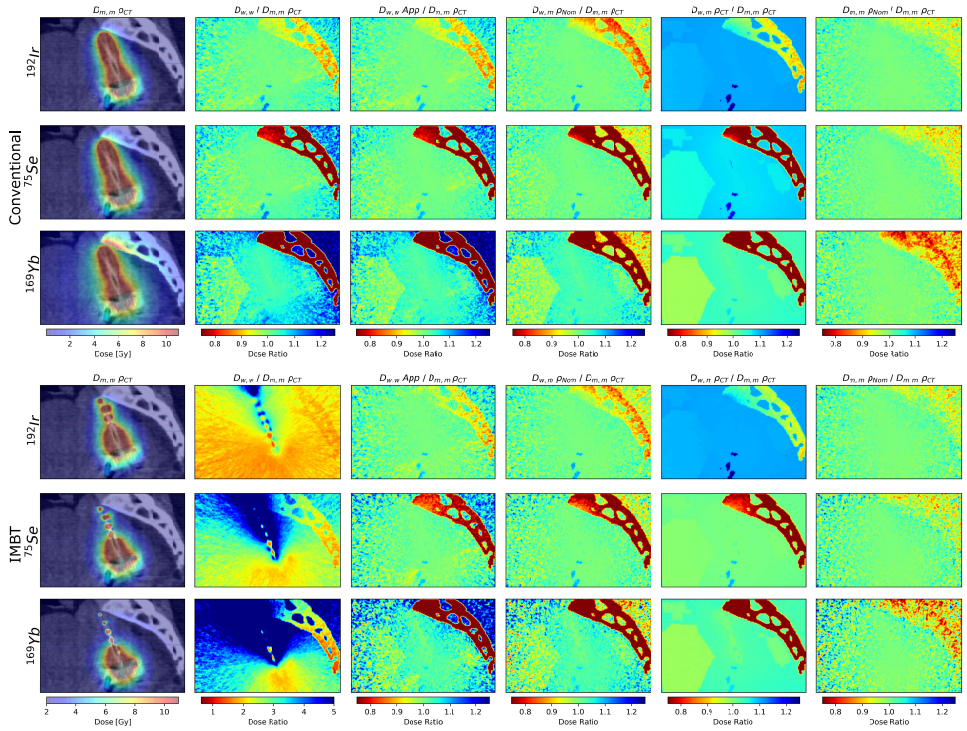


Figure 5.3: Sagittal CT slice for a cervix brachytherapy case implanted with a Venezia applicator (model overlayed in teal). Dose distributions to medium in medium using CT-derived mass-densities (Dm,m(CT)) for 192Ir, 75Se and 169Yb are shown in the left-most column subplots for conventional (top panel) and IMBT (bottom panel), respectively. Dose ratio maps relative to Dm,m(CT) for all investigated dose specification and heterogeneity method combinations.

Finally, Table 5.5 shows the effect of different mass density assignment schemes by comparing nominal mass-density assignment per structure as opposed to CT-derived voxel-by-voxel mass density assignment. Assuming a nominal mass-density for a given structure (as a whole) overestimates doses by up to 1.6% for all radionuclide-structure combinations, except for $^{169}$Yb, where dose to bone was underestimated by 2.5 ± 0.7% (P=.003) for conventional brachytherapy and 2.4 ± 0.9% (P=.002) for IMBT.

## 5.4 Discussion

Cervix brachytherapy has entered an era of precision medicine, where MR guidance facilitates the treatment of advanced cancers and novel techniques such as IMBT promise to enable safe

Table 5.2: Effect of ignoring applicator material in conventional HDR (Dw,w), represented as a percent difference from the case where the applicator material is modeled (Dw,w-App).

| Dw,w vs Dw,w-App (%) | 192Ir | 75Se | 169Yb |
|---|---|---|---|
| CTV D90 | 0.2±0.0 (P<.001) | 0.2±0.0 (P<.001) | 0.7±0.1 (P<.001) |
| Bladder D2cc | 0.4±0.2 (P<.001) | 0.3±0.2 (P=.001) | 1.0±0.3 (P<.001) |
| Rectum D2cc | 1.0±0.2 (P=.003) | 1.1±0.2 (P=.004) | 1.9±0.3 (P=.002) |
| Sigmoid D2cc | 0.2±0.1 (P=.078) | 0.1±0.1 (P=.142) | 0.6±0.1 (P=.022) |
| Bowel D2cc | 0.2±0.1 (P=.070) | 0.2±0.1 (P=.035) | 0.7±0.1 (P=.016) |
| Bone D2cc | 0.7±0.3 (P=.002) | 0.6±0.2 (P=.001) | 1.3±0.4 (P=.001) |

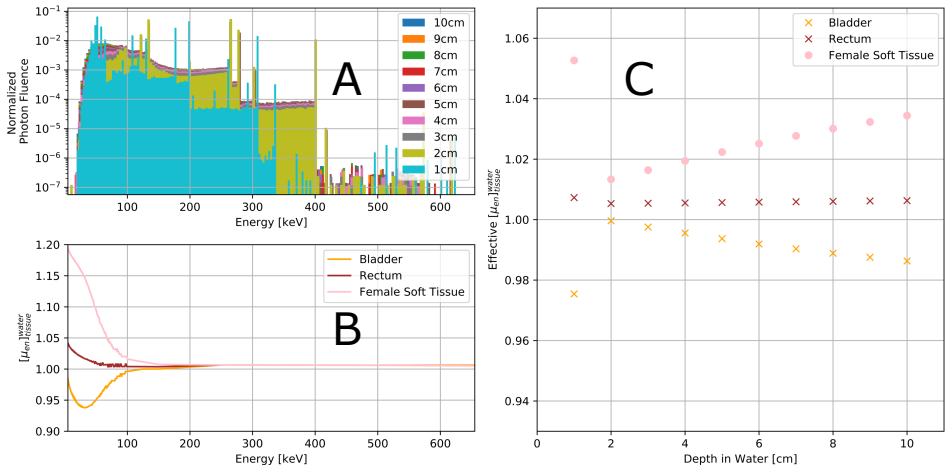


Figure 5.4: Results from simulations of a 169Yb source centered in a spherical water phantom with 30 cm radius. (A) Energy fluence as a function of depth in water. (B) Mass-energy absorption ratios (rel. to water) as a function of photon energy. (C) Effective mass-energy absorption ratios as a function of depth.

Table 5.3: Effect of ignoring patient heterogeneities, represented as a percent difference between Dw,w-App and Dm,m (CT).

| Dw,w-App vs Dm,m (CT) (%) | 192Ir | | 75Se | | 169Yb | |
|---|---|---|---|---|---|---|
| | Conv | IMBT | Conv | IMBT | Conv | IMBT |
| CTV D90 | 0.3±0.5 (P=.088) | 0.5±0.5 (P=.023) | 0.8±0.4 (P=.005) | 0.9±0.5 (P=.012) | 3.9±0.4 (P<.001) | 3.5±0.8 (P=.004) |
| Bladder D2cc | 0.4±0.3 (P=.033) | 0.4±0.2 (P=.018) | 0.1±0.5 (P=.494) | 0.0±0.4 (P=.707) | -1.2±0.6 (P=.011) | -1.1±0.6 (P=.003) |
| Rectum D2cc | 0.8±0.6 (P=.023) | 0.8±0.6 (P=.027) | 1.1±0.9 (P=.030) | 0.8±0.9 (P=.070) | 2.0±1.2 (P=.017) | 1.7±1.7 (P=.049) |
| Sigmoid D2cc | 0.8±0.3 (P=.010) | 0.8±0.5 (P=.030) | 1.0±0.5 (P=.011) | 1.1±0.9 (P=.042) | 1.6±0.7 (P=.012) | 1.3±1.3 (P=.037) |
| Bowel D2cc | 1.3±0.9 (P=.002) | 1.0±0.5 (P=.007) | 2.2±2.2 (P=.022) | 1.4±1.2 (P=.011) | 3.1±2.7 (P=.012) | 1.4±1.2 (P=.039) |
| Bone D2cc | -6.5±2.8 (P=.004) | -5.0±3.3 (P=.019) | -26.6±4.0 (P<.001) | -22.6±5.4 (P=.001) | -59.7±1.5 (P<.001) | -56.2±3.3 (P=.001) |

tumor dose escalation. [17] Dosimetry in this context was assessed in this study by using a variety of dose reporting and tissue/density assignment schemes in order to help the brachytherapy community bridge the gap between MBDCAs and the vast historical experience based on TG-43. Due to the absence of extensive dosimetric data for MBDCAs, brachytherapy doses continue to be specified in terms of the TG-43. To fully transition to MDBCAs, site-specific dosimetric data must be collected so that it may be available for correlation with known clinical outcomes. Additionally, considering the growing interest in IMBT, where high Z metal shields are introduced and radionuclides emitting lower energy photons than $^{192}$Ir are favorable [3–5, 30], understanding how MBDCAs and the various degrees of approximations impact dosimetry are important for guiding professional societies establish guidelines for IMBT. In this work we note that the trends of various dose reporting schemes are consistent and between conventional brachytherapy and IMBT within 1% for non-bone tissues and therefore conclusions drawn from conventional brachytherapy generalize well for IMBT.

The current clinical practice is to ignore the applicator. Dose uncertainties due to this effect can lead to systematic shifts in dose-response curves [31]. Hofbauer et al. observed that Dw,w

Table 5.4: Effect of reporting dose to small mass of water (Dw,m), represented as a percent difference from scoring dose to a small mass of medium (Dm,m).

| Dw,m (CT) vs Dm,m (CT) (%) | 192Ir | | 75Se | | 169Yb | |
|---|---|---|---|---|---|---|
| | Conv | IMBT | Conv | IMBT | Conv | IMBT |
| CTV D90 | 0.2±0.0 (P<.001) | 0.2±0.0 (P=.001) | 0.5±0.1 (P<.001) | 0.4±0.1 (P=.001) | 3.9±0.2 (P<.001) | 2.9±0.5 (P=.003) |
| Bladder D2cc | 0.0±0.0 (P=.117) | 0.0±0.0 (P=.013) | -0.4±0.0 (P=.001) | -0.4±0.0 (P<.001) | -1.7±0.1 (P=.001) | -1.5±0.1 (P<.001) |
| Rectum D2cc | 0.1±0.1 (P=.287) | 0.2±0.3 (P=.274) | 0.0±0.2 (P=.517) | 0.0±0.2 (P=.750) | 0.8±0.5 (P=.041) | 0.7±0.5 (P=.011) |
| Sigmoid D2cc | 0.2±0.3 (P=.353) | 0.1±0.2 (P=.281) | 0.1±0.4 (P=.525) | 0.1±0.4 (P=.518) | 0.8±0.3 (P=.016) | 0.6±0.3 (P=.014) |
| Bowel D2cc | 0.0±0.0 (P=.046) | 0.0±0.0 (P=.033) | 0.0±0.1 (P=.468) | 0.0±0.1 (P=.194) | 0.7±0.1 (P=.009) | 0.3±0.2 (P=.194) |
| Bone D2cc | -7.6±2.5 (P=.001) | -6.2±3.2 (P=.004) | -28.5±3.8 (P<.001) | -24.5±5.4 (P<.001) | -62.8±1.1 (P=.001) | -59.0±3.0 (P=.001) |

overestimates target and OAR doses by up to 2%, relative to Dw,m, when using a titanium tandem and ring applicator for $^{192}$Ir-based brachytherapy [32]. Desbiens et al., observed an up to 1% change to target and OAR DVH metrics due to plastic (polyphenylsulfone) applicator and tissue heterogeneities for $^{192}$Ir brachytherapy using a Syed-Neblett implant [9]. Our results presented in Table 5.2 show that ignoring the applicator material overestimates DVH metrics by 0.2% to 0.6% for conventional HDR brachytherapy delivered with $^{192}$Ir, which is consistent with the aforementioned studies based on the thin-walled plastic Venezia applicator used. Due to its lower energy, $^{169}$Yb produced up to a 1.0% and 1.9% overestimation in bladder and rectum D2cc when ignoring the applicator. Dose differences between Dw,w-App and Dw,m were all within 1% for non-bone tissues for conventional and IMBT using all three radionuclides as illustrated in Table 5.2 and Figures 1 and 2. As expected, differences are generally not clinically relevant for $^{192}$Ir as the disagreements are small compared to combined uncertainties. [33] While differences may be statistically significant with intermediate-energy radionuclides, differences smaller than 1% are not appropriate for drawing conclusions in light of the estimated combined

Table 5.5: Effect of assuming nominal mass-density (Dm,m nom), represented as a percent difference relative to using per voxel CT-derived mass-densities (Dm,m CT).

| Dm,m (Nom) vs Dm,m (CT) (%) | 192Ir | | 75Se | | 169Yb | |
|---|---|---|---|---|---|---|
| | Conv | IMBT | Conv | IMBT | Conv | IMBT |
| CTV D90 | 0.4±0.2 (P=.009) | 0.4±0.2 (P=.003) | 0.5±0.2 (P=.007) | 0.6±0.3 (P=.007) | 0.5±0.3 (P=.015) | 0.7±0.4 (P=.016) |
| Bladder D2cc | 0.5±0.1 (P=.004) | 0.4±0.2 (P=.006) | 0.5±0.3 (P=.011) | 0.4±0.2 (P=.011) | 0.6±0.4 (P=.029) | 0.4±0.3 (P=.036) |
| Rectum D2cc | 0.8±0.4 (P=.002) | 0.7±0.4 (P=.017) | 1.1±0.5 (P=.004) | 0.9±0.6 (P=.035) | 1.2±1.0 (P=.015) | 1.2±1.1 (P=.049) |
| Sigmoid D2cc | 0.6±0.3 (P=.015) | 0.5±0.3 (P=.012) | 0.7±0.3 (P=.011) | 0.6±0.4 (P=.015) | 0.6±0.5 (P=.023) | 0.6±0.4 (P=.021) |
| Bowel D2cc | 1.0±0.5 (P=.001) | 0.7±0.4 (P=.004) | 1.3±0.7 (P=.001) | 0.8±0.7 (P=.015) | 1.4±0.8 (P=.001) | 0.3±0.3 (P=.118) |
| Bone D2cc | 1.6±0.4 (P=.001) | 1.2±0.7 (P=.029) | 1.4±0.7 (P=.006) | 1.4±0.7 (P=.025) | -2.5±0.7 (P=.003) | -2.4±0.9 (P=.002) |

uncertainties (Table B.4).

It is well known that substantial differences in mass-energy absorption coefficients of patient tissues and water are observed with lower energy photon sources due to the increasing importance of the photoelectric effect. Differences between Dw,w and Dm,m to bone are known to be significant especially in the lower photon energy range [1]. For CTVHR and non-bone OARs, Dw,w compared to Dm,m overestimates dose by up to about 1% and 2% for $^{192}$Ir and $^{75}$Se, respectively, with the largest differences for bowel. A simultaneous 4% overestimation (Dw,m/Dm,m and Dw,wApp/Dm,m) of CTVHR and 2% underestimation of bladder was noted for $^{169}$Yb-based brachytherapy. This finding is due to the considerably different effective mass-energy absorption ratios in the depths relevant for gynecologic brachytherapy OAR evaluation (5-20 mm). For example, using a $^{169}$Yb source, the effective mass-energy absorption ratios (relative to water) for female soft tissue and bladder are approximately 1.053 and 0.975 at a depth of 1 cm, respectively, and reach 1.013 and 0.999 at 2 cm. Simulation results for energy spectra as a function of depth and the resulting effective $(\mu_{en}/\rho)$ presented in

Figure 4 confirm our conclusions. Therefore, groups publishing dosimetric planning studies must clearly define their dose scoring method as their results may exaggerate the benefits of using low-to-intermediate energy sources if they are not explicitly reporting Dm,m. Effects on IMBT cases were still present yet slightly ( 1%) suppressed due to the higher effective energies due to the shielding caused attenuation.

In the intermediate-to-high brachytherapy source photon energy range investigated in this study, Dw,m underestimates bone by approximately 8% (6%), 29% (25%) and 63% (59%) for conventional brachytherapy (IMBT) with $^{192}$Ir, $^{75}$Se and $^{169}$Yb, respectively. These results are consistent with AAPM TG-186 and TG-286, [1, 19] and more recently, reported in a recent prostate planning study, which also investigated $^{169}$Yb. [34] Pelvic insufficiency fractures have been observed in gynecologic cancer patients after pelvic irradiation [35]. Based on the results obtained in this study, when $^{169}$Yb or $^{75}$Se is used for cervical cancer brachytherapy, dose to bone should be considered.

Brachytherapy for the treatment of locally advanced cervical cancer has undergone major transformations over the last couple of decades, transitioning from 2D to 3D-based planning with an increasing number of centers performing MR image-only brachytherapy guidance (12–14). Our findings presented in Table 5.5 indicate that MR-based dosimetry (material assigned to contours) for conventional HDR brachytherapy and IMBT for treatment of cervical cancer result in a soft tissue dose overestimation on the order of 1% for $^{192}$Ir, $^{75}$Se and $^{169}$Yb, despite the loss of voxel-by-voxel mass-density information, and is consistent with that found from a recent endorectal brachytherapy investigation by Shoemaker et al [29]. This result is encouraging in view of the on-going MR-guided EMBRACE studies. Furthermore, obviating the need for CT would eliminate the uncertainties introduced by CT-to-MRI fusion and would reduce the time/resource of acquiring a CT.

## 5.5 Conclusions

In summary, our results show that ignoring the thin plastic applicator material has a minor effect on dosimetry for $^{192}$Ir and $^{75}$Se but can overestimate the absorbed dose to the target and OAR by up to 2% for $^{169}$Yb. Although bone is not typically close to the cervix applicator, our results suggest that care need to be taken to evaluate the bone dose, especially for conventional HDR brachytherapy or IMBT delivered with $^{75}$Se and especially with $^{169}$Yb. Scoring dose to

water (Dw,wApp or Dw,m) leads to an overestimation of dose to most tissues relative to Dm,m which increases with decreasing photon energy. The proximity of CTVHR and bladder to the applicator in cervix brachytherapy coupled with a significant dip in the effective mass-energy absorption ratios at these depths for $^{169}$Yb may lead to a simultaneous overestimation of absorbed dose to the target and underestimation to the OAR if Dw,m dose reporting scheme is used. Hence, we strongly recommend dose reporting clearly stated to avoid artificially overstating dosimetric effects. Dose reporting variation trends between conventional brachytherapy and IMBT are similar. In addition, our results indicate that using structure-by-structure, rather than voxel-by-voxel, mass-density assignment for MR-guided brachytherapy results in an acceptable approximation of Dm,m on the order of 1%, for conventional brachytherapy delivered with intermediate-to-high energy brachytherapy sources.

**Acknowledgements:** This research was undertaken, in part, thanks to funding from the Canada Research Chairs Program, Collaborative Health Research Projects (# 248490) and the Natural Sciences and Engineering Research Council of Canada (#241018). Computations were made on the supercomputers MP2 and Graham managed by Calcul Québec and Compute Canada. The operation of these supercomputers are funded by the Canada Foundation for Innovation (CFI), the ministère de l'Économie, de la science et de l'innovation du Québec (MESI) and the Fonds de recherche du Québec - Nature et technologies (FRQ-NT).

**Conflict of interest:** MM and SAE have an international patent on brachytherapy shields for intensity modulated brachytherapy (PCT/CA2020/050821). ANV reports personal fees from Elsevier - Seminars in Radiation Oncology, outside the submitted work.

**Supplementary material:** Supplementary material for this article can be found in Appendix B.

# References

[1] Beaulieu L, Carlsson-Tedgren A, Carrier JF. Report of the Task Group 186 on model-based dose calculation methods in brachytherapy beyond the TG-43 formalism: Current status and recommendations for clinical implementation. Med Phys;39:6208–6236. Available from: https://doi.org/10.1118/1.4747264.

[2] Rivard MJ, Coursey BM, Dewerd LA. Update of AAPM Task Group;. Report: A revised AAPM protocol for brachytherapy dose calculations. 2004. Available from: https://doi.org/10.1118/1.1646040.

[3] Morcos M, Enger SA. Monte Carlo dosimetry study of novel rotating MRI-compatible shielded tandems for intensity modulated cervix brachytherapy. Phys Medica;71:178–184. Available from: https://doi.org/10.1016/j.ejmp.2020.02.014.

[4] Famulari G, Duclos M, Enger SA. A novel 169Yb-based dynamic-shield intensity modulated brachytherapy delivery system for prostate cancer. Med Phys;47:859–868. Available from: https://doi.org/10.1002/mp.13959.

[5] Hopfensperger KM, Adams Q, Kim Y. Needle-Free Cervical Cancer Treatment Using Helical Multi-Shield Intracavitary Rotating Shield Brachytherapy with the 169;. Yb Isotope. Med Phys February 2020. Available from: https://doi.org/10.1002/mp.14101.

[6] Safigholi H, Han DY, Soliman A, Song WY. Direction modulated brachytherapy (DMBT) tandem applicator for cervical cancer treatment: Choosing the optimal shielding material. Med Phys;45:3524–3533. Available from: https://doi.org/10.1002/mp.13030.

[7] Flynn RT, Adams QE, Hopfensperger KM, Wu X, Xu W, Kim Y. Efficient 169 Yb high-dose-rate brachytherapy source production using reactivation. Med Phys;46:mp.13563. Available from: https://doi.org/10.1002/mp.13563.

[8] Safigholi H, Meigooni AS, Song WY. Comparison of 192Ir, 169Yb, and 60Co high-dose rate brachytherapy sources for skin cancer treatment. Med Phys;44:4426–4436. Available from: https://doi.org/10.1002/mp.12335.

[9] Desbiens M, D'Amours M, Afsharpour H. Monte Carlo dosimetry of high dose rate gynecologic interstitial brachytherapy. Radiother Oncol;109:425–429. Available from: https://doi.org/10.1016/j.radonc.2013.09.010.

[10] Enger SA, Ahnesjö A, Verhaegen F, Beaulieu L. Dose to tissue medium or water cavities as surrogate for the dose to cell nuclei at brachytherapy photon energies. Phys Med Biol;57:4489–4500. Available from: https://doi.org/10.1088/0031-9155/57/14/4489.

[11] Tedgren AC, Carlsson GA. Specification of absorbed dose to water using model-based dose calculation algorithms for treatment planning in brachytherapy. Phys Med & Biol;58(2561).

[12] Ma CM, Li J. Dose specification for radiation therapy: dose to water or dose to medium? Phys Med & Biol;56(3073).

[13] Anderson R, Armour E, Beeckler C. Interventional Radiation Oncology (IRO): Transition of a magnetic resonance simulator to a brachytherapy suite. Brachytherapy;17:587–596. Available from: https://doi.org/10.1016/j.brachy.2018.01.007.

[14] Chino J, Annunziata CM, Beriwal S. Radiation Therapy for Cervical Cancer: Executive Summary of an ASTRO Clinical Practice Guideline. Pract Radiat Oncol;2020:220–234. Available from: https://doi.org/10.1016/j.prro.2020.04.002.

[15] Famulari G, Marc-AndréRenaud CMP, Evans MDC, Seuntjens J, Enger SA. RapidBrachyMCTPS: a Monte Carlo-based treatment planning system for brachytherapy applications. Phys Med Biol;63(175007). Available from: https://doi.org/10.1088/1361-6560/aad97a.

[16] Agostinelli S, Allison J, Amako K. Geant4—a simulation toolkit. Nucl Instruments Methods Phys Res Sect A Accel Spectrometers. Detect Assoc Equip;506:250–303. Available from: https://doi.org/10.1016/S0168-9002(03)01368-8.

[17] Morcos M, Antaki M, Viswanathan AN, Enger SA. A novel minimally invasive dynamic-shield, intensity-modulated brachytherapy system for the treatment of cervical cancer;. Med Phys 2020. Available from: https://doi.org/10.1002/mp.14459.

[18] Enger SA, Landry G, D'Amours M. Layered mass geometry: A novel technique to overlay seeds and applicators onto patient geometry in Geant4 brachytherapy simulations. Phys Med Biol;57:6269–6277. Available from: https://doi.org/10.1088/0031-9155/57/19/6269.

[19] Sechopoulos I, Rogers DWO, Bazalova-Carter M. RECORDS: improved Reporting of montE CarlO RaDiation transport Studies: Report of the AAPM Research Committee Task Group 268. Med Phys;45:e1–e5. Available from: https://doi.org/10.1002/mp.12702.

[20] File TJENSD;. Online]. Available:. Available from: http://www.nndc.bnl.gov/ensdf/.

[21] Geant4 Collaboration Physics lists for electromagnetic processes;. Available at. Available from: http://geant4.web.cern.ch/geant4/collaboration/workinggroups/electromagnetic/physlist.shtml.

[22] Williamson JF. Monte Carlo evaluation of kerma at a point for photon transport problems. Med Phys;14:567–576. Available from: https://doi.org/10.1118/1.596069.

[23] Glickman H, Antaki M, Deufel C, Enger SA. RapidBrachyMCTPS 2.0: A Comprehensive and Flexible Monte Carlo-Based Treatment Planning System for Brachytherapy Applications;. ArXiv Prepr arXiv200702902 2020.

[24] Antaki M, Deufel C, Enger SA. Fast mixed integer optimization (FMIO) for high dose rate brachytherapy. Phys Med & Biol.

[25] White DR, V GR, Wilson IJ. Report 46. J Int Comm Radiat Units Meas.

[26] Walters B, Kawrakow I, Rogers DWO, et al. DOSXYZnrc users manual. Nrc Rep Pirs;794:1–125.

[27] Kawrakow I. Accurate condensed history Monte Carlo simulation of electron transport. I. EGSnrc, the new EGS4 version. Med Phys;27:485–498.

[28] Mann-Krzisnik D, Verhaegen F, Enger SA. The influence of tissue composition uncertainty on dose distributions in brachytherapy. Radiother Oncol;126:394–410. Available from: https://doi.org/10.1016/j.radonc.2018.01.007.

[29] Shoemaker T, Vuong T, Glickman H, Kaifi S, Famulari G, Enger SA. Dosimetric Considerations for Ytterbium-169, Selenium-75, and Iridium-192 Radioisotopes in High-Dose-Rate Endorectal Brachytherapy. Int J Radiat Oncol;105:875–883. Available from: https://doi.org/10.1016/J.IJROBP.2019.07.003.

[30] Safigholi H, Han DY, Mashouf S. Direction modulated brachytherapy (DMBT) for treatment of cervical cancer: A planning study with 192Ir, 60Co, and 169Yb HDR sources: A. Med Phys;44:6538–6547. Available from: https://doi.org/10.1002/mp.12598.

[31] Nesvacil N, Tanderup K, Kallehauge J, Lindegaard J, Pötter R, Kirisits C. OC-0360: Impact of random dosimetric uncertainties on dose-response curves for HDR cervix cancer brachytherapy. Radiother Oncol;106:S141.

[32] Hofbauer J, Kirisits C, Resch A. Impact of heterogeneity-corrected dose calculation using a grid-based Boltzmann solver on breast and cervix cancer brachytherapy. J Contemp Brachytherapy;8:143–149. Available from: https://doi.org/10.5114/jcb.2016.59352.

[33] Andreo P, Burns DT, Salvat F. On the uncertainties of photon mass energy-absorption coefficients and their ratios for radiation dosimetry. Phys Med Biol;57:2117–2136. Available from: https://doi.org/10.1088/0031-9155/57/8/2117.

[34] Famulari G, Alfieri J, Duclos M, Vuong T, Enger SA. Can intermediate-energy sources lead to elevated bone doses for prostate and head & neck high-dose-rate brachytherapy? Brachytherapy;19:255–263. Available from: https://doi.org/10.1016/j.brachy.2019.12.004.

[35] Shih KK, Folkert MR, Kollmeier MA. Pelvic insufficiency fractures in patients with cervical and endometrial cancer treated with postoperative pelvic radiation. Gynecol Oncol;128:540–543. Available from: https://doi.org/https://doi.org/10.1016/j.ygyno.2012.12.021.

# Chapter 6

# Conclusions & Outlook

This dissertation presents a novel dynamic-shield IMBT tandem-based applicator for the treatment of locally advanced cervical cancer. Our IMBT applicator, which is compatible with commercial high dose rate BT afterloading systems is also MRI-compatible - enabling its use in MRI-guided BT, which has be shown to improve patient outcomes [1] as it allows us to more clearly define the extent of the tumor growth and to therefore treat the entire tumor. BT in the course of the definitive treatment of cervical cancer is undoubtedly the factor that results in high (>90%) local control rates as evidenced by the large retroEMBRACE study [2]. However, these outcomes are only possible if the patient receives BT in the first place.

The grim reality is that women around the world do not have access to this standard of care. The reasons for the gaps in care are multi-factorial but are mainly caused by the fact that there are not many residency-trained BT practitioners comfortable in intracavitary/interstitial BT implantation. There also exists a subset of patients unable to receive complex interstitial implants due to procedure and anesthesia-related toxicities [3]. IMBT offers the promise of minimal invasiveness, i.e., needle-free, intracavitary-only BT, which can produce dose distributions superior to conventional intracavitary BT implants and equal to hybrid intracavitary/interstitial BT implants. Specifically, we have demonstrated that IMBT with the ubiquitous $^{192}$Ir or the lower energy alternatives $^{75}$Se or $^{169}$Yb improves the tumor (HR-CTV) dose coverage by up to 6.7% with the largest improvements achieved with the lowest energy radionuclides ($^{169}$Yb$\rightarrow^{75}$Se$\rightarrow^{192}$Ir). For context, a 6.7% increase in tumor dose translates to about 6.3% increase in local control in the 70 to 80 Gy region for patients with FIGO stage III-IV disease according to analysis of retroEMBRACE data [4].

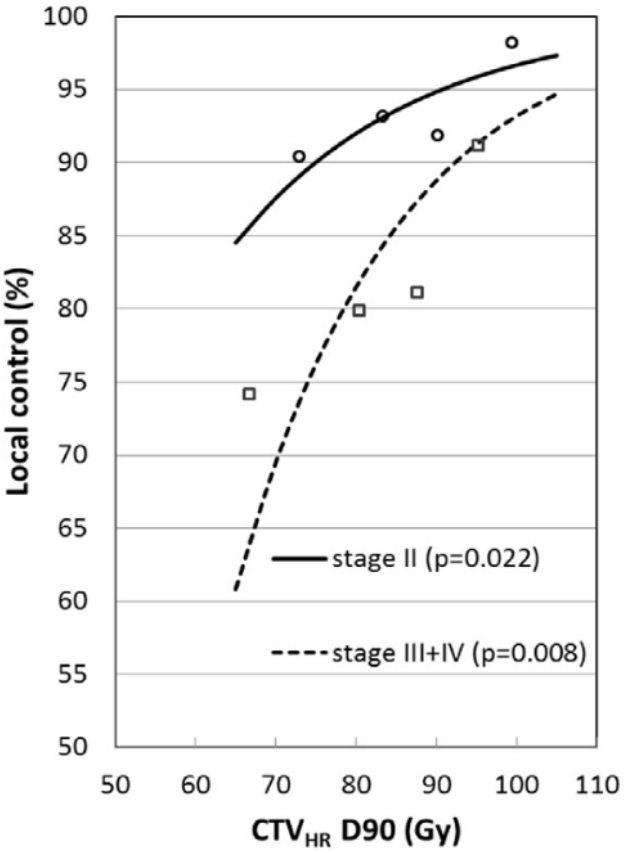


Figure 6.1: Dose response curves indicating the 3-year local control rates as a function of HR-CTV D90 dose. Reproduced from Tanderup *et al.* [4]

For patients with large (> 30 cm$^3$) irregular tumors, retroEMBRACE has shown that the addition of interstitial needles (hybrid intracavitary/interstitial BT) improves the therapeutic ratio and leads to a 10% high local control rate compared to patients who receive intracavitary BT. For this group of patients, we have shown that the needle-free IMBT can achieve similar dosimetry to conventional hybrid intracavitary/interstitial BT, thereby improving the survival rates of women who do not have access to intracavitary/interstitial BT and improving the quality of life in terms of a procedure which is minimally invasive and could be performed in an out-patient setting. Larger dosimetric studies will help confirm the findings from this body of works and determine the subset of patients with advanced disease which are suitable for IMBT.

The clinical implementation of dynamic shield IMBT is contingent on the adoption of model-based dose calculation algorithms (MBDCAs) capable of accurately calculating dose in the presence of tissue and applicator heterogeneities, specifically, high-Z shields. Clinically available, commercial MBDCAs have been made available for nearly a decade but have been adopted in a limited fashion mainly due to lack of clinical outcome evidence based on dose-to-medium ($D_{m,m}$) as opposed to dose-to-water ($D_{w,w}$). Our current understanding of dose response outcome and toxicity data is based on nearly a century of ($D_{w,w}$) experience. Translating the clinical standard to dose-to-medium requires collection of real clinical dosimetry data calculated in both media (water and medium) to be able to draw firm conclusions on how prescription doses are to change. Unlike conventional BT, dynamic shield IMBT dose distributions cannot be estimated by ignoring all tissue/material heterogeneities and assuming patients and applicators are composed of water. Therefore the development of a MBDCA that can take the attenuation of the radiation by the shield material and handle dynamic shield motions is paramount. In Chapter 3, the ability to handle dynamic motion of the shields, independent of the motion of the cable-driven BT source was added to the Monte Carlo based treatment planning system RapidBrachyMCTPS [5, 6]. Optimization algorithms (fast mixed integer and column generation) were added to RapidBrachyMCTPS for dwell time, dwell position and shield angle optimization by Antaki *et al.* [7] This formed the framework which enabled patient-specific dwell position/time and shield angle optimization followed by patient-specific dose calculations which were used in our retrospective patient study (Chapter 4).

In our manuscript titled "On the impact of absorbed dose specification, tissue heterogeneities, and applicator heterogeneities on Monte Carlo-based dosimetry of Ir-192, Se-75, and Yb-169 in conventional and intensity-modulated brachytherapy for the treatment of cervical cancer" (Chapter 5) [8], we showed the potential dosimetric benefits of IMBT, the next step was to help the BT community bridge the gap between the vast historical experience with $D_{w,w}$ and MBDCA-based $D_{m,m}$ dosimetry. $D_{w,w}$ makes the assumption that the patient is composed entirely of uniform density water. Whereas $D_{m,m}$ represents the most realistic dose by taking into consideration the the mass density and material composition of the patient, BT applicators and shields. MBDCAs are capable of outputting an intermediate dose to $D_{w,w}$ and $D_{m,m}$, referred to dose-to-water-in-medium ($D_{w,m}$), which takes into consideration material/density heterogeneities for the purposes of radiation transport (same as $D_{m,m}$) but scores dose to a small mass of water. The arguments in favor of using $D_{w,m}$ are based on the fact that current clinical knowledge is based on dose to water and that this intermediate dose reporting method may help

intuitively. Additionally, radiation effects in tissue are due to DNA damage in the cell nucleus (which can be approximated as water). The clinical impact of prescribing $D_{m,m}$ versus $D_{w,m}$ is outside the scope of our work. In this context, our study aimed to present dosimetric data in the setting of gynecologic BT to help shed light on the matter.

While the impact of soft tissues in the pelvis are not clinically relevant in the photon energy range covered by BT sources used in high dose rate BT, our study investigated whether any tissue heterogeneity corrections needed to be applied for accurate clinical dosimetry. The main takeaway was that although pelvic bones are typically not in close proximity to the treatment area, care should be taken to evaluate the dose to bone to avoid radiation-induced fractures. The dose to bone increases with decreasing photon energies, a potential concern for $^{169}$Yb. Another important consideration in the era of MRI-guided BT is that by leaving CT based treatment planning, we now lose mass-density information. The reason for this is that CT Hounsfield Units are bilinearly related to mass density. Doing away with CT leaves us with the responsibility of estimating mass densities for dose calculation. Our study assessed the impact of assigning a nominal mass density to an entire organ which is done in MRI-based dosimetry performed with MBDCA, compared with voxel by voxel mass density assignment done in CT-based dosimetry which was assumed to be the ground truth. We found that assigning nominal mass densities to organs resulted in an acceptable approximation of the dosimetry on the order of 1%. Our most important, non-intuitive, finding with $^{169}$Yb-based BT/IMBT was that dose to the tumor (HR-CTV) was overestimated while the dose to the bladder was underestimated. The proximity of the HR-CTV and bladder to the BT implant coupled with a substantial dip in the effective mass-energy absorption ratio (at these depths) lead to these findings when reporting dose using the intermediate dose reporting method of transporting radiation through medium but scoring it locally to a small mass of water ($D_{w,m}$). Our recommendation is that practitioners should clearly state the dose reporting method used to avoid inadvertently misrepresenting dosimetric improvements.

The outlook for IMBT in the treatment of cervical cancer is positive. The cervix is one of the few anatomical sites that can be reached through a naturally occurring cavity in the body. Coupled with the evidence that IMBT is superior to intracavitary BT and equal to complex intracavitary/interstitial BT, there exists an imminent evolution in BT. Before entering the clinical trial phase, dynamic shield IMBT will require considerable collaborations between academic and industrial partners. These partnerships will need to focus on incorporation of the developed treatment planning optimization algorithms, MBDCAs, dynamic shield systems by

the academic partners into clinical solutions provided by the industry. Further collaboration regarding radionuclide production is needed. In addition, academic partners, clinicians and industry need to collaborate closely through AAPM and GEC-ESTRO to provide guidelines and recommendations for quality assurance, clinical adoption and future studies. In light of the surge of enthusiasm and promise of IMBT for impacting clinical care, the American Association of Physicists in Medicine (AAPM)'s task group #337 has been tasked with defining the possibilities and limitations of improving conventional BT by using IMBT techniques and is actively working on the technological review and clinical recommendations which will be needed to translate IMBT into clinical use. This provides societal support of the IMBT technique and is a strong indication that IMBT shall enter clinical trials within the decade.

# References

[1] Fokdal L, Sturdza A, Mazeron R. Image guided adaptive brachytherapy with combined intracavitary and interstitial technique improves the therapeutic ratio in locally advanced cervical cancer: Analysis from the retroEMBRACE study. Radiother Oncol;120:434–440. Available from: https://doi.org/10.1016/j.radonc.2016.03.020.

[2] Sturdza A, Pötter R, Fokdal LU. Image guided brachytherapy in locally advanced cervical cancer: Improved pelvic control and survival in RetroEMBRACE, a multicenter cohort study. Radiother Oncol;120:428–433. Available from: https://doi.org/10.1016/j.radonc.2016.03.011.

[3] Lim KH, Lu JJ, Wynne CJ, Back MF, Mukherjee R, Razvi K, et al. A study of complications arising from different methods of anesthesia used in high-dose-rate brachytherapy for cervical cancer. American journal of clinical oncology. 2004;27(5):449–451.

[4] Tanderup K, Fokdal LU, Sturdza A, Haie-Meder C, Mazeron R, van Limbergen E, et al. Effect of tumor dose, volume and overall treatment time on local control after radiochemotherapy including MRI guided brachytherapy of locally advanced cervical cancer. Radiotherapy and Oncology. 2016;120(3):441–446. Available from: https://www.sciencedirect.com/science/article/pii/S0167814016311173.

[5] Glickman H, Antaki M, Deufel C, Enger SA. RapidBrachyMCTPS 2.0: a comprehensive and flexible Monte Carlo-based treatment planning system for brachytherapy applications; 2020. arXiv:2007.02902.

[6] Famulari G, Marc-AndréRenaud CMP, Evans MDC, Seuntjens J, Enger SA. RapidBrachyMCTPS: a Monte Carlo-based treatment planning system for brachytherapy applications. Phys Med Biol;63(175007). Available from: https://doi.org/10.1088/1361-6560/aad97a.

[7] Antaki M, Deufel C, Enger SA. Fast mixed integer optimization (FMIO) for high dose rate brachytherapy. Phys Med Biol. 2020;65(21):215005.

[8] Morcos M, Viswanathan AN, Enger SA. On the impact of absorbed dose specification, tissue heterogeneities, and applicator heterogeneities on Monte Carlo-based dosimetry of Ir-192, Se-75, and Yb-169 in conventional and intensity-modulated brachytherapy for the treatment of cervical cancer. Medical physics. 2021;48(5):2604–2613.

# Appendix A

# Supplementary material of Chapter 4

Table A.1: Elemental composition and nominal densities of tissues.

| Material | Element (% mass) | | | | | | | | | | | | | Mass density (g cm-3) |
|---|---|---|---|---|---|---|---|---|---|---|---|---|---|---|
| | H | C | N | O | Na | Mg | P | S | Cl | Ar | K | Ca | Other | |
| Water | 11.2 | | | 88.8 | | | | | | | | | | 0.998 |
| Air | 0.1 | | 75 | 23.6 | | | | | | 1.3 | | | | 0.0012 |
| Soft Tissue (Female) | 10.6 | 31.5 | 2.4 | 54.7 | 0.1 | | 0.2 | 0.3 | 0.2 | | 0.2 | | | 1.02 |
| Bladder | 10.8 | 3.5 | 1.5 | 83 | 0.3 | | 0.1 | 0.1 | 0.5 | | 0.2 | | | 1.03 |
| Rectum/Sigmoid/Bowel | 10.6 | 11.5 | 2.2 | 75.1 | 0.1 | | 0.1 | 0.1 | 0.2 | | 0.1 | | | 1.03 |
| Cortical bone | 3.4 | 15.5 | 4.2 | 43.5 | 0.1 | 0.2 | 10.3 | 0.3 | | | | 22.5 | | 1.92 |
| PPSU (Applicator) | 4 | 72 | | 16 | | | | | | | | | S(8.0) | 1.29 |
| Fiberglass (Applicator) | 2.6 | 27.3 | 0.2 | 36.6 | | 3.7 | | | | | | 6 | B(2.0),Al(4.9),Si(16.7) | 2.1 |
| Tungsten (Shield) | | | | | | | | | | | | | W(100) | 19.3 |

Table A.2: Conversion from Hounsfield units (HU) to mass density.

| Hounsfield unit (HU) | Mass density (g cm-3) |
|---|---|
| -1000 | 0.0012 |
| -659 | 0.330 |
| -516 | 0.480 |
| -97 | 0.945 |
| -57 | 0.980 |
| 0 | 1.000 |
| 14 | 1.052 |
| 69 | 1.094 |
| 217 | 1.155 |
| 220 | 1.157 |
| 456 | 1.335 |
| 809 | 1.561 |
| 1230 | 1.824 |
| 3000 | 2.874 |
| 5000 | 3.920 |

# Appendix B

# Supplementary material of Chapter 5

Table B.1: Elemental composition and nominal densities of tissues.

| Material | Element (% mass) | | | | | | | | | | | | | Mass density (g cm-3) |
|---|---|---|---|---|---|---|---|---|---|---|---|---|---|---|
| | H | C | N | O | Na | Mg | P | S | Cl | Ar | K | Ca | Other | |
| Water | 11.2 | | | 88.8 | | | | | | | | | | 0.998 |
| Air | 0.1 | | 75 | 23.6 | | | | | | 1.3 | | | | 0.0012 |
| Soft Tissue (Female) | 10.6 | 31.5 | 2.4 | 54.7 | 0.1 | | 0.2 | 0.3 | 0.2 | | 0.2 | | | 1.02 |
| Bladder | 10.8 | 3.5 | 1.5 | 83 | 0.3 | | 0.1 | 0.1 | 0.5 | | 0.2 | | | 1.03 |
| Rectum/Sigmoid/Bowel | 10.6 | 11.5 | 2.2 | 75.1 | 0.1 | | 0.1 | 0.1 | 0.2 | | 0.1 | | | 1.03 |
| Cortical bone | 3.4 | 15.5 | 4.2 | 43.5 | 0.1 | 0.2 | 10.3 | 0.3 | | | | 22.5 | | 1.92 |
| PPSU (Applicator) | 4 | 72 | | 16 | | | | | | | | | S(8.0) | 1.29 |
| Fiberglass (Applicator) | 2.6 | 27.3 | 0.2 | 36.6 | | 3.7 | | | | | | 6 | B(2.0),Al(4.9),Si(16.7) | 2.1 |
| Tungsten (Shield) | | | | | | | | | | | | | W(100) | 19.3 |

Table B.2: Conversion from Hounsfield units (HU) to mass density.

| Hounsfield unit (HU) | Mass density (g cm-3) |
|---|---|
| -1000 | 0.0012 |
| -659 | 0.330 |
| -516 | 0.480 |
| -97 | 0.945 |
| -57 | 0.980 |
| 0 | 1.000 |
| 14 | 1.052 |
| 69 | 1.094 |
| 217 | 1.155 |
| 220 | 1.157 |
| 456 | 1.335 |
| 809 | 1.561 |
| 1230 | 1.824 |
| 3000 | 2.874 |
| 5000 | 3.920 |

Table B.3: Monte Carlo simulation methods based on the recommendations of TG-268.

| Item name | Description |
|---|---|
| Code, version | Geant4 10.02.p02,RapidBrachyMCTPS. |
| Computation Time | 3 cpu-hours for 1E8 histories on a 2.8 GHz Intel Core i7 processor. |
| Geometry | Voxelized geometry (egsphant) extracted from DICOM CT images and DICOM RT Structure Set files. CT grid interpolated to grid with voxel size 1mm3. |
| Materials | a)Homogeneous water phantom(TG-43) orb) heterogeneous phantom(TG-186), with elemental composition of tissues, CT-to-density conversion, and tissue properties assignment schemes provided in Tables A.1-A.2. |
| Source description | FlexiSource source geometry(active core consists of192Ir,75Se or169Yb).<br>Explicit simulation of radioactive decay using photon decay spectra from ENSDF. Source positions and orientations imported from DICOM RT Plan files. Dwell times imported from RapidBrachyMCTPS plan files. |
| Cross sections | EPDL97, EEDL97, EADL97. |
| Transport parameters | PENELOPE low-energy electromagnetic physics list with default transport parameters.Electron transport off.Production cut: 0.1 mm. |
| Variance reduction technique | Track length estimator using mass-energy absorption coefficient library provided in RapidBrachyMCTPS. |
| Scored quantities | Absorbed dose (collisional kerma approximation)scored to a) water or b) medium. Voxel size of 1mm3 |
| # histories/statistical uncertainty | 1E8photon histories (decay events). Type A uncertainties(k=1)<1%for voxels inside 100% isodose volume and <2% for voxels contained within 50% isodose volume. |
| Statistical methods | History-by-history method. |

Table B.4: Total uncertainty budget for Monte Carlo simulations. A range of uncertainties is reported for voxels of organs/structures used in calculated dose-volume metrics of interest in this work. Bowel tends to be sufficiently far from the implant relative to the CTV and other organs and is at the upper range of the uncertainty.

| Source of uncertainty | Type | Uncertainty (%) | Reference |
|---|---|---|---|
| Statistics | A | 0.3-2.0 | |
| Source geometry | B | 0.5 | |
| Source photon spectrum | B | 0.5 | (*) |
| MC radiation transport | B | 0.2 | (*) |
| Interaction cross sections ($\mu/\rho$) | B | 0.1 | (*) |
| Scoring cross sections ($\mu_{en}/\rho$) | B | 1.0 | (*) |
| Tally volume averaging | B | 0.2 | |
| Standard uncertainty (k=1) | | 1.3-2.4 | |
| Expanded uncertainty (k=2) | | 2.6-4.8 | |

*DeWerd, Larry A., et al. "A dosimetric uncertainty analysis for photon-emitting brachytherapy sources: Report of AAPM Task Group No. 138 and GEC-ESTRO." Medical Physics. 2011 Feb;38(2):782-801